



# CLIMATE CHANGE AND RENEWABLES

PROGRESSING TOWARDS A  
GREENER AND CLEANER FUTURE



# CLIMATE CHANGE AND RENEWABLES

PROGRESSING TOWARDS A GREENER AND CLEANER FUTURE

## **Editors**

Nurfadzilah Ahmad

Muhammad Azfar Shamil Abd Aziz



**SEMARAK ILMU**  
PUBLISHING

202103268166 (003316878 - P)

Share your knowledge for a better tomorrow

**Semarak Ilmu Publishing**

No. 7-G, Jalan Puteri 3A/7

Bandar Puteri Bangi

43000 Kajang, Selangor

2023

© Solar Research Institute (SRI) 2023

All right reserved, no part of this publication may be reproduced, stored in a retrieval system or transmitted in any form or by any means, mechanical, electronic, photocopying, recording or any other way without the permission of Solar Research Institute (SRI), UiTM.

eISBN 978-629-98779-0-5

*Published in Malaysia by*  
SEMARAK ILMU PUBLISHING  
No. 7-G, Jalan Puteri 3A/7  
Bandar Puteri Bangi  
43000 Kajang, Selangor  
Tel: 017-7541097  
Website:<https://semarakilmu.com.my/>

## Project Management

Nurfadzilah Ahmad

*Acquisition Editor*

Muhammad Azfar Shamil Abd Aziz

*Editor*

Nurliyana Baharin

*Paper Author*

Muhammad Ikram Ahmad

*Paper Author*

Nur Fadhilah Jamaludin

*Paper Author*

Nur Alfarina Pirdaus

*Paper Author*

Sharina Safiee

*Paper Author*

Norhasnelly Anuar

*Paper Author*



# FOREWORD

## by Director of Solar Research Institute (SRI)



More than three years after the declaration of a global emergency for Covid-19, the World Health Organization (WHO) is now saying it is over as we enter the endemic phase.

As nations globally learn to live with the virus, we see businesses and societies set to recover to the state they once were in. This coupled with the increasingly evident consequences of climate change, have accelerated efforts in developing more sustainable and renewable sources of energy.

Likewise, in Malaysia, the Government has stepped up efforts to increase the use of renewable energy to decrease its dependency on fossil fuel and further commit to its endeavour in becoming a carbon-neutral nation as early as 2050.

The Solar Research Institute (SRI) of Universiti Teknologi MARA (UiTM) has always been in support of these actions with constant collaborations, innovations, and research with diverse parties and stakeholders.

Additionally, SRI has always worked closely with the university in engaging and nurturing bright young talents as we work towards securing a greener tomorrow for the nation.

SRI pledges to give its utmost effort and dedication in backing the country's commitment towards achieving the UN Sustainable Development Goals (SDGs) and a carbon-neutral nation by 2050.

I would like to extend my heartfelt gratitude to all the authors, contributors, and researchers whose dedication has brought this invaluable resource to life. I also extend my appreciation to all the readers who share in the vision of a better tomorrow.


May this work serve as a catalyst for positive change and inspire us all to be steadfast in our commitment to creating a better world through solar power and sustainability.

Thank you and happy reading.

**Associate Professor Ir. Dr. Nofri Yenita Dahlan**  
Director, Solar Research Institute (SRI)  
Universiti Teknologi MARA (UiTM)

## Table of contents

<b>01. Overview on Electric Bus Charging Scheduling: A Case Study of a Battery Electric Bus as Campus Transportation in UTeM Main Campus</b> .....	<b>01</b>
I. Introduction	02
II. Related works	03
III. System model	04
IV. Assumptions	05
V. Results and discussion	05
VI. Conclusions and recommendations	07
<b>02. Forecasting Generation of 50MW Gambang Large Scale Solar (LSS) Photovoltaic Plant Using Non-Linear Autoregressive Exogenous (NARX) – Artificial Neural Network (ANN)</b> .....	<b>09</b>
I. Introduction	10
II. Methodology	11
III. Results	13
IV. Conclusions	14
<b>03. Designing a 2755 kW Photovoltaic System for Grid Integration for Empowering Renewable Energy</b> .....	<b>15</b>
I. Introduction	16
II. Overview of the 2775 kW LSSPV	17
III. The 2775 kW LSSPV design component	17
IV. LSSPV calibrated simulation model implementation in MATLAB Simulink	19
V. Conclusion	21
<b>04. Comparison between Titanium Dioxide Synthesis by Sol-Gel and Titanium Dioxide Commercial Properties for Dye-Sensitized Solar Cell Application</b> .....	<b>23</b>
I. Introduction	24
II. Methodology	25
III. Results and discussion	25
IV. Conclusion	27
<b>05. A Review of the KNX System in Addressing Climate Change and Energy Efficiency</b> .....	<b>28</b>
I. Introduction	29
II. KNX system in climate change mitigation and energy efficiency	30
III. Summary	32
<b>06. A Fuzzy C-Means Clustering Analysis of Global Horizontal Irradiance – A Case Study in Gambang, Pahang, Malaysia</b> .....	<b>34</b>
I. Introduction	35
II. Methodology	36
III. Result and discussion	36
IV. Conclusion	39
<b>07. List of contributors</b> .....	<b>40</b>
<b>08. Index</b> .....	<b>41</b>



# Overview on Electric Bus Charging Scheduling: A Case Study of a Battery Electric Bus as Campus Transportation in UTeM Main Campus

01

# Overview on Electric Bus Charging Scheduling: A Case Study of a Battery Electric Bus as Campus Transportation in UTeM Main Campus

Nurliyana Binti Baharin  
Fakulti Kejuruteraan Elektrik,  
Universiti Teknikal Malaysia Melaka,  
Melaka, Malaysia  
liyana@utem.edu.my

Nofri Yenita Dahlan  
UiTM Solar Energy Research Institute  
Universiti Teknologi MARA  
Shah Alam, Selangor  
nofriyenita012@uitm.edu.my

Mohamad Fani Sulaima  
Fakulti Kejuruteraan Elektrik,  
Universiti Teknikal Malaysia Melaka,  
Melaka, Malaysia  
fani@utem.edu.my

**Abstract**— BEB has a wide range of usage, from short- to long distance travel. In 2023, Malaysia's government's encouragement towards BEB has supported the projection of the transition of diesel buses to electric buses in the National Automotive Policy 2020. The aims of this paper are: 1) to review the BEB technologies and method to optimize BEB charging scheduling and 2) to develop fuzzy logic model to optimize the BEB charging scheduling in for BEB as in-campus shuttle. Comprehensive overview of relevant literature on BEB technology, charging specification and BEB charging scheduling. BEB charging scheduling was developed using Fuzzy Logic model to determine priority of BEB charging through two inputs and one output in Fuzzy Logic model. The findings show that the energy demand shows that there is a significant spike occur on the load profile due to BEB charging loads. Besides, by applying enhanced time-of-use (eToU) tariff, there is increment in overall electricity bill for the campus.

**Keywords**—BEB, charging scheduling, Fuzzy logic, load profile, eToU

## I. INTRODUCTION

Transport sector is one of the sectors that contributed to the air pollution around the world besides the other big sectors such as residential, energy, industry, agriculture and from windblown dust. By country, North America has the largest contributing air pollution by transport sector with 14.8% of total air pollution by sector in North America. It is followed by Europe with 8.7%, Latin America and Caribbean with 8.5%, Asia and Pacific 7.4%, West Asia 6.3% and the lowest is Africa with 3.6% [1]. Hence, many countries shifted from internal combustion engine (ICE) to the zero-emission vehicle (ZEV) includes passengers to heavy duty vehicles. Among these, battery electric buses (BEB) have emerged as a promising solution for reducing emissions in the public transportation sector which it is projected that the sales of BEB will be increase in 25% from 2022 to 2030 [2]. Over the past decade, the adoption of BEB has witnessed substantial growth worldwide. According to statistics, as of the most recent data available, there are approximately 670,000 electric buses operating globally. China has been at the forefront of this shift, accounting for most electric bus deployments. In fact, China alone represents over 99% of the total electric bus fleet, with more than 450,000 electric buses in operation in 2017. China continues to dominate the electric bus market, and new registrations are rising as they have in past years. The adoption of plug-in electric buses is not limited to China alone. Several other countries have recognized the potential of electric buses in achieving sustainable urban transportation. Europe has seen significant progress in this area, with countries like the Netherlands, Germany, and France leading the way. Furthermore, cities such as London, Paris, and Amsterdam have implemented policies to phase out diesel

buses and transition to electric alternatives [3]. Consequently, in order to save energy and prevent congestion in the power system when charging the BEB from the grid, a proper BEB charging schedule needs to be designed. 2. According to NAP 2020, government encourage to use EB to replace conventional buses [4]. However, electric bus operation has a few limitations to consider which BEB typically have a limited driving range per charge compared to diesel buses' fuel range due to the battery capacity and route, the availability and accessibility of charging infrastructure and need high power to charge the battery. Therefore, optimum BEB charging scheduling need to be considered to achieve optimum BEB operations. 4. In Malaysia, there is absence of specific tariff scheme for EB charging load in campus facility. The existing tariff that available is eToU tariff by TNB applied for campus facility is based on commercial tariff for electrical load. The effectiveness of the existing eToU tariff in promoting the use of EB in the campus is yet to be explored and investigated. Therefore, it is critical to formulate an optimum eToU tariff that is suitable for both existing campus load and EB charging load that can create benefits to both consumers and the power utility in Malaysia [5]

Driven by the motives, BEB charging scheduling has been extensively studied in recent years (will be reviewed in the next section). Most of the works that are currently in existence, in particular, take into account BEB charging scheduling outside of campus networks. As a result, this paper will highlight the BEB charging scheduling in campus network, where BEB serves as on-campus transportation for students. The energy demand of the campus will be analysed based on a comparison of load profiles and electricity bills before and after BEB charging loads are added to the existing campus network. The main objective of this paper is to review the BEB charging scheduling research and to analyse the effect of charging BEB in campus network by using Fuzzy Logic model.

Contributions of this paper are: 1) review on the BEB technologies and method to optimize BEB charging scheduling and 2) to develop fuzzy logic model to optimize the BEB charging scheduling in for BEB as in-campus shuttle. The impact of the BEB charging activity on the campus load profile and energy cost will be analyzed.

The rest of this paper is organized as follows. Theory about BEB and its technology and related works regarding BEB charging scheduling represented in Section II. The proposed scheduling algorithm with the fuzzy logic control is described in Section III. The assumption used in this work were explained in Section IV. In Section V, the simulation results of the Fuzzy logic model and the impact of BEB charging to

the grid and transformers are provided. Finally, conclusions and recommendations are given in Section VI.

## II. RELATED WORKS

This section explained the facts of the electric buses, latest BEB charging technologies and related works that investigated the BEB charging impact. The BEB charging method that was covered by previous researchers will also be elaborated in this section.

### A. Electric Buses and BEB Charging Technology

Four types of familiar zero-emission buses that have been used in road are hybrid electric bus (HEB), plug-in hybrid electric bus (PHEB), battery electric bus (BEB) and Fuel Cell Electric Buses (FCEB). These varieties differ in the technologies used for fuelling, which in turn affects the routes and purposes these buses can best serve. Here are some basic explanations about all the listed electric buses. A HEB typically keeps a diesel engine but uses additional equipment to drive the bus when needed. There are many types of hybrid system currently in operation called series and parallel HEBs. On a hybrid bus when the driver brakes, the hybrid system captures kinetic energy and stores for use later when it is required for propulsion. The next time the bus accelerates, the stored energy is fed back to the driving wheels, this process called as regenerative braking system. The diesel is conserved by the energy produce from the electric energy produce from regenerative braking system. PHEB incorporate the advantages of hybrid and battery electric buses. They are equipped with an internal combustion engine as a fallback for extended range or when the batteries are depleted. PHEBs can be charged using either external power sources or regenerative braking. BEB, also known as pure electric buses, are driven by one electric motor or more electric motors that utilise energy from an on-board high voltage battery. A high-voltage battery is defined as any voltage with a value of 50 volts and above. Usually, BEB battery packs are manufactured between 400V and 800V. BEBs are charged by plugging into charging stations, and their range is determined by battery capacity. They are widely used in urban areas and for short to medium distance routes. FCEB use hydrogen fuel cells to generate electricity, which is then used to power the electric motor. The only byproduct of the fuel cells' conversion of hydrogen and oxygen into electricity is water vapour. FCEBs have longer ranges and quicker refuelling periods than battery electric buses, making them ideal for long-distance routes [6].

The charging system for electric buses is a crucial component of their operation, allowing their batteries to be refuelled and ensuring continuous operation. As technology advances, electric bus charging systems continue to evolve with improvements in charging speeds, interoperability, and smart grid integration. Three main types of electric charging systems widely used on the road are plug-in, pantograph, and inductive or wireless charging systems. Two of them are pantograph and plug-in charging systems, both made by a well-known company, ABB. The plug-in charging system includes AC and DC fast charging. Plug-in AC charging systems use CCS cables that consist of AC and DC power. There are two types of pantographs charging designs from ABB: pantograph down and pantograph up. The difference between these two types of pantographs charging systems is the charging connection, where up refers to the pantograph coming from the electric bus and down refers to the pantograph coming from the charging pole [[7], [8]. ABB also

provides the design for smart charging for electric bus depots, where the buses can be charged in sequence automatically to avoid peak demand [9]. Along with these, the charging system is also assigned other names, such as plug-in, also called overnight charging. Both pantographs up and down can be opportunities, and overnight charging depends on where the pantograph is installed, either in the depot or on the single pole Depot charging refers to the buses being charged while they are parked at the depot, typically during off-peak hours. This method allows for a longer charging time and can be more cost-effective. On the other hand, single pole charging involves installing pantographs on individual poles along the bus route, allowing for quick and convenient charging during regular stops.

### B. BEB Charging Impact and Charging Scheduling

When charging, electric buses use a substantial amount of power, especially when several buses are doing it at once. The high-power demand during the charging process can put additional stress on the electrical distribution network [10], [11] impacts to both transformers and grids. Normally, transformer were installed with reserved capacity for future grid expand however, BEB charging load consume huge amount of energy which can contributes to several effects such as overload of transformer [12], increase maintenance cost [13], increase power loss on transformer [31], shorter the life of transformer [14], [15], increase temperature on transformer [16] and additional cost due to new installation of transformer[17]. BEB charging loads also gave negative effect to the grid where it can increase peak load demand [18]–[22], increase power losses [23]–[27], severe voltage drop [21], decrease reserve margins [28]–[31], degradation of power efficiency [32], BEB charger can inject more harmonics [25], upgrade of distribution system [33] and overload on the distribution line [34]. Due to these conditions, proper BEB charging scheduling need to be done.

BEB charging scheduling refers to the process of determining when and how electric buses should be charged to ensure they have sufficient battery capacity for their scheduled operations. It involves creating a schedule that specifies the charging times and durations for individual buses within a fleet. The objectives of BEB charging scheduling are to minimise operational cost, charging cost, and infrastructure cost and fully utilise the charging infrastructure to have optimum operations. To optimise BEB charging scheduling, two methods were used in previous research: the mathematical method and the artificial intelligence method. One of the popular mathematical methods is mixed-integer linear programming (MILP), which has been extensively used in previous research to minimise different kinds of costs involved in charging infrastructure and the impact on the grid Fast-charging station deployment for battery electric bus systems considering electricity demand charges [31], [35]–[39]. The other mathematical methods used are the general modelling system [40] and non-linear programming optimisation (NLP) [41]. These mathematical methods have proven to be effective in optimising charging infrastructure and managing its impact on the grid. Additionally, artificial intelligence methods, such as machine learning algorithms, have also been employed in previous research to address these challenges [42]–[47]. These AI methods have shown promising results in predicting charging demand and optimising charging schedules to minimise costs and grid stress.



To analyse the effect of charging costs, previous researchers considered the demand response. Time-of-Use (ToU) pricing allows for different electricity rates at different times of the day, incentivizing users to shift their charging demand to off-peak hours when electricity costs are lower. By considering the single depot charging infrastructure, research has been done to minimise the charging cost using ToU as the electricity tariff price [22], [48]–[51]. Usually, a single depot is used for overnight charging systems. Multi depot charging infrastructures can usually be applied for opportunity charging and overnight charging, which means that beside the main depot, the charging system also has on-route charging infrastructure. This kind of charging system has been used in research [47], [52] to minimise BEB charging costs. There is also research using day ahead tariff prices to optimise the operating system cost using wireless charging systems [53].

### III. SYSTEM MODEL

As depicted in Figure 1, the battery electric bus (BEB) charging depot discovery employs a beacon signal between the charging stations (CS) and BEB, and the beacon signal is powered by a local area network (LAN) such as Wi-Fi or Bluetooth. Through the discovery of BEB charging depots, the CS is aware of the number of BEB in the area, and vice versa. BEB and CS transmit data to the centralised control system via cellular or wireless network following the discovery of the BEB charging depot. The CS data contains the condition of charging pads. Consequently, the control system is informed of the number of accessible pads that are not occupied by the BEB. The information of BEB comprises the state of charge (SOC) and charging time of the BEB battery. The charging period indicates the duration of BEB's stay at the CS for charging. The BEB provides the specific charging time to the CS, and if the charging time expires, the BEB departs the CS. As a result, the SOC of the BEB battery and the charging time serve as inputs for the fuzzy logic control. Using the data from BEB and CS, the control system generates a priority matrix, which is the output of fuzzy logic control. The priority matrix is utilised by the control system's algorithm for charging scheduling. The control system prioritises minimising charging wait time and balancing the charging request rate.

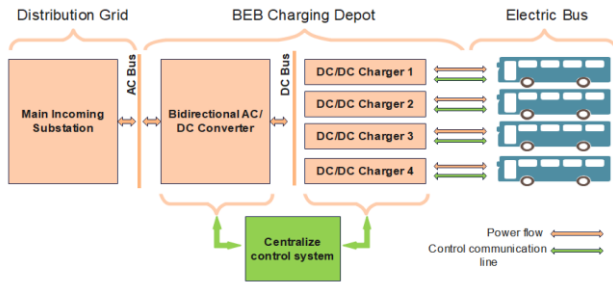


Figure 1: BEB charging scheduling diagram.

#### A. BEB and Charging Stations Specifications

BEB model that have been selected in this paper have energy storage of 330kW and assumed using overnight charging system using CCS cable. The battery can be charged using 150kW charging stations. Hence, maximum time to charge one bus is 2.2 hours but we consider as 3hours because the kWh is considering one hour full for the energy usage. These specifications will be applied to the case study in section IV.

#### B. Fuzzy Logic Model for Priority Determination

In this paper, a fuzzy logic control is developed to determine the BEB charging priority. By considering the inputs as state-of-charge (SoC) and stay time (duration of charging) while the output is charging priority. To acquire the fuzzy charging priority of each electric vehicle, the inputs are fuzzified and sent through an inference system with fuzzy rules. The fuzzy logic control system can be referred to Figure 2.

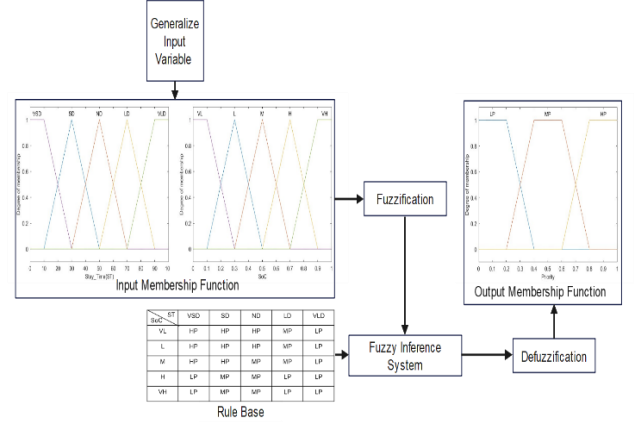


Figure 2: Fuzzy Logic Model

The membership functions of the two inputs are used to express the fuzziness of the inputs. Table I shows the details of both input and output variables of fuzzy inference system. The first input is SoC that is defined by triangular and trapezium membership functions with five fuzzy states: Very Low (VL), Low (L), Medium (M), High (H), and Very High (VH). The second input is Stay Time (ST) that is defined by triangular and trapezium membership functions with five fuzzy states: Very Short Duration (VSD), Short Duration (SD), Normal Duration (ND), Long Duration (LD) and Very Long Duration (VLD). The output of the fuzzy inference system is the charging priority which is defined using trapezium membership functions with three fuzzy states: Low Priority (LP), Medium Priority (MP), and High Priority (HP).

TABLE I: THE MEMBERSHIP FUNCTION OF FL

Input		Input		Output	
SoC (%)		Stay Time		Priority	
State	Symbol	State	Symbol	State	Symbol
VL	Very Low	VSD	Very Short Duration	LP	Low Priority
L	Low	SD	Short Duration	MP	Medium Priority
M	Medium	ND	Normal Duration	HP	High Priority
H	High	LD	Long Duration		
VH	Very High	VLD	Very Long Duration		

#### C. Enhanced Time-of-Use Tariff (eToU)

In Peninsular Malaysia, the eToU tariff applicable for the consumers under commercial and industrial segment. TNB introduced enhanced time-of-use (eToU) to improve the ToU tariff structure. The enhanced time of use (ETOU) rate is available to all commercial and industrial categories (including C1, E1, C2, and E3) with three time zones,

whereas previous TOU tariffs only have two zones [54]. The ETOU tariff also includes six-time segmentations that incorporate off-peak, mid-peak, and peak zones, allowing consumers greater flexibility in evaluating load management options to minimize power consumption costs. Nonetheless, as of the end of 2017, this initiative had garnered a negligible number of participants, and the goal had not been met [55]. ETOU electricity price tariff is shown in TABLE II.

TABLE II: ETOU ELECTRICITY TARIFF PRICE

Time Zone	Time	Energy Charge (sen/kWh)	
		Weekdays	Weekend
off-peak	0-1	0.281	0.281
	1-2	0.281	0.281
	2-3	0.281	0.281
	3-4	0.281	0.281
	4-5	0.281	0.281
	5-6	0.281	0.281
	6-7	0.281	0.281
mid-peak	7-8	0.281	0.281
	8-9	0.357	0.281
	9-10	0.357	0.281
peak	10-11	0.357	0.281
	11-12	0.584	0.281
mid-peak	12-13	0.357	0.281
	13-14	0.357	0.281
peak	14-15	0.584	0.281
	15-16	0.584	0.281
	16-17	0.584	0.281
mid-peak	17-18	0.357	0.281
	18-19	0.357	0.281
	19-20	0.357	0.281
	20-21	0.357	0.281
	21-22	0.357	0.281
off-peak	22-23	0.281	0.281
	23-24	0.281	0.281

#### IV. ASSUMPTIONS

The case study in main campus UTeM has been selected to become the BEB charging scheduling application. Currently, UTeM only provides the services of conventional buses as shuttle bus in main campus. However, there is a plan to use BEB on campus in future. Hence, it is important to investigate the impact of adding new charging loads to the existing grid in this campus. To be precise, 20 BEBs and 4 BEB charging stations are assumed to be installed in a single depot in the Development Management Office which is nearer to the main incoming substation. By neglecting the route of the BEB, the BEB charging scheduling is developed based on the fuzzy logic model.

## V. RESULTS AND DISCUSSION

### A. BEB Charging Scheduling

In this section, the output from the fuzzy logic model has been used to construct the BEB charging schedule. Table III shows the priority determination based on inputs and output that has been set in fuzzy logic model. For example, if the stay time is 80 and SoC value is 0.2, the priority is 0.373 fall under low priority category. This means that any BEB that has been detected with SoC value 0.2 will have low priority. The BEB with high priority will be charged first, followed by medium and low priority.

TABLE III: PRIORITY DETERMINATION USING FL OUTPUT

Stay Time	SoC	Charging Time	CCS	Priority	
80	0.2	2.2	30	0.373	LP
70	0.3	1.98	147	0.5	MP
60	0.4	1.76	114	0.627	HP
50	0.5	1.54	81	0.5	MP
40	0.6	1.32	48	0.627	HP
30	0.7	1.1	15	0.5	MP
20	0.8	0.88	132	0.373	LP
10	0.9	0.66	99	0.153	LP

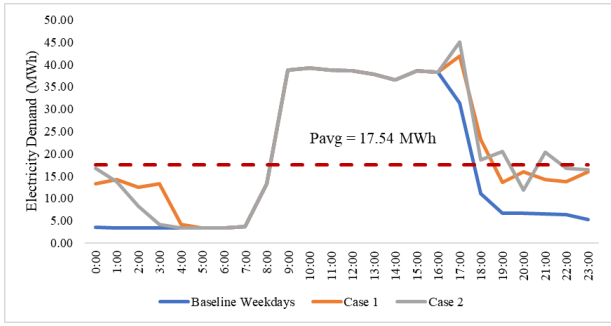
In Table IV in Appendix A represented the BEB charging scheduling for 20 BEBs using 4 charging stations. Overnight charging will start at 1800 and end at 0700 before the bus start to reoperates. The first 4 BEB that will be charged are Bus 3, 5, 11 and 13 because it has high priority. The process is continued with the bus that have medium and low priority and repeated until all 20 buses are complete the charging process. The last session of charging is done by Bus 17 at charging station 4 (CS4) at 0400. The reading of the energy usage is captured by the metering system installed in this campus distribution system.

### B. Impact of BEB charging to Grid

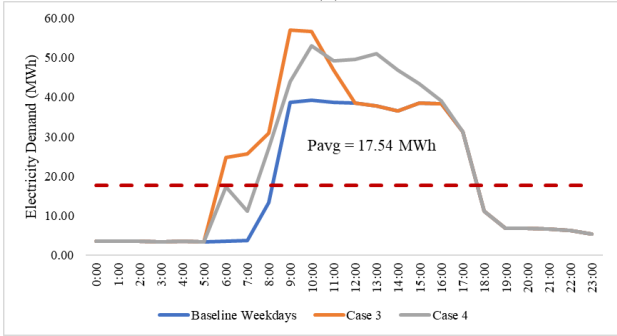
The historical data of the power consumption for the main campus network has been used in this work. To see the impact of charging BEB to grid, case scenarios were created as follows:

- 1) Case 1-Night Charging – OppCharge (charging started 1800) – 2 charging stations (CS – CS1,CS2)
- 2) Case 2-Night Charging – CCS (charging started 1800) – charging stations (CS– CS1,CS2,CS3,CS4)
- 3) Case 3-Day Charging - OppCharge (charging started 0700) - 2 charging stations (CS – CS1,CS2)
- 4) Case 4-Day Charging - CCS (charging started 0700) - 4 charging stations (CS– CS1,CS2,CS3,CS4)

Another type of charging station has been added which is 2 pantograph charging stations. The charging session is also now assumed to be held during the day for weekday and weekend.



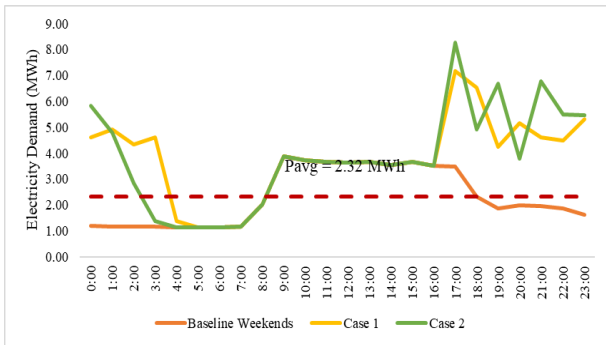
(a)



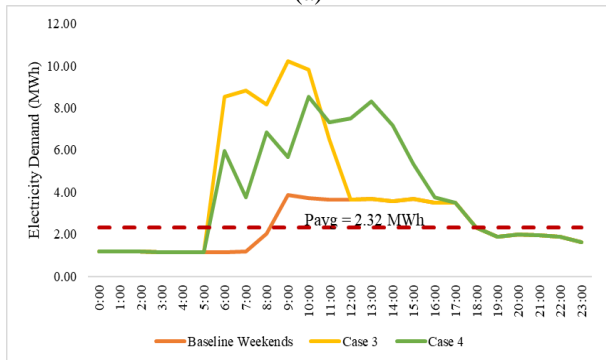
(b)

Figure 3: Electricity Demand (MWh) for weekday.

From Figure 3 (a), the comparison of the BEB charging Case 1 and Case 2 has been presented. Case 1 and Case 2 refer to Overnight charging where there is peak load started to grow from the time BEB start to charge. While in Figure 3(b), the load profile comparison for Case 3 and 4 shows that additional peak load during day charging. This will affect the reserve margin for the energy demand in this campus. The same pattern shows for weekend cases as shown in Figure 4(a) and (b). However, the increment of energy usage for weekend is higher compared to weekdays.



(a)



(b)

Figure 4: Electricity Demand (MWh) for weekend.

TABLE V: ENERGY DEMAND INCREMENT PERCENTAGE

	Pantograph	CCS
Weekdays	24.91%	24.88%
Weekends	65.51%	65.42%

As shown in TABLE V, by using the Pantograph charging system, the increment of energy demand is 24.91%, compared to 24.88% using the CCS charging system. However, the weekend cases show a higher percentage increase in energy demand compared to weekdays, with 65.51% and 65.42% for the pantograph and CCS charging systems, respectively. This suggests that the Pantograph charging system is slightly more efficient in meeting energy demands compared to the CCS charging system. Additionally, the higher percentage increase in energy demand on weekends may be attributed to increased usage of BEB for recreational purposes or longer trips.

### C. Impact of BEB charging to Energy Cost

There are several costs that should be considered in developing the BEB charging system, such as BEB cost, BEB charging depot cost, and energy cost. However, in this work, the energy cost was analyzed based on the eToU tariff set by TNB. The energy cost in this paper is the overall electricity price before and after BEB charging loads are added to the existing loads. TABLE VI indicates the electricity price for Cases 1, 2, 3, and 4 for weekends and weekdays. The baseline electricity price for weekdays is RM 181,862.19, while for weekends it is RM 15,647.93. The prices for Case 1, Case 2, Case 3, and Case 4 vary slightly from the baseline in both weekday and weekend scenarios. There are distinguishable changes in price increments before and after the BEB charging system. As illustrated in TABLE VII, the energy cost for Case 4 is increased by 18.14% during the weekdays and 22.96% on weekends. This indicates that the energy cost for charging BEBs is higher on weekends compared to weekdays. Additionally, the energy cost for Case 4 remains consistent across all four cases, with an increment percentage of 65.42%.

TABLE VI: ELECTRICITY PRICE COMPARISON

WEEKDAY ELECTRICITY PRICE(RM)				
Baseline	Case 1	Case 2	Case 3	Case 4
181862.19	214857.43	215400.74	217880.25	223623.19
WEEKEND ELECTRICITY PRICE(RM)				
Baseline	Case 1	Case 2	Case 3	Case 4
15647.93	25898.81	25885.32	25898.81	25885.32

TABLE VII: ELECTRICITY PRICE PERCENTAGE OF INCREMENT COMPARISON

Weekday			
Case 1	Case 2	Case 3	Case 4
18.14%	18.44%	19.81%	22.96%
Weekend			
Case 1	Case 2	Case 3	Case 4
65.51%	65.42%	65.51%	65.42%

## VI. CONCLUSIONS AND RECOMMENDATIONS

This paper proposes BEB charging scheduling using a fuzzy logic model. A fuzzy logic model has been developed for the priority development of the BEB charging system. The output of the fuzzy logic model was obtained to build the BEB charging schedule. Additional BEB charging loads affect peak load demand and energy costs for the UTeM main campus network. It is recommended that the BEB charging schedule be optimised to minimise peak load demand and energy costs. Additionally, further research could explore the potential benefits of implementing smart grid technologies to improve the efficiency of the BEB charging system.

## REFERENCES

- [1] UNEP, "Pollution Action Note – Data you need to know." [https://www.unep.org/interactive/air-pollution-note/?gclid=CjwKCAjwyqWkBhBMEiwAp2yUFgb1Ffm1it-WqjZMwHsnKvdZXRcfzC1GsVCTzRxMe107Mbw6SnB6BoCORMQAvD\\_BwEhttps://www.unep.org/interactive/air-pollution-note/?gclid=CjwKCAjwyqWkBhBMEiwAp2yUFgb1Ffm1it-WqjZMwHsnKvdZXRcfzC1GsVCTzRxMe107Mbw6SnB6BoCORMQAvD\\_BwE](https://www.unep.org/interactive/air-pollution-note/?gclid=CjwKCAjwyqWkBhBMEiwAp2yUFgb1Ffm1it-WqjZMwHsnKvdZXRcfzC1GsVCTzRxMe107Mbw6SnB6BoCORMQAvD_BwEhttps://www.unep.org/interactive/air-pollution-note/?gclid=CjwKCAjwyqWkBhBMEiwAp2yUFgb1Ffm1it-WqjZMwHsnKvdZXRcfzC1GsVCTzRxMe107Mbw6SnB6BoCORMQAvD_BwE) (accessed Jun. 05, 2023).
- [2] International Energy Agency, "Historical of EV sales, cars, World, 2010-2022," *International Energy Agency*, Apr. 26, 2023. <https://www.iea.org/data-and-statistics/data-tools/global-ev-data-explorer> (accessed Jul. 01, 2023).
- [3] International Energy Agency and Clean Energy Ministerial, "Global EV Outlook 2022," France, May 2022. Accessed: Jun. 21, 2023. [Online]. Available: <https://www.iea.org/reports/global-ev-outlook-2022>
- [4] Ministry of International Trade and Industry, "NAP2020 Booklet," 2020.
- [5] Tenaga Nasional Berhad (TNB), "TNB ENHANCED TIME OF USE (ETOU)." <https://www.tnb.com.my/faq/etou/> (accessed Aug. 15, 2022).
- [6] The Low Carbon Vehicle Partnership, G. Esposito, D. Hayes, and D. Eastlake, "The Low Emission Bus Guide," London, Nov. 2016. [Online]. Available: <http://www.lowcvp.org.uk/initiatives/leb/LEBCertificates.htm>
- [7] ABB, "Electric bus pantograph up," ABB. <https://new.abb.com/ev-charging/pantograph-up> (accessed Jul. 10, 2023).
- [8] ABB, "Pantograph down for electric buses," ABB. <https://new.abb.com/ev-charging/pantograph-down> (accessed Jul. 10, 2023).
- [9] ABB, "HVC360 ABB Smart Charging System," ABB. <https://e-mobility.abb.com/products-services/hvc360/> (accessed Jul. 10, 2023).
- [10] E. Sortomme, M. M. Hindi, S. D. J. MacPherson, and S. S. Venkata, "Coordinated charging of plug-in hybrid electric vehicles to minimize distribution system losses," *IEEE Trans Smart Grid*, vol. 2, no. 1, pp. 198–205, 2011, doi: 10.1109/TSG.2010.2090913.
- [11] N. Korolko and Z. Sahinoglu, "Robust Optimization of EV Charging Schedules in Unregulated Electricity Markets," *IEEE Trans Smart Grid*, vol. 8, no. 1, pp. 149–157, Jan. 2017, doi: 10.1109/TSG.2015.2472597.
- [12] M. A. Azzouz, M. F. Shaaban, and E. F. El-Saadany, "Real-Time Optimal Voltage Regulation for Distribution Networks Incorporating High Penetration of PEVs," *IEEE Transactions on Power Systems*, vol. 30, no. 6, pp. 3234–3245, Nov. 2015, doi: 10.1109/TPWRS.2014.2385834.
- [13] P. S. Georgilakis and E. I. Amoiralis, "Distribution transformer cost evaluation methodology incorporating environmental cost," *IET Generation, Transmission and Distribution*, vol. 4, no. 7, pp. 861–872, Jul. 2010, doi: 10.1049/iet-gtd.2009.0638.
- [14] C. Z. El-Bayeh, I. Mougharbel, D. Asber, M. Saad, A. Chandra, and S. Lefebvre, "Novel approach for optimizing the transformer's critical power limit," *IEEE Access*, vol. 6, pp. 55870–55882, 2018, doi: 10.1109/ACCESS.2018.2873077.
- [15] A. Ahmadian, M. Sedghi, M. Aliakbar-Golkar, M. Fowler, and A. Elkamel, "Two-layer optimization methodology for wind distributed generation planning considering plug-in electric vehicles uncertainty: A flexible active-reactive power approach," *Energy Convers Manag*, vol. 124, pp. 231–246, Sep. 2016, doi: 10.1016/j.enconman.2016.07.025.
- [16] T. Committee of the IEEE Power and E. Society, "IEEE Guide for Loading Mineral-Oil-Immersed Transformers and Step-Voltage Regulators Sponsored by the Transformers Committee," 2012.
- [17] P. Balducci, L. Schienbein, T. Nguyen, D. Brown, and E. Fathelrahman, "An examination of the costs and critical characteristics of electric utility distribution system capacity enhancement projects," in *IEEE PES Power Systems Conference and Exposition, 2004.*, IEEE, pp. 484–484. doi: 10.1109/PSCE.2004.1397503.
- [18] H. M. Abdullah, A. Gastli, and L. Ben-Brahim, "Reinforcement Learning Based EV Charging Management Systems—A Review," *IEEE Access*, vol. 9, pp. 41506–41531, 2021, doi: 10.1109/ACCESS.2021.3064354.
- [19] A. Dubey, S. Santoso, M. P. Cloud, and M. Waclawiak, "Determining Time-of-Use Schedules for Electric Vehicle Loads: A Practical Perspective," *IEEE Power and Energy Technology Systems Journal*, vol. 2, no. 1, pp. 12–20, Mar. 2015, doi: 10.1109/JPETS.2015.2405069.
- [20] B. Sun, Z. Huang, X. Tan, and D. H. K. Tsang, "Optimal Scheduling for Electric Vehicle Charging with Discrete Charging Levels in Distribution Grid," *IEEE Trans Smart Grid*, vol. 9, no. 2, pp. 624–634, Mar. 2018, doi: 10.1109/TSG.2016.2558585.
- [21] E. Karfopoulos and N. Hatzigaryriou, "Distributed coordination of electric vehicles for conforming to an energy schedule," *Electric Power Systems Research*, vol. 151, pp. 86–95, Oct. 2017, doi: 10.1016/j.epsr.2017.05.018.
- [22] R.-C. Leou and J.-J. Hung, "Optimal Charging Schedule Planning and Economic Analysis for Electric Bus Charging Stations," *Energies (Basel)*, vol. 10, no. 4, p. 483, Apr. 2017, doi: 10.3390/en10040483.
- [23] O. Erdinc, A. Tascikaraoglu, N. G. Paterakis, I. Dursun, M. C. Sinim, and J. P. S. Catalao, "Comprehensive Optimization Model for Sizing and Siting of DG Units, EV Charging Stations, and Energy Storage Systems," *IEEE Trans Smart Grid*, vol. 9, no. 4, pp. 3871–3882, Jul. 2018, doi: 10.1109/TSG.2017.2777738.
- [24] Q. Kang, S. Feng, M. Zhou, A. C. Ammari, and K. Sedraoui, "Optimal Load Scheduling of Plug-In Hybrid Electric Vehicles via Weight-Aggregation Multi-Objective Evolutionary Algorithms," *IEEE Transactions on Intelligent Transportation Systems*, vol. 18, no. 9, pp. 2557–2568, Sep. 2017, doi: 10.1109/TITS.2016.2638898.
- [25] M. K. Gray and W. G. Morsi, "Power quality assessment in distribution systems embedded with plug-in hybrid and battery electric vehicles," *IEEE Transactions on Power Systems*, vol. 30, no. 2, pp. 663–671, Mar. 2015, doi: 10.1109/TPWRS.2014.2332058.
- [26] S. Bohn, M. Agsten, A. Dubey, and S. Santoso, "A Comparative Analysis of PEV Charging Impacts -An International Perspective," Apr. 2015. doi: 10.4271/2015-01-0300.
- [27] K. Clement-Nyns, E. Haesen, and J. Driesen, "The Impact of Charging Plug-In Hybrid Electric Vehicles on a Residential Distribution Grid," *IEEE Transactions on Power Systems*, vol. 25, no. 1, pp. 371–380, Feb. 2010, doi: 10.1109/TPWRS.2009.2036481.
- [28] P. Samaras, A. Fachantidis, G. Tsoumakas, and I. Vlahavas, "A prediction model of passenger demand using AVL and APC data from a bus fleet," in *Proceedings of the 19th Panhellenic Conference on Informatics*, New York, NY, USA: ACM, Oct. 2015, pp. 129–134. doi: 10.1145/2801948.2801984.
- [29] C. Zhou, P. Dai, and R. Li, "The Passenger Demand Prediction Model on Bus Networks," in *2013 IEEE 13th International Conference on Data Mining Workshops*, IEEE, Dec. 2013, pp. 1069–1076. doi: 10.1109/ICDMW.2013.20.
- [30] J. Mendes-Moreira, L. Moreira-Matias, J. Gama, and J. Freire De Sousa, "Validating the coverage of bus schedules: A Machine Learning approach," *Inf Sci (N Y)*, vol. 293, pp. 299–313, Feb. 2015, doi: 10.1016/j.ins.2014.09.005.
- [31] I. Zoltowska and J. Lin, "Optimal Charging Schedule Planning for Electric Buses Using Aggregated Day-Ahead Auction Bids," *Energies (Basel)*, vol. 14, no. 16, p. 4727, Aug. 2021, doi: 10.3390/en14164727.
- [32] T. Thiringer and S. Haghbin, "Power Quality Issues of a Battery Fast Charging Station for a Fully-Electric Public Transport System

in Gothenburg City,” *Batteries*, vol. 1, no. 1, pp. 22–33, Nov. 2015, doi: 10.3390/batteries1010022.

[33] S. M. Arif, T. T. Lie, B. C. Seet, S. M. Ahsan, and H. A. Khan, “Plug-In Electric Bus Depot Charging with PV and ESS and Their Impact on LV Feeder,” *Energies (Basel)*, vol. 13, no. 9, p. 2139, Apr. 2020, doi: 10.3390/en13092139.

[34] T. Li *et al.*, “An Optimal Design and Analysis of a Hybrid Power Charging Station for Electric Vehicles Considering Uncertainties,” in *IECON 2018 - 44th Annual Conference of the IEEE Industrial Electronics Society*, IEEE, Oct. 2018, pp. 5147–5152. doi: 10.1109/IECON.2018.8592855.

[35] A. Abdelwahed, P. L. van den Berg, T. Brandt, J. Collins, and W. Ketter, “Evaluating and optimizing opportunity fast-charging schedules in transit battery electric bus networks,” *Transportation Science*, vol. 54, no. 6, pp. 1601–1615, Nov. 2020, doi: 10.1287/trsc.2020.0982.

[36] R. Patil, A. Rahegaonkar, A. Patange, and S. Nalavade, “Designing an optimized schedule of transit electric bus charging: A municipal level case study,” *Mater Today Proc.*, vol. 56, pp. 2653–2658, Jan. 2022, doi: 10.1016/J.MATPR.2021.09.220.

[37] Y. Wang, Y. Huang, J. Xu, and N. Barclay, “Optimal recharging scheduling for urban electric buses: A case study in Davis,” *Transp Res E Logist Transp Rev.*, vol. 100, pp. 115–132, Apr. 2017, doi: 10.1016/J.TRE.2017.01.001.

[38] Y. Jiang and T. He, “Optimal Charging Scheduling and Management with Bus-Driver-Trip Assignment considering Mealtime Windows for an Electric Bus Line,” *Complexity*, vol. 2022, pp. 1–19, Mar. 2022, doi: 10.1155/2022/3087279.

[39] Y. He, Z. Song, and Z. Liu, “Fast-charging station deployment for battery electric bus systems considering electricity demand charges,” *Sustain Cities Soc.*, vol. 48, Jul. 2019, doi: 10.1016/j.scs.2019.101530.

[40] J.-M. Clairand, M. Gonzalez-Roriguez, P. G. Teran, I. Cedenno, and G. Escriva-Escriva, “The impact of charging electric buses on the power grid,” in *2020 IEEE Power & Energy Society General Meeting (PESGM)*, IEEE, Aug. 2020, pp. 1–5. doi: 10.1109/PESGM41954.2020.9282014.

[41] A. Houbbadi, R. Trigui, S. Pelissier, E. Redondo-Iglesias, and T. Bouton, “Optimal Scheduling to Manage an Electric Bus Fleet Overnight Charging,” *Energies (Basel)*, vol. 12, no. 14, p. 2727, Jul. 2019, doi: 10.3390/en12142727.

[42] K. Gkiotsalitis, “Bus Holding of Electric Buses with Scheduled Charging Times,” *IEEE Transactions on Intelligent Transportation Systems*, vol. 22, no. 11, pp. 6760–6771, Nov. 2021, doi: 10.1109/TITS.2020.2994538.

[43] N. Olsen and N. Kliewer, “Scheduling Electric Buses in Public Transport: Modeling of the Charging Process and Analysis of Assumptions,” Berlin, Germany, Mar. 2020. doi: 10.23773/2020\_4.

[44] D. Huang and S. Wang, “A two-stage stochastic programming model of coordinated electric bus charging scheduling for a hybrid charging scheme,” *Multimodal Transportation*, vol. 1, no. 1, p. 100006, Mar. 2022, doi: 10.1016/J.MULTRA.2022.100006.

[45] H. Hu, B. Du, and P. Perez, “Integrated optimisation of electric bus scheduling and top-up charging at bus stops with fast chargers,” in *2021 IEEE International Intelligent Transportation Systems Conference (ITSC)*, IEEE, Sep. 2021, pp. 2324–2329. doi: 10.1109/ITSC48978.2021.9564617.

[46] A. Jahic, M. Eskander, and D. Schulz, “Charging Schedule for Load Peak Minimization on Large-Scale Electric Bus Depots,” *Applied Sciences*, vol. 9, no. 9, p. 1748, Apr. 2019, doi: 10.3390/app9091748.

[47] B. R. Ke, Y. H. Lin, H. Z. Chen, and S. C. Fang, “Battery charging and discharging scheduling with demand response for an electric bus public transportation system,” *Sustainable Energy Technologies and Assessments*, vol. 40, p. 100741, Aug. 2020, doi: 10.1016/J.SETA.2020.100741.

[48] Y. He, Z. Liu, and Z. Song, “Optimal charging scheduling and management for a fast-charging battery electric bus system,” *Transp Res E Logist Transp Rev.*, vol. 142, p. 102056, Oct. 2020, doi: 10.1016/J.TRE.2020.102056.

[49] J. A. Manzolli, J. P. F. Trovão, and C. Henggeler Antunes, “Electric bus coordinated charging strategy considering V2G and battery degradation,” *Energy*, vol. 254, p. 124252, Sep. 2022, doi: 10.1016/J.ENERGY.2022.124252.

[50] G.-J. Zhou, D.-F. Xie, X.-M. Zhao, and C. Lu, “Collaborative Optimization of Vehicle and Charging Scheduling for a Bus Fleet Mixed with Electric and Traditional Buses,” *IEEE Access*, vol. 8, pp. 8056–8072, 2020, doi: 10.1109/ACCESS.2020.2964391.

[51] A. Bagherinezhad, A. D. Palomino, B. Li, and M. Parvania, “Spatio-Temporal Electric Bus Charging Optimization with Transit Network Constraints,” *IEEE Trans Ind Appl.*, vol. 56, no. 5, pp. 5741–5749, Sep. 2020, doi: 10.1109/TIA.2020.2979132.

[52] H. Hu, B. Du, W. Liu, and P. Perez, “A joint optimisation model for charger locating and electric bus charging scheduling considering opportunity fast charging and uncertainties,” *Transp Res Part C Emerg Technol.*, vol. 141, p. 103732, Aug. 2022, doi: 10.1016/J.TRC.2022.103732.

[53] C. Yang, W. Lou, J. Yao, and S. Xie, “On Charging Scheduling Optimization for a Wirelessly Charged Electric Bus System,” *IEEE Transactions on Intelligent Transportation Systems*, vol. 19, no. 6, pp. 1814–1826, Jun. 2018, doi: 10.1109/TITS.2017.2740329.

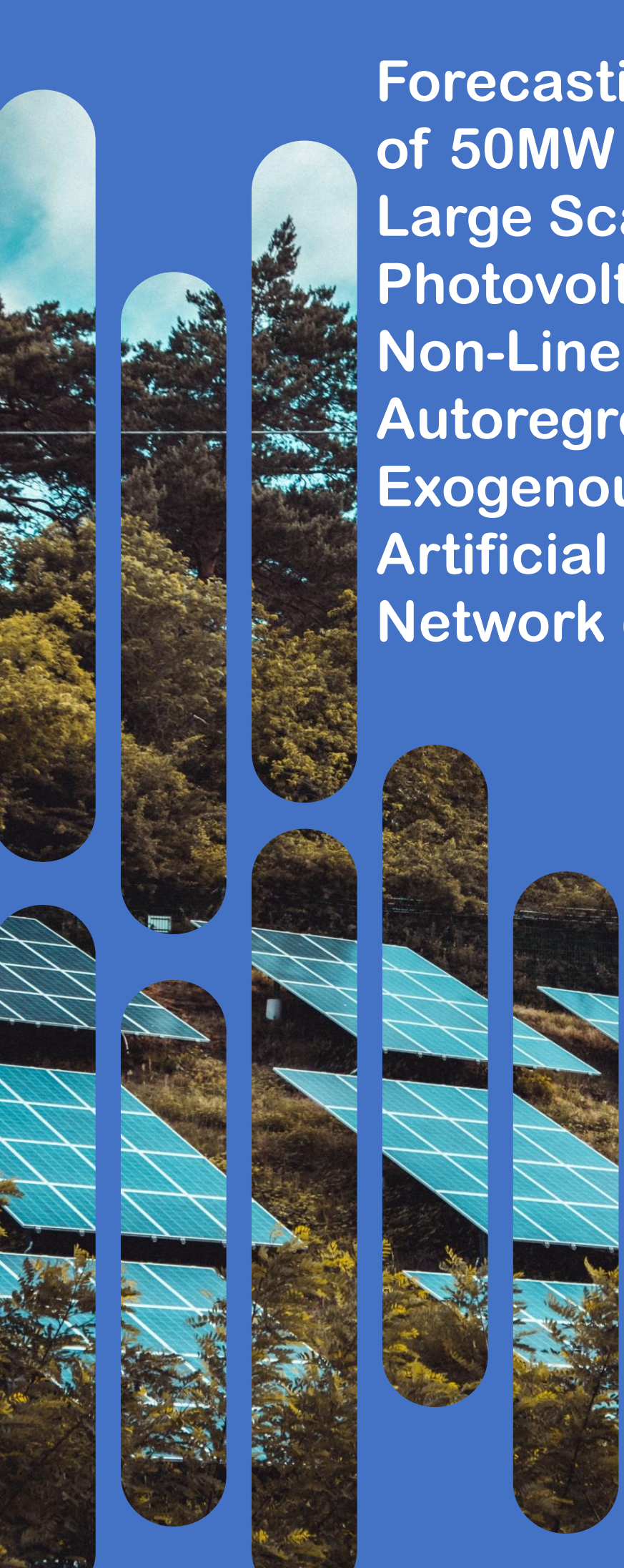
[54] Tenaga Nasional Berhad, “Enhanced Time-of-Use Tariff,” *Tenaga Nasional Berhad*, 2021. <https://www.mytnb.com.my/business/special-schemes/enhanced-time-of-use> (accessed Sep. 30, 2022).

[55] Energy Commission, “Energy Commission Annual Report 2016.”

## APPENDIX A

TABLE IV: BEB CHARGING SCHEDULING BASE ON FUZZY LOGIC MODEL

Priority	LP	MP	HP	MP	HP	MP	LP	LP	LP	MP	HP	MP	HP	MP	LP	LP	LP	MP	HP	MP
SoC	20	30	40	50	60	70	80	90	20	30	40	50	60	70	80	90	20	30	40	50
	CS1	CS1	CS1	CS1	CS2	CS2	CS1	CS2	CS2	CS2	CS3	CS3	CS3	CS4	CS3	CS3	CS4	CS4	CS4	CS4
Time	Bus 1	Bus 2	Bus 3	Bus 4	Bus 5	Bus 6	Bus 7	Bus 8	Bus 9	Bus 10	Bus 11	Bus 12	Bus 13	Bus 14	Bus 15	Bus 16	Bus 17	Bus 18	Bus 19	Bus 20
1	150								150											
2	150								150											
3	30								30											
4																				
5																				
6																				
7																				
8																				
9																				
10																				
11																				
12																				
13																				
14																				
15																				
16																				
17																				
18			150		150						150		150							
19			114		48						114		48							
20				150		150								150						150
21				81		15								15						114
22		150								150		150								150
23		147								147		81								81
24								132	99							99		150		

The background features a solid blue color. On the left side, there are several vertical panels of varying heights and widths, each with a rounded top and bottom. These panels contain images of a lush green forest and rows of blue solar panels. The text is positioned on the right side of the slide.

# Forecasting Generation of 50MW Gambang Large Scale Solar (LSS) Photovoltaic Plant Using Non-Linear Autoregressive Exogenous (NARX) – Artificial Neural Network (ANN)

02

# Forecasting Generation of 50MW Gambang Large Scale Solar (LSS) Photovoltaic Plant Using Non-Linear Autoregressive Exogenous (NARX) – Artificial Neural Network (ANN)

Muhammad Ikram bin Ahmad  
Zaidi

*Solar Research Institute*  
Universiti Teknologi MARA  
Shah Alam, Selangor  
muhammadikramzaidi@gmail.com

Assoc. Prof. Ir. Dr. Nofri Yenita binti  
Dahlan

*Solar Research Institute*  
Universiti Teknologi MARA  
Shah Alam, Selangor  
nofriyenita012@uitm.edu.my

Assoc. Prof. Ir. Ts. Dr. Ahmad Ihsan  
bin Mohd Yassin

*Microwave Research Institute*  
Universiti Teknologi MARA  
Shah Alam, Selangor  
ihsan.yassin@gmail.com

Dr. Rijalul Fahmi bin Mustapha

*Faculty of Electrical Engineering*  
Universiti Teknologi MARA  
Pasir Gudang, Johor  
rijalulfahmi@yahoo.com

**Abstract**—Malaysia is one of the countries that strongly dependent on the non-renewable energy such as coal to empower electricity industry and it cause decreasing in natural reserves and climate change. In Malaysia, solar energy is one of the renewable energies that plays a crucial role in reducing greenhouse gas emissions and addressing climate change. Geographical location shows that Malaysia is one of the best countries to use solar energy to empowering electricity for the country since it can collect high number of energies from Sun. Towards the planning of changing direction to the solar industry, many challenges had been addressed by Independent Power Producers (IPP) such as the uncertainty of output power from photovoltaic (PV) due to instability of weather conditions. This paper addressed the issues faced by the IPP and UiTM 50MW LSSPV in Gambang, Pahang has been used as case study. Forecasting power generation model of NARX-ANN has been developed. This paper can contribute to understand the Malaysia's solar industry.

**Keywords**—Artificial Neural Network, Photovoltaic, Large-Scale Solar, Mean Square Error (MSE), regression.

## I. INTRODUCTION

Nowadays, the number of demands for energy in Malaysia had been increased followed by the increasing number of populations. Currently, main energy generated from coal power plant. Since Malaysia is planning to shift energy towards renewable energy, accurate forecasting method become a crucial topic to be discussed among the power producers. Currently there are numerous types of renewable energy had been implemented in Malaysia. Solar energy, wind energy, and mini hydro energy are among the most developed and popular renewable energy, but all of it have the uncertainties issue related on energy produced. Solar energy become the most attractive among the renewable energy stakeholder since many policies have been initiated to minimise the greenhouse gas emission and contribute to less severity on climate change [1]. There are two types of technology for solar energy which are solar thermal energy and solar photovoltaic technology. The most developed technology is solar photovoltaic technology which converting energy from Sun into energy.

Currently Malaysia is rapidly developing solar energy industry where the cost of installation of PV system becomes more affordable. In Australia, government providing two incentives scheme aimed to reduce installation cost of small-scale PV system and large-scale solar PV system. The scheme named as Small-scale Renewable Energy Scheme (SRES) and Large-scale Renewable Energy Target (LRET) [2]. An initiative launched by the Indian government named as Solar Alliance in 2015 aimed to provide platform to increase the use of solar energy to meet energy demands [3]. In 2019, UK's government has legislated for net zero emission by 2050 due to scientific evidence [4].

Solar energy found to have great problem due to uncertainties in form of producing energy. The dependency on weather cost the power producer and grid operator to plan the production of solar energy injected into grid. The uncertainty of energy produced by solar energy potentially disrupting the power grid [5]. Therefore, it is one of the most important issues to tackle to ensure stable and efficient energy supplied into the electricity grid. It also can protect the power grid system from experiencing low supply that does not meet the demand energy. Power supply company requires to submit their energy generation planning for grid operators. Planning from grid operators is important as used to strategize the distribution of energy depending on the demand for the country [6].

Therefore, there are numerous methods had been introduced to cater the problem of instability of power produced by solar energy. Study in [7] discussed on various types of method used to predict solar power which are Back Propagation Neural Network (BPNN), Elman Neural Network (ENN), Nonlinear Autoregressive Neural Network with Exogenous Inputs (NARX-ANN), Random Forest (RF), and Support Vector Regression (SVR). From the study, it found that NARX-ANN is most superior over other technique due to its dynamic feedback mechanism. In [8], study said that main important part of forecasting is historical data to train the forecast model. The author used neuro-fuzzy based model to model short-term load forecasting. Another study in [9] discussed on different artificial intelligence method which is

StatCast-Solar. that generate short-term predictions of solar irradiance using the algorithm. In [10], there are numerous techniques had been analysed for the purpose of comparison. Results show that method of CNN-LSTM is better technique for forecasting compare with other methods.

This paper will focus on the forecasting model using NARX-ANN and comparison with the Multi Linear Regression technique using Microsoft Excel. This research will benefit the power producer and grid operator in term of planning the power dispatch, generated and reserve. It also used to determine and forecast the energy and revenue produced by solar power plant.

## II. METHODOLOGY

### A. Historical Data Acquisition and Filtration

A set of data is taken to be sampled for training purposes. Historical data is extremely important to training the model of forecasting before testing on real data. For this case study at UiTM 50MW LSSPV in Gambang, Pahang, 5 weather stations had been located suit with the area of the solar farm. Figure 2 shows the weather station used to collect raw data of weather at Gambang LSS Farm. The data will be recorded every minute and uploaded to Google Drive for processing purposes. For this paper, the data used as input from the 1<sup>st</sup> of August 2020 until end of July 2021.



Figure 2: Weather station located at Gambang LSS Farm

The data collected from the weather station will be considered as input variable data. The input variable data includes ambient temperature, wind speed, PV module temperature, global irradiance on module plane, total global horizontal irradiance, total slope irradiation, and total horizontal irradiation while the output variable is AC output power collected from the iSolarCloud system which recorded every 5 minutes. The numerous sets of data could include certain errors where it can interrupt the efficacy of forecasting model. Therefore, preprocessing data is extremely necessary to minimize the error of the input variable for forecasting model. The data also will undergo mathematical analysis to obtain an average value for every 30 minutes. The process is important since the model is developed using 30 minutes of time interval for one year. Before developing the forecasting model, each input variables regression was analyzed to determine the relationship between the input variables and output variable. Figures 3, 4, 5, 6, 7, 8 and 9 show the graph of output variables and each input variable.

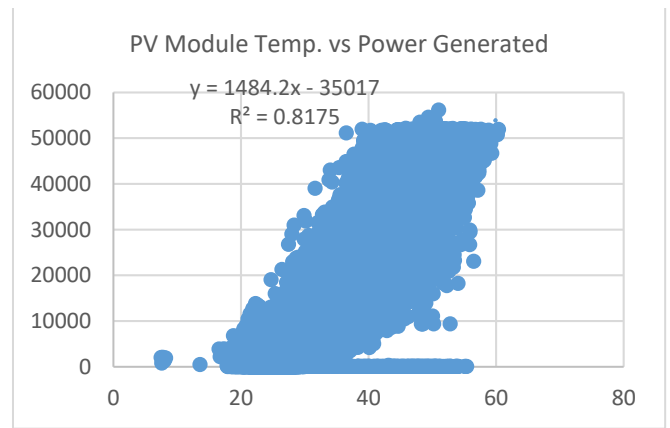


Figure 3: Graph of PV Module Temperature and Output Power Generated

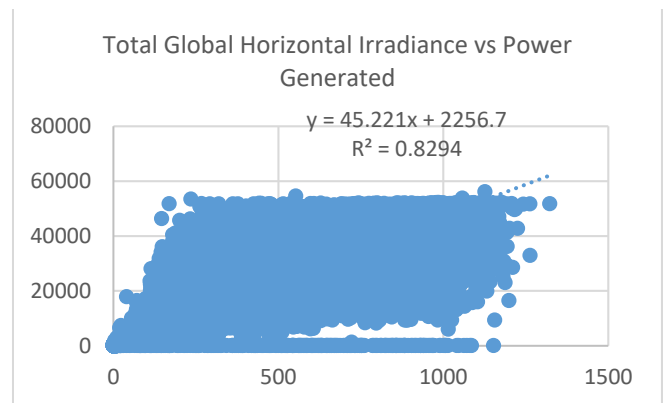


Figure 4: Graph of Total Global Horizontal Irradiance and Output Power Generated

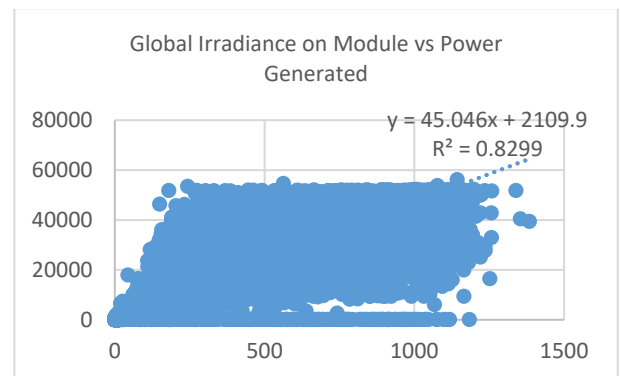


Figure 5: Graph of Global Irradiance on Module and Output Power Generated

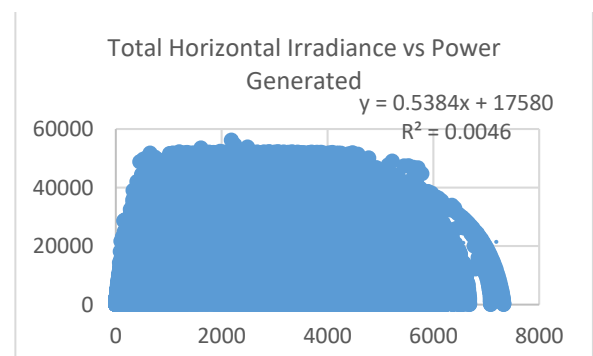




Figure 6: Graph of Total Horizontal Irradiance and Output Power Generated

Total Horizontal Irradiance	0.0046
Ambient Temperature	0.4918
Total Slope Irradiation	0.0045
Wind Speed	0.2100

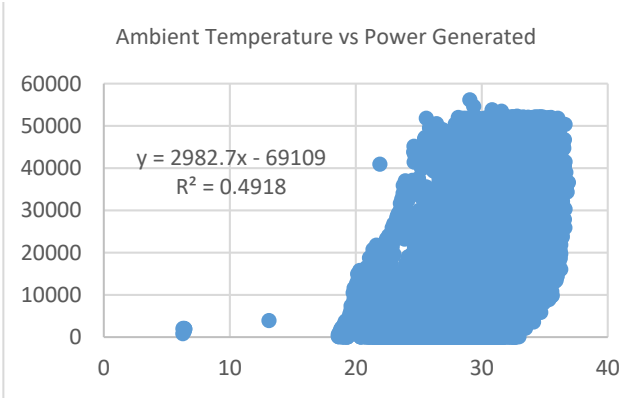


Figure 7: Graph of Ambient Temperature and Output Power Generated

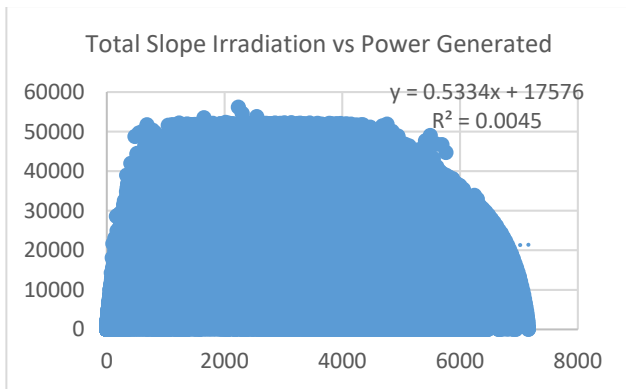


Figure 8: Graph of Total Slope Irradiation and Output Power Generated

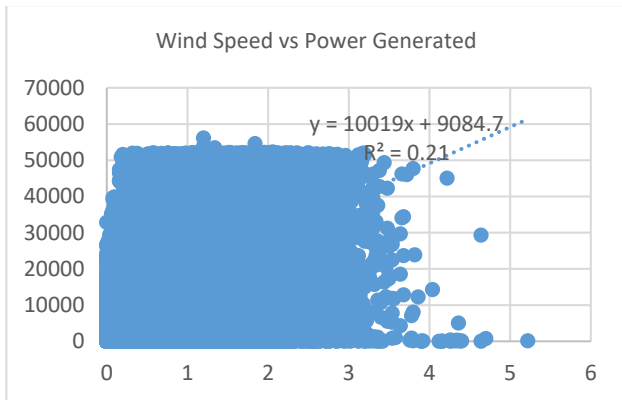


Figure 9: Graph of Wind Speed and Output Power Generated

TABLE 1: REGRESSION BETWEEN INPUT VARIABLE AND OUTPUT VARIABLE

Input Variable	Regression, $R^2$
PV Module Temperature	0.8175
Total Global Horizontal Irradiation	0.8294
Global Irradiance on Module	0.8299

7 input variables had been selected as input variables in developing forecasting model.

### B. Design of NARX-ANN Model

For this paper, NARX-ANN will be developed using MATLAB. Initially the NARX-ANN model will experience training process, the training input and output variables will be defined and normalized to a value between -1 and 1. These data need to be normalized to a common scale to increase rate of convergence since these data have different range of values. Once the data normalization has completed, the type of back propagation algorithm will be set for the training process. Lavenberg-Marquardt algorithm (trainlm) is chosen for the training process since it is proven to have faster rate of convergence and widely used in many forecasting studies. The 'trainlm' algorithm will update the NARX-ANN weight and bias at every epoch and its performance will be evaluated based on the MSE value. The number of input lags or delays is 10 and the number of output lag is 12.

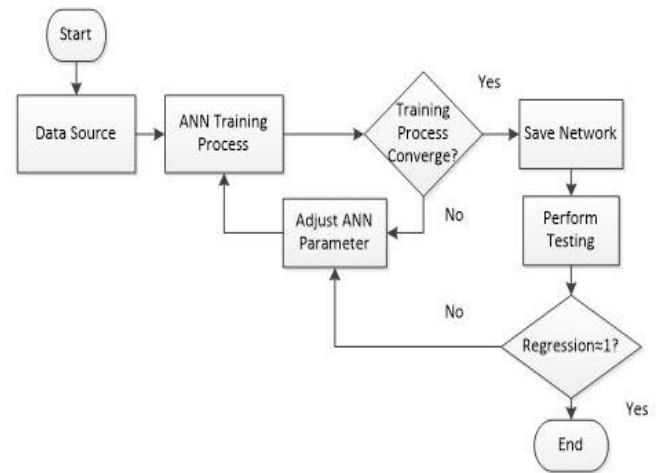


Figure 10: Flowchart of NARX-ANN training and testing process

ANN black box can be configured by adjusting the ANN learning rate, momentum rate and the number of neurons in hidden layer. The process of determining the correct values for these parameters to produce precise forecasting model will be time consuming as it is a try and error process. The 'trainlm' algorithm and adjusting the NARX-ANN parameters do not guarantee the optimum solution can be found easily since the NARX-ANN method is well known to have its solution trap at the local minima. The trained NARX-ANN data will be denormalized and saved at the end of the training process.

For the testing process, the testing input and output variables are first called out. These data will undergo the

same process as in during training process where it will be normalized and denormalized at the end of the program. During testing, the data will undergo post processing process in which it will output the regression value and linear equation. The AC forecast data will be evaluated as having a strong regression if the testing process has a value approximately approaching to 1.

In this research, series-parallel architecture will be implemented since the availability of true past values of time-series as well as it has higher precision compares with parallel architecture. Based on Figure 11 below, series-parallel model uses the true values as input feedforward network rather than parallel model which use prediction value as input feedforward network.

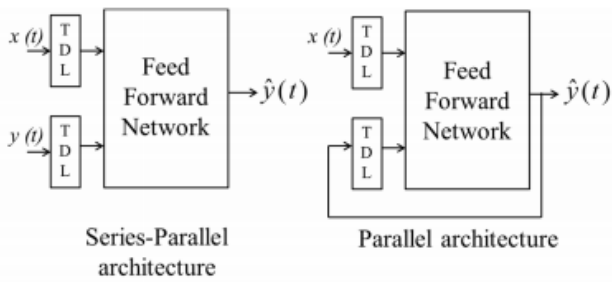


Figure 11: Design architecture of NARX-ANN model

### III. RESULTS

The analysis comprises of inspection on regression of each input variables with the output variables as well as the process of preprocessing raw set of data. Total set of data are 52,058 with 30 minutes of time interval. The results obtained from the forecasting model will be compare with the Multi Linear Regression method which using Microsoft Excel. The performance is evaluated based on the regression value. Less value in regression shows a weak correlation between the input and output variables. Table 2 below shows the value of multiple linear regression for 7 input variables which is 0.9449 and the value of  $R^2$  is 0.8928.

TABLE 2: REGRESSION STATISTIC OF MLR

<i>Regression Statistics</i>	
Multiple R	0.944907898
R Square	0.892850936
Adjusted R Square	0.892836525
Standard Error	4760.679889
Observations	52058

Figure 12 below shows the value of regression for testing which is at 0.99451 and the value of  $R^2$  is 0.98905. Based on these two results obtained, it shows that NARX-ANN have better performance compare with MLR.

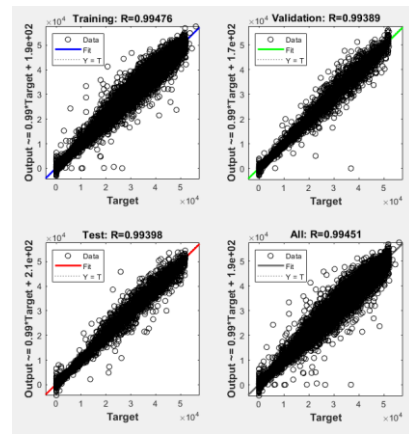


Figure 12: Regression performance of NARX-ANN

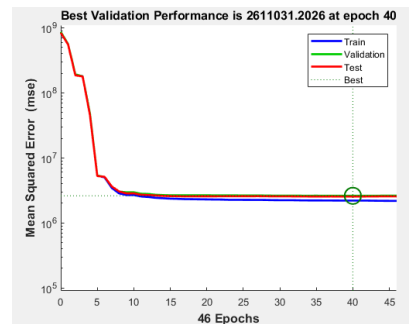


Figure 13: MSE performance of NARX-ANN

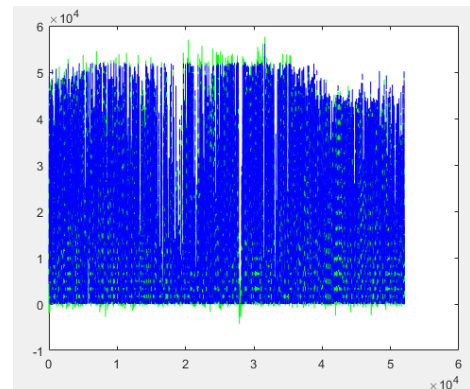


Figure 14: Graph of predicted output and actual output

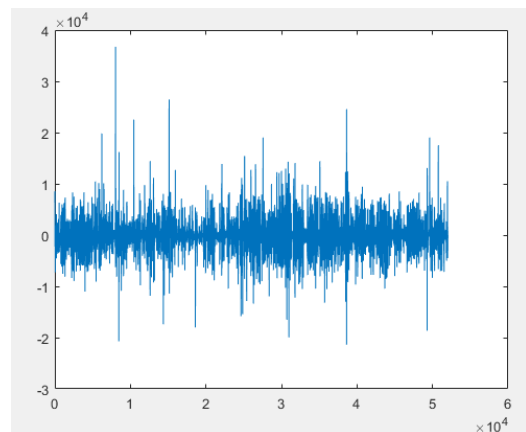


Figure 15: Graph of residual value of actual and predicted value

Figure 14 shows the graph of predicted output (green line) and the actual output (blue line). The difference of both output is called residual as shown in Figure 15. The efficiency of the forecasting model is greater if the residual value lesser.

#### IV. CONCLUSIONS

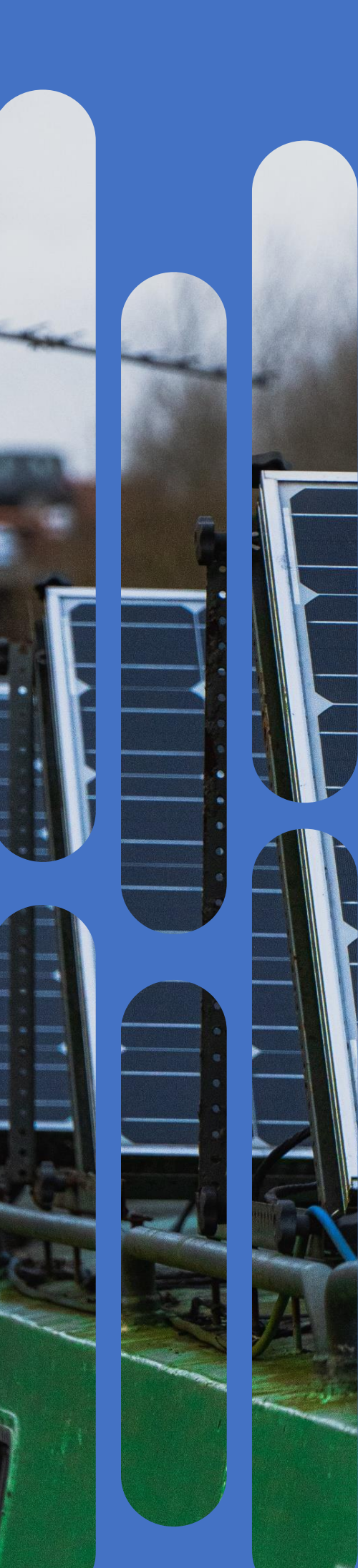
In this paper, NARX-ANN model is being developed to increase the performance of forecasting model compared to MLR. A total 52,058 sets of data are used for training and testing of both method of prediction. From the results obtained, it shows that NARX-ANN model has better performance compared to MLR model in term of regression and MSE value.

#### ACKNOWLEDGMENT

The authors would like to thank Univesiti Teknologi Mara (UiTM) and UiTM Energy Facility Sdn. Bhd. (UEFB) for providing data used in this study. This study is supported by the Ministry of Education Malaysia through the research grant 600-RMI/FRGS 5/3(316/2019).

#### REFERENCES

- [1] M. Vaka, R. Walvekar, A. Khaliq, and M. Khalid, "A review on Malaysia's solar energy pathway towards carbon-neutral Malaysia beyond Covid'19 pandemic," *J. Clean. Prod.*, no. July, 2020.
- [2] S. Rahman *et al.*, "A framework to assess voltage stability of power grids with high penetration of solar PV systems," *Int. J. Electr. Power Energy Syst.*, vol. 139, no. November 2021, 2022, doi: 10.1016/j.ijepes.2021.107815.
- [3] S. Jain, T. Sharma, and A. K. Gupta, "End-of-life management of solar PV waste in India: Situation analysis and proposed policy framework," *Renew. Sustain. Energy Rev.*, vol. 153, no. July 2021, p. 111774, 2022, doi: 10.1016/j.rser.2021.111774.
- [4] N. Stognief, P. Walk, and P.-Y. Oei, *Political economy of climate and energy policies in the United Kingdom*. 2022.
- [5] Y. R. O., J. J., A. K. Chakraborty, and J. M. Guerrero, "Stochastic optimal power flow in islanded DC microgrids with correlated load and solar PV uncertainties," *Appl. Energy*, vol. 307, no. November 2021, p. 118090, 2022, doi: 10.1016/j.apenergy.2021.118090.
- [6] H. H. H. Aly, "A proposed intelligent short-term load forecasting hybrid models of ANN, WNN and KF based on clustering techniques for smart grid," *Electr. Power Syst. Res.*, vol. 182, no. July 2019, p. 106191, 2020, doi: 10.1016/j.epsr.2019.106191.
- [7] D. Su, E. Batzelis, and B. Pal, "Machine Learning Algorithms in Forecasting of Photovoltaic Power Generation," *SEST 2019 - 2nd Int. Conf. Smart Energy Syst. Technol.*, 2019, doi: 10.1109/SEST.2019.8849106.
- [8] M. Malekizadeh, H. Karami, M. Karimi, A. Moshari, and M. J. Sanjari, "Short-term load forecast using ensemble neuro-fuzzy model," *Energy*, vol. 196, p. 117127, 2020, doi: 10.1016/j.energy.2020.117127.
- [9] S. E. Haupt *et al.*, "Combining Physical Modeling with Artificial Intelligence for Solar Power Forecasting," *Conf. Rec. IEEE Photovolt. Spec. Conf.*, vol. 2020-June, pp. 2051–2053, 2020, doi: 10.1109/PVSC45281.2020.9300434
- [10] Alam, A. M., Nahid-Al-Masood, Iqbal Asif Razee, M., & Zunaed, M. (2021). Solar PV power forecasting using traditional methods and machine learning techniques. *2021 IEEE Kansas Power and Energy Conference, KPEC 2021*. <https://doi.org/10.1109/KPEC51835.2021.9446199>



# Designing a 2755 kW Photovoltaic System for Grid Integration for Empowering Renewable Energy

03

# Designing a 2755 kW Photovoltaic System for Grid Integration for Empowering Renewable Energy

Nur Fadhilah Jamaludin  
School of Electrical Engineering  
College of Engineering  
Universiti Teknologi MARA Shah  
Alam  
Selangor, Malaysia  
nurfadhilah2765@uitm.edu.my

Nofri Yenita Dahlan  
Solar Research Institute (SRI)  
Universiti Teknologi MARA Shah  
Alam  
Selangor, Malaysia  
nofriyenita012@uitm.edu.my

**Abstract**— Nowadays, the development of different Large-Scale Solar Photovoltaic (LSSPV) configurations with different capacity levels using various software tools to analyse the performance of the solar plant has become an interest in researchers and solar providers. This increase is attributed to the system's dependence on solar radiation, which serves as an abundant and environmentally sustainable energy source. However, the uncertain characteristics of the LSSPV significantly affect the efficiency of the solar system components, especially the inverter and transformer that supply power to the grid system. Therefore, to overcome this problem, it is crucial to develop the calibrated model of the LSSPV to ensure accurate and robust pre-analyses are done before replacing the malfunctioning components in the plant. In this paper, the calibrated model of a 2775 kW LSSPV grid connected based on UiTM Solar Park 1 at Gambang, Pahang, is used as a case study. The calibrated model is designed using MATLAB and Simulink, with power, AC and DC voltage, and power tolerances measured and analysed based on the Malaysia Energy Commission Standard.

**Keywords**—Large-Scale Solar Photovoltaic, Matrix Laboratory, Maximum Power Point Tracking, Perturb and Observe, Standard Test Condition, Distributed Combiner Box

## I. INTRODUCTION

Large Scale Solar Photovoltaic (LSSPV) is a solar PV plant with a minimum installed power rating of 1 MW<sub>AC</sub> up to a maximum of 50 MW<sub>AC</sub> connected to either a Transmission Network or Distribution Network in Peninsular Malaysia, Sabah, or Labuan as approved by the Malaysia Energy Commission [1],[2]. The awareness of the government to reduce carbon dioxide emissions along with the depletion of non-renewable resources became the catalyst for the change in energy resources from non-renewable energy resources such as oil, coal, and fuel to renewable energy resources such as wind, biomass, and solar.

The location of Malaysia, which is strategically located close to the equator, provides a benefit as a potential country in Asia for LSS applications. Monthly solar irradiation for Malaysia is calculable at 400–600 MJ/ m<sup>2</sup> [3]. The irradiation is higher throughout the North-East monsoon once the wind direction returns from central Asia to the South China Sea through Malaysia and eventually to Australia between November and March. Lower irradiation occurs during the South-West monsoon once the wind direction changes and yields from Australia and moves towards Sumatera Island before reaching the Straits of Malacca between May and September [3]. Generally, Malaysia encompasses a high potential for solar generation considering it is hot and humid

all year round, with the calculable potential for solar generation reaching up to 6500 MW [4]-[5].

Previously, various models of LSSPV using different software tools to analyse the performance of LSSPV have been studied. The calibration of a 1 MW PV system at PV array, inverter, and transformer levels based on standard irradiance and temperature values of 1000 kW/m<sup>2</sup> and 25 °C using MATLAB Simulink has been studied in [6]. The 3180 of the TSM-315pa14a PV module can retain the voltage across the boost converter at 1500 V and match the transformer value to the grid with varied irradiance and temperature. Additionally, another study in [7] investigated the performance of the solar model in three different regions in Turkey, which are Izmir, Ankara, and Istanbul. The 35,460 units of PV polycrystalline module with 250 W at a 30° tilt solar panel angle and 391 units of GW20K-DTL inverter provide efficiency up to 98.4%. The PV module based on the monocrystalline type has been proposed in [8] and [9]. In [8], the 1428 unit of Sharp PV monocrystalline module of 175Wp with the titled angle of 10 ° is used to design a 250 kW grid-connected solar plant in Iraq. The 10 units of SMA solar inverters with the 400 V inverter output produce total annual energy up to 346692 kWh. Meanwhile, in [9], the 704 units of Sunmodule SW 285 monocrystalline modules with a titled angle of 25 ° were used to design a 200 kW solar plant in Dubai. The 3 units of Sungrow SG60KTL with a capacity of 60 kVA, produce a total annual energy of 352.6 MWh. The studies in [6],[7], [8] and [9] provide valuable insights into the performance of PV systems. But the calibrations in [6],[7], [8] and [9] do not comply with the Malaysia Grid Code [1],[2].

The studies in [10] and [11] have examined the potential of LSSPV systems in Sabah. In the study [10], a total solar capacity of 5 MW was achieved using 15,625 units of multi-crystalline PV modules provided by JA Solar. Furthermore, in [11], a total solar capacity of 48 MW was achieved using 24 units of Huawei WECC dynamic PV inverters. However, these studies provide limited discussion on the specific parameters and specifications of the inverters and transformers used in the design of the LSSPV model.

It is crucial for the PV system developers, installers, and operators to ensure the LSSPV design is in compliance with the specific requirements outlined in the Malaysia Grid Code. This compliance prevents potential grid disturbances, ensures safe operation, and maintains the overall integrity of the power supply as the PV systems are in alignment with the required technical standards and specifications. Therefore, it is important to develop a calibrated model of the LSSPV to avoid suboptimal design and false analysis of the LSSPV performance.

In this research, a 2775 kW LSSPV system is designed utilising a PV polycrystalline module from JinKO Solar and the Sungrow SG2500 MW solar inverter. The design and calibration processes of an LSSPV involve the utilisation of MATLAB and Simulink software. The performance of the simulation model of an LSSPV at the DC and AC sides is calibrated based on Malaysian Standard in [12], [13], [14] and [15].

## II. OVERVIEW OF THE 2775 kW LSSPV

The 50 MW UiTM Solar Park 1 located in Gambang, Pahang, was used as a case study. It consists of 22 blocks, with each block consisting of 88 units of sub-inverters and 22 units of transformers. Each block has the capability to generate up to 2775 MW. However, in this paper, one block of the PV system in UiTM Solar Park 1 is analysed as shown in Figure 1.

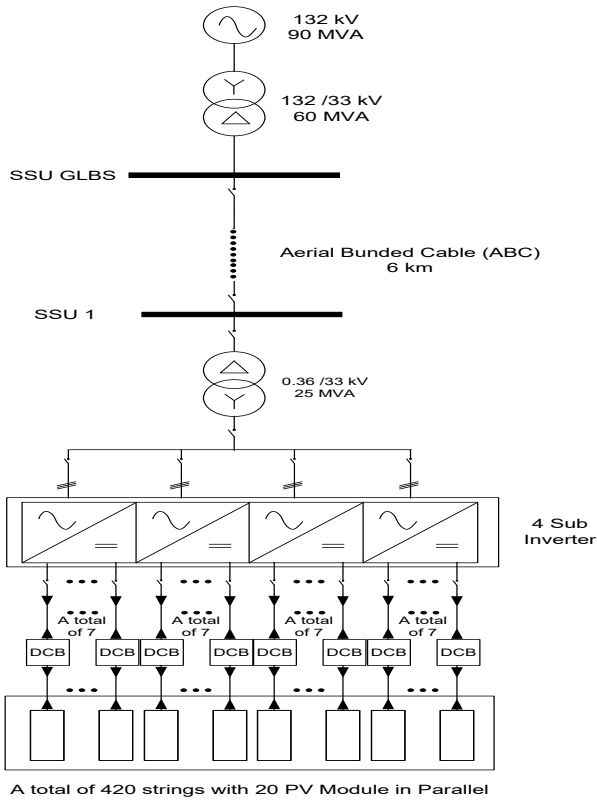


Fig. 1. The single line diagram of 2775 kW LSSPV connected to the grid system.

Figure 1 shows the single line diagram of a 2775 kW LSSPV connected to the grid system. Generally, it can be divided into DC and AC sides. On the DC side, there are 7 smart PV DC Combiner Boxes (DCB) with 16 strings in parallel, consisting of 20 solar PV modules connected in series. This connection is crucial to ensuring the numerous outputs from the PV module feed each sub-inverter efficiently. On the AC side, it consists of 4 sub-unit inverters and 1 unit of transformer. The 7 smart PV DCBs with 16 strings in parallel connected to each sub-unit inverter construct a total of 420 strings in parallel to the PV array. The output from the inverter is then stepped up through a 360 kV/33 kV transformer before the power is delivered to the grid connection point.

## III. THE 2775 kW LSSPV DESIGN COMPONENT

The single-line diagram of the 2775 kW LSSPV used in this research is shown in Figure 2.

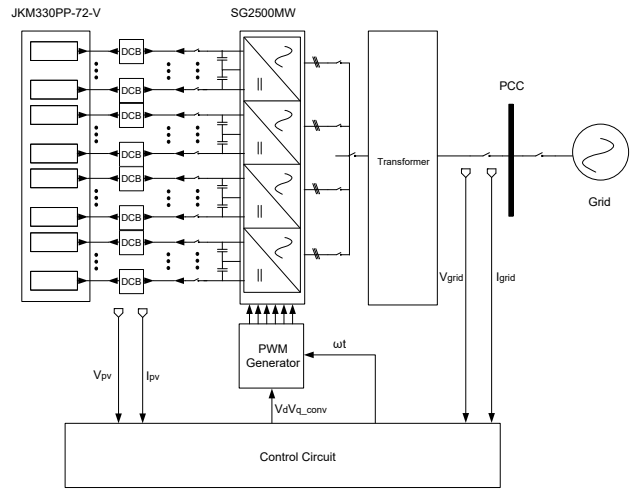


Fig. 2. The 2775 kW LSSPV component and control circuit.

It is shown that the LSSPV system consists of a PV array, DC filter, three-phase inverter, step-up transformer, and grid interconnection point. The PV array is connected to the DC filter before the DC output is converted to the AC output. The output from the DC filter will then be converted to the AC output using a three-phase inverter before being stepped up to a 33 kV transformer. The output from the transformer will then be delivered to the grid system. The details explanation on the parameter, configuration and control system of the component used are explained in the section below.

### A. Jinko Solar PV Module

The JKM330PP-72-V PV Panel from Jinko Solar Co., Ltd. [16] is used as a PV module array in this research. The 72 poly-crystalline cells of solar modules can generate power up to 330 Wp. The PV array specification for JKM330PP-72-V is shown in Table I.

TABLE I. THE SYSTEM SPECIFICATION FOR THE 330W OF JKM330PP-72-V

No.	Parameter	Rating
1	Maximum Power Voltage ( $V_{mp}$ )	37.8 V
2	Maximum Power Current ( $I_{mp}$ )	8.74 A
3	Open-Circuit Voltage ( $V_{oc}$ )	46.9 V
4	Short-Circuit Current ( $I_{sc}$ )	9.14 A
5	Module Efficiency STC (%)	46.9 V
6	Operating Temperature ( $^{\circ}C$ )	$-40^{\circ}C \sim +85^{\circ}C$

In the first stage of PV system design, the PV array is constructed by determining the total number of series connections for the PV modules, ( $N_s$ ) and the total number of parallel strings, ( $N_p$ ). In this research, 420 parallel strings with 20 PV modules in series are used to build the PV array. The expected PV array voltage and power obtained under Standard Test Conditions (STC) for solar irradiance of  $1000 \text{ W/m}^2$  and a temperature of  $25^{\circ}C$  can be calculated using eq (1) and (2).

$$N_s = \frac{V_{pv}}{V_{mp}} \quad (1)$$

$$20 = \frac{V_{pv}}{37.8}$$

$$V_{pv} = 756 \text{ V}$$

$$N_p = \frac{P_{max}}{\frac{V_{pv}}{I_{mp}}} \quad (2)$$

$$420 = \frac{P_{max}}{\frac{756}{8.74}}$$

$$P_{max} = 2775 \text{ kW}$$

From eq (1) and (2) with respect to the data specification in Table I, it shows that the expected voltage and power of the JKM330PP-72-V with 420 parallel strings and 20 PV modules in series are 720 V and 2775 kW at STC level.

### B. Sungrow Medium Voltage Turnkey Station Inverter

In this research, the DC output from the JKM330PP-72-V will be converted to the AC output using the SG2500-MV Inverter from Sungrow Power Supply Co.[17]. The MV turnkey station is a comprehensive and fully integrated solution that is specifically designed to operate in conjunction with the SG2500-MV inverter. It encompasses a range of essential components such 4-unit sub inverters integrated with one Maximum Power Point Tracking (MPPT), a transformer, switchgear, protection devices, monitoring systems and control system as shown in Figure 3.

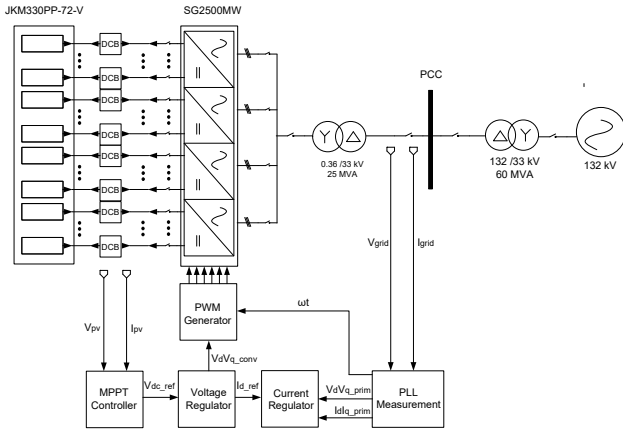


Fig. 3. The SG2500 MW inverter with MPPT controller, PQ measurement and switching control.

These elements are combined to ensure the effective and efficient functioning of the voltage generation from the PV array at the desired voltage level for grid connection. To ensure the inverter extracts the maximum available power from the PV array under varying irradiance or temperature, the MPPT based on the Perturb and Observe (P&O) algorithm [18] is implemented as shown in Figure 4.

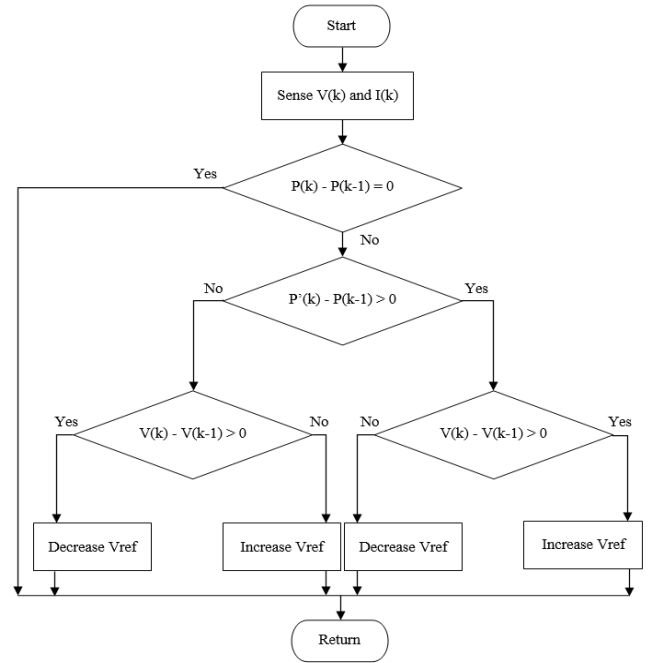


Fig. 4. The flow diagram of the Perturb and Observe (P&O) algorithm.

The MPPT system continuously measures the input PV array DC voltage,  $V(k)$ , and current,  $I(k)$ , to calculate the measured output power,  $P(k)$ , of the PV panel at the current duty cycle. The reference power output,  $P(k-1)$ , obtained from previous iterations will be compared with  $P(k)$ . If  $P(k) - P(k-1)$  is equal to zero, then the algorithm will maintain the duty cycle since the PV system has reached the MPPT. If  $P(k) - P(k-1)$  is larger than zero, the  $V_{ref}$  will decrease by a small step size to move the voltage towards the MPPT since the power has increased with the perturbation. Meanwhile, if the  $P(k) - P(k-1)$  is smaller than zero, the  $V_{ref}$  will increase by a small step size to move the voltage towards the MPPT since the power has decreased with the perturbation.

The iteration of the P&O algorithm will continuously measure the input PV array voltage and current, calculate the output power, and adjust its operating voltage within the MPPT range. To track the MPP of the PV array, the reference voltage,  $V_{ref}$  is modified within the voltage range of 520 V to 850 V. This adjustment allows the algorithm to automatically vary the  $V_{dc\_ref}$  signal of the inverter to ensure optimal operation and power extraction from the PV array.

The  $V_{dc\_ref}$  generated from the MPPT will be compared with the  $V_{dc}$  measured in the voltage regulator to determine the active current reference,  $I_{d\_ref}$ . In addition, the three-phase grid voltage,  $V_{grid}$ , and current,  $I_{grid}$ , are measured and transformed into an active and reactive voltage,  $V_d V_q\_prim$  and current,  $I_d I_q\_prim$ . Both outputs from the voltage regulator and PLL feed to the current regulator to determine the required reference voltages for the inverter,  $V_d V_q\_conv$ . Then, the PWM generator will inject the signal to the IGBT to control the flow of current in the inverter circuit and hence convert the DC output to AC voltage based on the reference generation voltage,  $U_{ref}$ . The IGBT will control the switching of the inverter to ensure the inverter generates a desired output voltage waveform within the AC voltage range. The SG2500 MW inverter specifications are shown in Table II.

TABLE II. THE SYSTEM SPECIFICATIONS FOR THE SUNGROW SG2500 MW SOLAR INVERTER

No.	Inverter	Parameter	Rating
1	DC	Maximum PV input voltage	1000 V
2		Minimum PV input voltage	520 / 540 V
3		MPP voltage range for nominal power	520 - 850 V
6	AC	AC output power	2520 kVA at 50 °C
7		Maximum inverter output current	4444 A
8		AC voltage range	6 - 40.5 kV
9		Adjustable power factor	> 0.99 / 0.8 leading - 0.8 lagging

From Table II, it is shown that the inverter can produce the AC voltage output within the range of 6 kV up to 40.5 kV to ensure compatibility with the AC grid and compliance with applicable harmonic distortion limits standards as stated in Engineering Recommendation ER G5/4-1[19]. As depicted in Figure 3, the Dy11 transformer integrated with the inverter improves the reliability and efficiency of the power transmission from the inverter to the grid. The transformer enables efficient power transfer and minimises voltage mismatches or imbalances by stepping up or stepping down the output voltage of the inverter to match the grid voltage requirement. Table III shows the detailed specification of the transformer integrated with the inverter.

TABLE III. THE DELTA-WYE TRANSFORMER SPECIFICATION

No.	Parameter	Rating
1	Rated Power	2500 kVA
2	Primary Voltage	33 ± 2*2.5 % kV
3	Secondary Voltage	0.36 kV
4	Impedance Voltage	6.0 %

Table III indicates that at rated power of 2500 kVA, the 33 kV delta connection at the primary transformer connected to the grid side to handle higher voltage levels varies from 31.35 kV to 34.65 kV with a voltage tolerance of ±2\*2.5%. Meanwhile, the inverter will be connected to the 0.36 kV wye connection at the secondary transformer with a fixed voltage rating. It is important to ensure the plant does not contribute zero-sequence current to the grid system during fault occurrences [19].

### C. 132 kV Grid Connected Transformer

The YNd1 transformer from Changzhou XD Transformer [20] is used at the transmission level as shown in Figure 2. The transformer used to step up the voltage from 33 kV to 132 kV to facilitate the connection of the PV system to the high-voltage grid. The integration of 0.36/33 kV transformers and the 132/33 kV transformer enables efficient transmission and distribution of the generated electricity from the PV system to feed power into the electrical grid at a higher voltage level. Table IV shows the detailed specification of the 132/33 kV transformer.

TABLE IV. THE SYSTEM SPECIFICATIONS FOR THE 132/33 kV TRANSFORMER

No.	Parameter	Rating
1	Transformer Rating	60 MVA
2	Upper limit on controlled voltage, Vmax	145.23 kV
3	Lower limit on controlled voltage, Vmin	112.16 kV

## IV. LSSPV CALIBRATED SIMULATION MODEL IMPLEMENTATION IN MATLAB SIMULINK

In this research, the design model based on MATLAB and Simulink is used as shown in Figure 5.

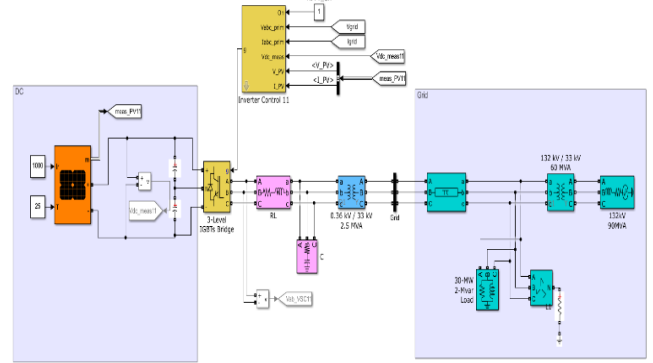


Fig. 5. The 2775 kW design model using MATLAB and Simulink.

Using Figure 5, the PV array voltage, power and Total Harmonic Distortion (THD) at a nominal temperature of 25 °C were simulated and analyzed for three distinct irradiance levels such as STC, moderate, and low. The 1000 W/m<sup>2</sup> irradiance values indicate the STC irradiance level. It is used as the baseline for PV module testing and comparison to assess the performance of PV modules under ideal temperature and irradiance levels. To analyse the performance of the PV module at moderate irradiance levels during normal daylight conditions, the 600 W/m<sup>2</sup> and 800 W/m<sup>2</sup> irradiance values are implemented. Meanwhile, the 200 W/m<sup>2</sup> and 400 W/m<sup>2</sup> irradiance values are used to analyse the PV module performance at the low irradiance level during cloudy or partially shaded environments.

### A. PV Array Voltage and Power at 25 °C under Varying Irradiance Conditions

Figure 1 shows the actual PV array voltage, V<sub>pv</sub> and power, P<sub>pv</sub> values vary as the irradiance value varies from 200 W/m<sup>2</sup> to 1000 W/m<sup>2</sup> at a constant temperature of 25 °C.

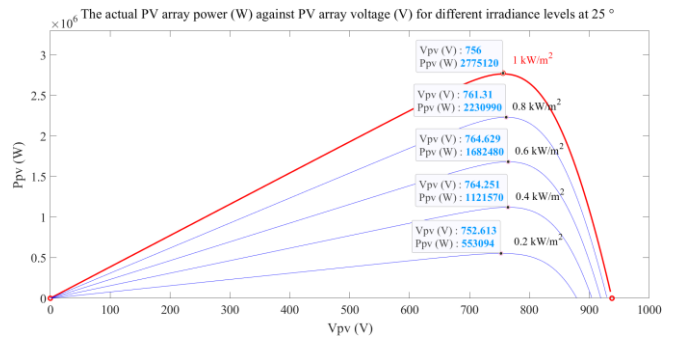
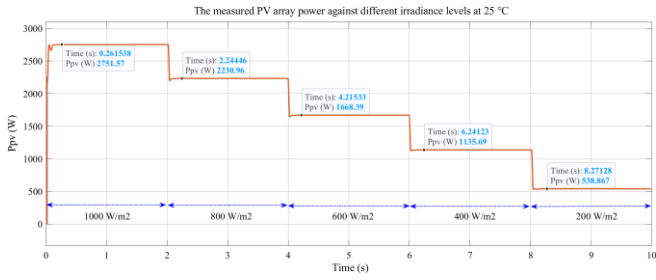


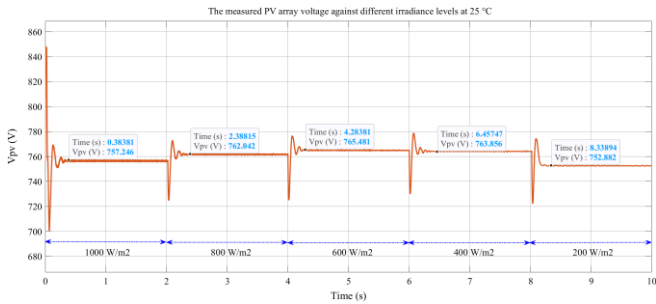
Fig. 6. The actual PV array voltage and power for different irradiance levels at 25 °C



The actual PV array voltage,  $V_{pv}$  and power,  $P_{pv}$  values at the STC irradiance level are 756 V and 2775120 W, which approximate the calculated PV array voltage and power values in eq. (1) and (2). Figure 6 shows the measured PV array voltage and power obtained through the simulation.



(a)



(b)

Fig. 7. The measured output waveform of a PV array for different irradiance levels at 25 °C (a) PV array voltage and (b) PV array power.

The comparison between actual and measured PV array voltage and power based on IEC 61727 [12] and the manufacture standard at a constant temperature of 25 °C in Figures 5 and 6 has also been analysed in Table IV.

TABLE V. COMPARISON BETWEEN ACTUAL AND MEASURED PV ARRAY VOLTAGE AND POWER BASED ON IEC 61727 AND THE MANUFACTURE STANDARD

Irradiance (W/m <sup>2</sup> )	PV Array Voltage (V)			PV Array Power (kW)		
	Actual Value (V)	Measured Value (V)	Voltage Tolerance ( $\pm 1\%$ )	Actual Value (kW)	Measured Value (kW)	Power Tolerance ( $\pm 3\%$ )
200	752.613	752.882	-0.035	553.094	538.867	2.572
400	764.251	763.856	0.051	1121.570	1135.69	-0.012
600	764.629	765.481	-0.111	1682.480	1668.39	0.008
800	761.31	762.042	-0.09	2230.990	2230.96	0.001
1000	756	757.246	-0.164	2775.120	2751.57	0.848

Table III shows that the tolerance of the PV array voltage at varying irradiance levels is below  $\pm 1\%$  as required in the IEC 61727 standard. Meanwhile, the PV array power is below the power tolerance of  $\pm 3\%$  as specified in the JKM330PP-72-V datasheet at varying irradiance levels.

### B. Grid Connection Point Voltage and Power At 25 °C Under Varying Irradiance Level

The calibration of the LSSPV on the AC side has also been analysed. Figure 8 shows the measured DC voltage,  $V_{dc}$ , is aligned with the reference DC voltage,  $V_{dc\_ref}$ , by maintaining a voltage across the DC link at 756 V.

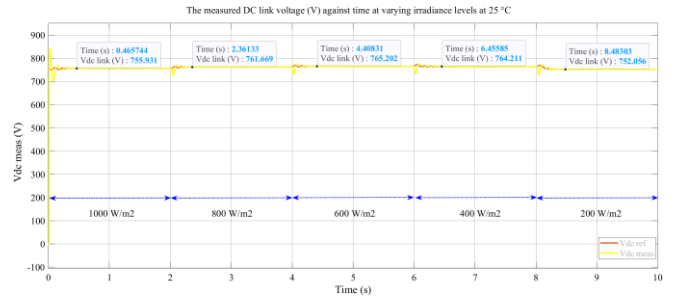


Fig. 8. The DC link voltage measure across the DC capacitor at varying irradiance level values at 25 °C.

The alignment of this DC voltage indicates the synchronization of the output from the transformer with the grid, as shown in Figures (8) and (9).

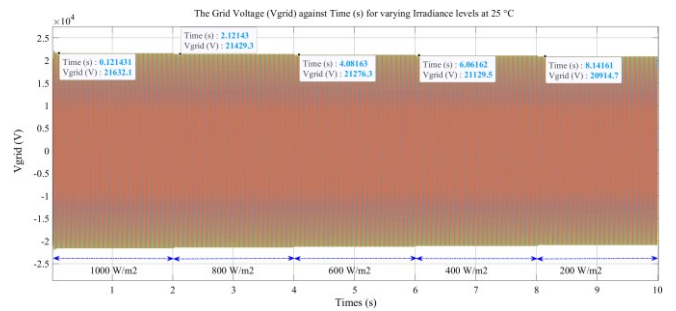


Fig. 9. The three-phase voltage at PCC at varying irradiance level values at 25 °C.

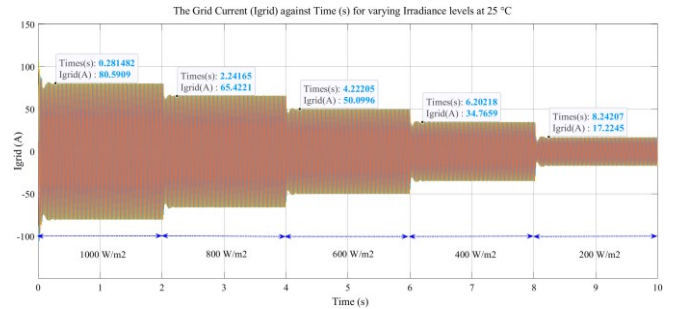
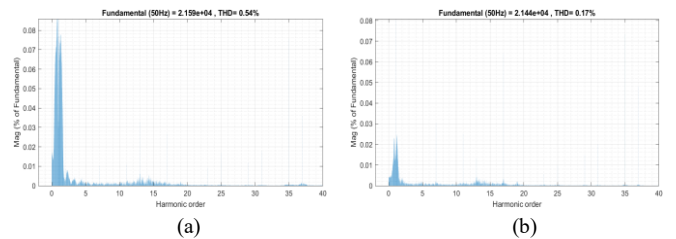


Fig. 10. The three-phase current ( $I_{ppc}$ ) at PCC against Time (s) for varying irradiance levels at 25 °C.

The alignment and synchronization of the system can be visually observed in Figure 10, where the output voltage and power waveform display a symmetrical and balanced condition with varying irradiation levels. Additionally, the alignment and synchronization of the transformer with the grid can be assessed by examining the Total Harmonic Distortion (THD) of the output voltage at the Point of Common Coupling (PCC), as depicted in Figure 11.



(a)

(b)

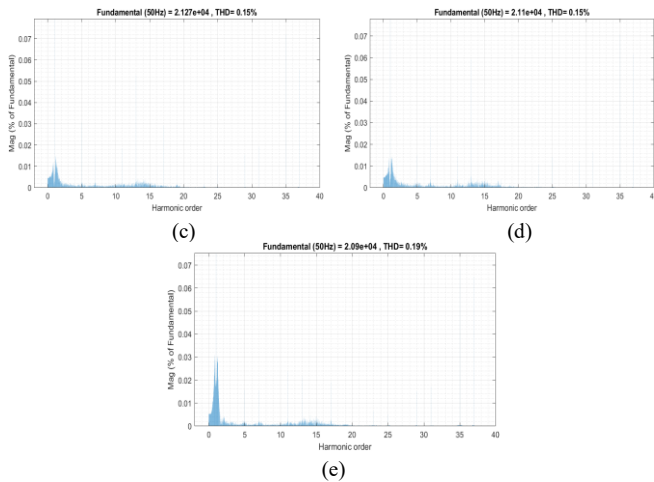


Fig. 11. The THD for Three-Phase Output Voltage at PCC at 25 °C (a) PV array at 1000 W/m<sup>2</sup> (b) PV array at 800 W/m<sup>2</sup> (c) PV array at 600 W/m<sup>2</sup> (d) PV array at 400 W/m<sup>2</sup> (e) PV array at 200 W/m<sup>2</sup>

It can be observed that the THD of the three-phase output voltage remains below the permissible limit of 3% at 33 kV, as mandated by ERG5/4 [19][21] for varying irradiance levels. From Figure 11(a), it is observed that at the highest irradiance level of 1000 W/m<sup>2</sup>, the THD is 0.54%, whereas the THD output voltage is 0.19% for the lowest irradiance level of 200 W/m<sup>2</sup>. It is crucial to ensure the voltage harmonic is within acceptable limits to maintain the quality and reliability of the power supply to the grid.

## CONCLUSION

In this research, a calibration model for a 2755 MW Large-Scale Solar Photovoltaic (LSSPV) system is developed using Matlab and Simulink software. The parameters and components utilised in the model are based on UiTM Solar Park 1, located in Gambang, Pahang. The analysis in this research primarily concentrates on evaluating the performance of the DC and AC sides of the LSSPV system under constant temperature conditions while varying irradiance levels such as output voltage, power, and Total Harmonic Distortion (THD) are considered. The obtained results show that the calibrated LSSPV system operates within the set parameters and satisfies the quality and performance requirements set forth by pertinent standards and regulations such as IEC 61727, ERG5/4, manufacturing standards, and the Grid Code for Peninsular Malaysia.


## ACKNOWLEDGMENT

We would like to express our gratitude and appreciation to the University Technology of MARA (UiTM) for providing us with the invaluable opportunity to advance the study. Sincere gratitude to Majlis Amanah Rakyat (MARA) for their generous sponsorship and unwavering support of this study under the Graduate Excellence Programme (GrEP).

## REFERENCES

- [1] Suruhanjaya Tenaga, "Guidelines on Large Scale Solar Photovoltaic Plant For Connection to Electricity Networks," *Laws Malaysia*, vol. 1990, no. July, pp. 1–103, 2016, [Online]. Available: [https://www.st.gov.my/en/contents/article/polisi/2016/01-Act\\_447\\_-\\_Electricity\\_Supply\\_Act\\_1990.pdf](https://www.st.gov.my/en/contents/article/polisi/2016/01-Act_447_-_Electricity_Supply_Act_1990.pdf).
- [2] "Large Scale Solar (LSS)," *Tenaga Nasional Berhad*. <https://www.mytnb.com.my/renewable-energy/large-scale-solar> (accessed Feb. 02, 2022).
- [3] M. A. A. Y. S. Mekhilef, A. Safari, W.E.S. Mustaffa, R. Saidur, R. Omar, "Solar energy in Malaysia: Current state and prospects," *Renew. Sustain. Energy*, vol. 16, no. 1, pp. 386–396, 2012, doi: <https://doi.org/10.1016/j.rser.2011.08.003>.
- [4] M. F. N. Gomesh, I. Daut, M. Irwanto, Y.M. Irwan, "Study on Malaysian's Perspective Towards Renewable Energy Mainly on Solar Energy," in *Energy Procedia*, 2013, vol. 36, pp. 303–312, doi: 10.1016/j.egypro.2013.07.035.
- [5] I. Daut, M. Irwanto, Y. M. Irwan, N. Gomesh, Rosnazri, and N. S. Ahmad, "Potential of solar radiation and wind speed for photovoltaic and wind power hybrid generation in Perlis, Northern Malaysia," *2011 5th Int. Power Eng. Optim. Conf. PEOCO 2011*, no. June, pp. 148–153, 2011, doi: 10.1109/PEOCO.2011.5970439.
- [6] A. Alblooshi and M. I. Masoud, "Design of a 1 MW Grid-tied Photovoltaic System," *7th Int. Conf. Eng. Emerg. Technol. ICEET 2021*, no. October, pp. 1–6, 2021, doi: 10.1109/ICEET53442.2021.9659704.
- [7] O. Ozcan and F. Ersoz, "Project and cost-based evaluation of solar energy performance in three different geographical regions of Turkey: Investment analysis application," *Eng. Sci. Technol. an Int. J.*, vol. 22, no. 4, pp. 1098–1106, 2019, doi: 10.1016/j.jestch.2019.04.001.
- [8] O. A. Ahmed, W. H. Habeeb, D. Y. Mahmood, K. A. Jalal, and H. K. Sayed, "Design and Performance Analysis of 250 kW Grid-Connected Photovoltaic System in Iraqi Environment Using PVsyst Software," *Indones. J. Electr. Eng. Informatics*, vol. 7, no. 3, 2019, doi: 10.52549/ijeei.v7i3.978.
- [9] M. Satish, S. Santhosh, and A. Yadav, "Simulation of a Dubai based 200 KW power plant using PVsyst software," *2020 7th Int. Conf. Signal Process. Integr. Networks, SPIN 2020*, pp. 824–827, 2020, doi: 10.1109/SPIN48934.2020.9071135.
- [10] M. Huda, K. Okajima, and K. Suzuki, "Tapping the Potential of Large Scale Solar PV System in Sabah: The Feasibility Analysis," *Energy Power Eng.*, vol. 09, no. 02, pp. 108–118, 2017, doi: 10.4236/epe.2017.92009.
- [11] M. Songkin, N. N. Barsoum, and F. Wong, "Impact Assessment of Large-Scale Solar Photovoltaic integration on Sabah Grid System," in *Computational Science and Technology*, 2020, pp. 659–668.
- [12] International Electrotechnical Commission, "IEC Standard Photovoltaic (PV) systems - characteristics of the utility interface," 2009.
- [13] D. A. H. A. S. S.; I. A. A. S. Mohamed, "TNB Technical Guidebook on Grid-interconnection of Photovoltaic Power Generation System to LV and MV Networks," 2013. [Online]. Available: <http://seda.gov.my/>.
- [14] Malaysian Government, "Electricity Supply Act 1990," *Laws Malaysia*, vol. 1990, no. July, pp. 1–103, 2016, [Online]. Available: [https://www.st.gov.my/en/contents/article/polisi/2016/01-Act\\_447\\_-\\_Electricity\\_Supply\\_Act\\_1990.pdf](https://www.st.gov.my/en/contents/article/polisi/2016/01-Act_447_-_Electricity_Supply_Act_1990.pdf).
- [15] Suruhanjaya Tenaga, "Grid Code For Peninsular Malaysia (Amendments) 2020.," 2020.
- [16] K. E. Y. Features and L. P. Warranty, "Eagle 72P 320-340 Watt Poly Crystalline Module," 2015.
- [17] "SG2500-MV MV Turnkey Station System Manual."
- [18] MathWorks, "MPPT Algorithm: Implement maximum power point tracking algorithms for photovoltaic systems using MATLAB and Simulink." <https://www.mathworks.com/solutions/electrification/mppt-algorithm.html> (accessed Feb. 21, 2022).
- [19] Energy Networks Association, "Guidelines on Large Scale Solar Photovoltaic Plant for Connection to Electricity Networks.," *2018 Energy Networks Assoc.*, no. 2, 2018.
- [20] C. X. T. C. LTD., "Details Technical Schedule for 60MVA, 132/33kV Power Transformer," 2016.
- [21] E. directorate of the energy networks Association, "A guide to ENA Engineering Recommendation G5/4-1," *Eng. Recomm. G5/4-1*, no. 4, 2005.





# Comparison between Titanium Dioxide Synthesis by Sol-Gel and Titanium Dioxide Commercial Properties for Dye-Sensitized Solar Cell Application

04

# Comparison between Titanium Dioxide Synthesis by Sol-Gel and Titanium Dioxide Commercial Properties for Dye-Sensitized Solar Cell Application

Nur Alfarina Pirdaus  
Solar Research Institute  
Universiti Teknologi MARA  
Shah Alam, Selangor, Malaysia  
nuralfarina13@gmail.com

Nurfadzilah Ahmad  
Solar Research Institute  
Universiti Teknologi MARA  
Shah Alam, Selangor, Malaysia  
nurfadzilah6344@uitm.edu.my

**Abstract**— Dye-sensitized solar cell (DSSC) has attracted great deal of interest in the recent years due to its easy and low-cost fabrication process compared to silicon solar cells.  $\text{TiO}_2$  is a transparent to visible light n-type wide band gap semiconductor. The DSSC convert visible light into electrical energy through charge separation in sensitizer dyes adsorbed on a wide band gap semiconductor.  $\text{TiO}_2$  paste in this study were prepared using  $\text{TiO}_2$  powder synthesised by the sol-gel method and commercial powder. The comparison study on the structural, morphological and optical characterisations of the  $\text{TiO}_2$  were carried out using X-ray diffraction (XRD), FESEM, and UV-vis spectroscopy in this study. The XRD pattern detects the formation of the amorphous phase of  $\text{TiO}_2$  structured thin films for both thin films when  $\text{TiO}_2$  supposed to be highly crystalline either in anatase or rutile phase. FESEM images show that  $\text{TiO}_2$  synthesis by sol-gel consist more uniform morphology compared to commercial  $\text{TiO}_2$  which consists highly agglomerated and uneven shape of particles. The bandgap energy of the  $\text{TiO}_2$  thin films were calculated based on the UV-visible absorbance spectra of  $\text{TiO}_2$  thin films were 2.16 eV and 3.05 eV for sol-gel synthesised and commercial  $\text{TiO}_2$  respectively. The results obtained suggest improvement on the coating for better optimisation for DSSC application.

**Keywords**— $\text{TiO}_2$ , sol-gel, commercial  $\text{TiO}_2$ , DSSC, solar cell

## I. INTRODUCTION

The third generation of solar cells, known as dye-sensitized solar cells (DSSC), were created in 1991 by O'Regan and Gratzel. Due to its remarkable effectiveness, affordable cost of production, lighter weight and low toxicity, DSSC have attracted a lot of interest [1]. Although they are still regarded as having lesser efficiency than crystalline solar cells, these solar cell forms are more efficient than other thin films [2]. Previously, large semiconductor materials like CdS, Si, or GaAs were used to make photoanodes for the older generation of solar cells. The disadvantage of these photoanodes is that they become electrochemically unstable due to photo-corrosion when exposed to light. The broad bandgap of the sensitised semiconductors (such ZnO,  $\text{TiO}_2$ , and  $\text{SnO}_2$ ) is around 3 eV. They provide a chemically stable cell when used in the creation of DSSC because they are resilient to the photo-corrosion [3]. In DSSC, wide bandgap semiconductors are sensitised which that sensitization then use to convert visible light into electricity [4].

As a result of their huge surface area for dye anchoring, nanostructured metal oxide coatings are particularly appealing for DSSCs. The semiconductor component which makes up the core of a photoelectrode (PE) must be chemically stable and undisturbed by electrolyte species. It should be existent in nanostructure form by a factor of a thousand to optimise the effective surface area for dye adsorption, hence enhancing the effectiveness of sunlight harvesting, and its lattice structure

should be suitable for dye bonding. It should have a conduction band that is just below the dye's LUMO level to facilitate electron injection [5].  $\text{TiO}_2$  is usually used as the photo-anode (working electrode) material and  $\text{I}^-$  or  $\text{I}_3^-$  as the redox couple in the most common and basic DSSC. [6].

Mesoporous  $\text{TiO}_2$  nanoparticles with surface areas ranging from 50 to 250  $\text{m}^2/\text{g}$  are the most commonly employed in DSSC fabrication. Transparent conductive oxide (TCO) glass's conductive side is covered with a  $\text{TiO}_2$  coating. The most common  $\text{TiO}_2$  coating techniques are screen printing, the doctor blade method, spin coating, electrophoretic deposition, and tape casting, followed by a high temperature heat treatment to remove organic binders and obtain a pure  $\text{TiO}_2$  film, as well as to enhance the inter-particle between  $\text{TiO}_2$  nanoparticles [3]. Within known synthesis methods, the sol-gel method is preferable for producing nanomaterials since it does not require complicated preparations and the synthesis process only require ambient temperature and pressure. The hydrolysis or condensation of a titanium precursor produces a sol and then a gel in sol-gel synthesis. Immediately after solvent evaporation, a xerogel is formed, which is milled and heat treated to yield highly crystalline  $\text{TiO}_2$  nanopowders [7].

Nanoporous  $\text{TiO}_2$  electrode with huge surface area per projected area was employed to maximise effective light absorption [8].  $\text{TiO}_2$  is found in three polymorphisms: rutile, anatase, and brookite. The rutile structure is the most thermodynamically stable of the three, whereas the other two are metastable.  $\text{TiO}_2$  from the anatase phase has a larger energy band gap of 3.2 eV than  $\text{TiO}_2$  from the rutile phase, which has a band gap of 3.0 eV, which improves photoactivity and makes it ideal for DSSC applications [9].

Considering its non-toxic nature, good optical and electrical capabilities, and great stability in DSSC and photocatalytic applications, titanium dioxide ( $\text{TiO}_2$ ) is a promising material for diverse applications among the numerous semiconducting metal oxide nanomaterials. Anatase- $\text{TiO}_2$  is employed as a photoanode in DSSC and as a photocatalyst for organic molecule degradation because it is an effective charge separator of photoexcited charge carriers. The efficacy of DSSC and photocatalytic applications is primarily determined by the amount of dye molecules adsorbed on  $\text{TiO}_2$  surfaces, the number of photons absorbed by the dye molecules for efficient electron harvesting, and the number of electron-hole pair recombinations. Several approaches have been used by researchers to move  $\text{TiO}_2$  absorption into the visible area [10].

## II. METHODOLOGY

### A. Preparation of TiO<sub>2</sub> Nanoparticles by Sol-Gel Method

The chemicals used are all analytical grade and have not been further refined. In order to prepare the sol-gel synthesised TiO<sub>2</sub>, 50 ml of titanium (IV) butoxide was mixed in absolute 50 ml of ethanol and agitated for an hour. After that, the solution was gradually diluted with 25 ml of deionised water. The resultant gel formed nearly instantaneously and was agitated for a few minutes more. After 24 hours, the solution will be filtered. It will then spend the next 12 hours in an oven set to 100°C, evaporating any remaining water and organic material. After drying, the material was processed into a fine powder.

### B. Preparation of TiO<sub>2</sub>-Coated Thin Film

To prepare TiO<sub>2</sub> paste from the prepared powder, 2 g of TiO<sub>2</sub> powder was mixed with 100 ml ethyl alcohol for 30 minutes until a homogeneous paste was produced. Keep the solution in the dark prior to use.

Prior to coating, the glass substrate was cleaned in the sonicator for 15 minutes with ethanol and deionised water alternately. After cleaning and drying, the substrate was placed on the spin coater holder and 10 drops of TiO<sub>2</sub> solution were dropped with 3000 rpm speed onto the cleaned glass substrates for 1 layer coating. After dispersing TiO<sub>2</sub> particles throughout the glass substrate, it was annealed at 100°C for 10 minutes. The coating procedure was repeated for the second layer. The final coating was annealed for 30 minutes at 500°C. The method was used for both paste using commercial and sol-gel synthesised TiO<sub>2</sub> powder.

### C. Characterisation

X-ray diffraction (XRD) was used to determine the phase of the thin film spin coated with different layers. FESEM was used to study the surface morphology of the TiO<sub>2</sub>. UV-Visible spectrometer was used to analyse the transmittance and bandgap energy of both type of TiO<sub>2</sub> in the range of 300 nm to 800 nm.

## III. RESULTS AND DISCUSSION

The photocatalytic property of titania is affected by various variables, including crystallinity, surface area, phase state, and bandgap [3]. To identify the phase composition of the TiO<sub>2</sub> anode for both commercial (C-TiO<sub>2</sub>) and sol-gel synthesised TiO<sub>2</sub> (SG-TiO<sub>2</sub>), XRD characterisations were carried out, and the resulting diffraction pattern was plotted as shown in Figure 1 with measurement ranges ranging from 10° to 90°. The XRD pattern detects the formation of the amorphous (non-crystalline phase) of TiO<sub>2</sub> structured thin films for both thin films when TiO<sub>2</sub> supposed to be highly crystalline either in anatase or rutile phase. However, tendency peak of anatase can be seen at 25° for both samples which shown that anatase supposed to be the dominant phase for both samples. This is due to the properties of anatase phase which exhibit a preferred orientation. Improvisation on the sample preparation (sol-gel and coating) should be done to avoid any impurities which lead to a reduction in the intensity of certain diffraction peaks or even their complete absence.

According to prior research, anatase phase was frequently observed in TiO<sub>2</sub> thin films used for photocatalysis. The observed anatase peaks occur at 25.24, 37.78, 48.12, 53.94, and 55.15, which are assigned to the (101), (004), (200), (15), and (211) planes, and are in good agreement with the standard

spectrum. (JCPDS NO.: 88-1175 and 84-1286) [11] [12]. In fact, it has been demonstrated that anatase functions as an indirect semiconductor, and hence electron desexcitation from the conduction band to the valence band is prohibited by selection criteria. As a result, anatase has a higher electron-hole lifetime than rutile, which works as a direct semiconductor with a shorter carrier lifetime [7].

In relation to the less-constrained molecular construction of anatase compared to rutile, the initial phase formation of crystalline TiO<sub>2</sub> in the synthesis of TiO<sub>2</sub> is generally anatase phase, and thus the short-range ordered TiO<sub>6</sub> octahedra can be easily arranged into long range anatase structure. In other words, because of its less limited structure and hence improved formation kinetics, anatase is the favoured phase production during TiO<sub>2</sub> synthesis. The sol-gel process is commonly used to convert kinetically stable anatase to thermodynamically stable rutile at increased temperatures ranging from 500°C to 700°C [13].

In general, the sol-gel generated precipitates in the sol gel technique are amorphous in nature. As a result, additional heat treatment is needed for crystallisation. To cause the transition from amorphous to anatase phase, an annealing temperature more than 300°C is usually necessary, resulting in a substantial increase in particle size. Titania's photocatalytic activity, on the other hand, is affected by particle size as well as crystallinity [14].

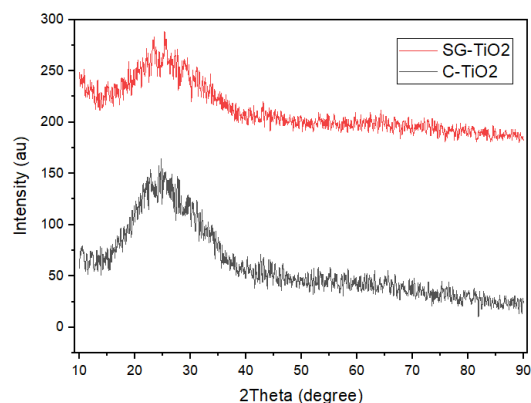


Fig. 1. XRD spectra of sol-gel synthesised and commercial TiO<sub>2</sub>

FESEM images in Figure 2 and 3 show that TiO<sub>2</sub> synthesised by sol-gel consist more uniform morphology compared to commercial TiO<sub>2</sub> which consists highly agglomerated and irregular shape of particles. It appeared that both samples had porous morphology, but there was a significant particle size difference between them. The particle size of the two samples was measured using Image J software, and their average was determined to be 586 nm and 327 nm for SG-TiO<sub>2</sub> and C-TiO<sub>2</sub> respectively.

The irregular particle agglomerates and aggregates that are mainly because of the high surface energy of the materials, which tend to cluster and clump together to minimise their surface energy [15]. The particle size of TiO<sub>2</sub> synthesized by sol-gel method were about the same size as the commercial but the nanoparticles agglomerated as colonies [16].

Previous research suggested that the particle size of SG-TiO<sub>2</sub> was approximately 60% smaller than that of C-TiO<sub>2</sub>, which can be attributed to the hydrolysis of Ti(OBu)<sub>4</sub> in an ethanol-water mixture, where water-immiscible byproducts

such as butanol functioned as a capping agent for the as-formed TiO<sub>2</sub> particles. The presence of nanoparticle agglomeration was apparent in both samples, which could be resulting to the usage of ethanol. Larger TiO<sub>2</sub> particle sizes result in poor photon diffusion towards the inner region of the TiO<sub>2</sub> layer. This decreases the amount of photogenerated carriers, resulting in a negligible contribution to the photocurrent. Furthermore, larger particle size increases the rate of electron-hole pair recombination. The quantity of charge carriers drops substantially when more electrons and holes recombine, resulting in reduced photocurrent detection. To account for the combination of these properties, SG-TiO<sub>2</sub> has a low photocurrent profile. [11]. The ideal nanoparticle size for TiO<sub>2</sub> paste synthesised is less than 20 nm to be deposited on a transparent conductive oxide (TCO) substrate. [17].

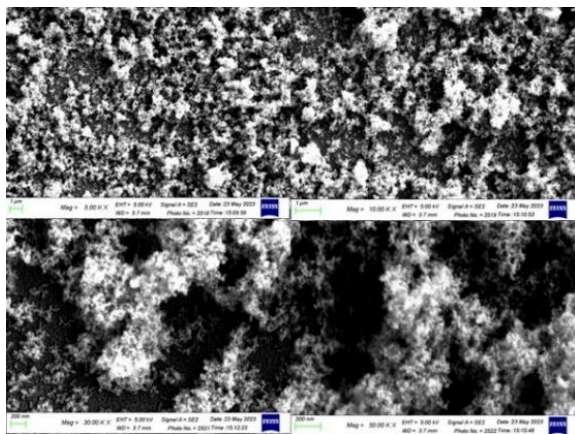


Fig. 2. FESEM images of commercial TiO<sub>2</sub>. Images 1 (5,000x magnification, bar = 1µm), Image 2 (10,000x magnification, bar = 1µm), Image 3 (30,000x magnification, bar 200nm) and Image 4 (50,000x magnification, bar =200nm).

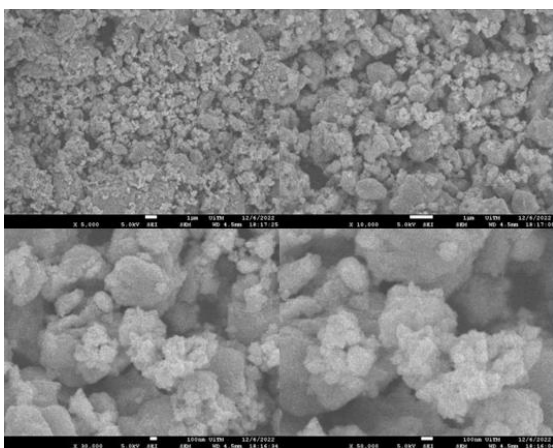


Fig. 3. FESEM images of sol-gel synthesised TiO<sub>2</sub>. Images 1 (5,000x magnification, bar = 1µm), Image 2 (10,000x magnification, bar = 1µm), Image 3 (30,000x magnification, bar 100nm) and Image 4 (50,000x magnification, bar =100nm).

The transmittance of C-TiO<sub>2</sub> and SG-TiO<sub>2</sub> has been reported to increase as a function of wavelength ranging from 300-800 nm, as illustrated in Fig. 4 . However, both have low transmittance values of 10-40% (C-TiO<sub>2</sub>) and 50-60% (SG-TiO<sub>2</sub>). High transmittance (>85%) for the sample is crucial in solar cell applications because energy requires being transported from one particle to another in the sample to achieve high efficiency [18].

Based on the absorbance spectra obtained from UV-Vis characterisation and using Beer's law, the optical band gap energy (E<sub>g</sub>) was estimated using Tauc's model by using this following equation:

$$\alpha h\nu = A(h\nu - E_g)^n \quad (1)$$

where  $\alpha$  is the absorption coefficient, E<sub>g</sub> is the nanoparticle band gap value, hν is energy of photon and A is the constant associated with the effective masses of the bands; n indicates the transition nature; n = 2 indicates allowed indirect transitions. It was estimated by extrapolating the linear portion of (αhν)<sup>2</sup> vs photon energy curve to the photon energy axis respectively [19].

The bandgap energy of the TiO<sub>2</sub> thin films measured were 2.16 eV and 3.05 eV for sol-gel synthesised and commercial TiO<sub>2</sub> respectively. According to the previous study, the energy band gap of the commercial TiO<sub>2</sub> obtained was larger than TiO<sub>2</sub> synthesised via sol-gel [15]. The rise in band gap is related to the decrease in crystallite size, which determines quantum size. Lowering the pH resulted in a noticeable drop in crystallite size, which can be associated with an increase in the band gap [20]. The transmittance value also reduces as the annealing temperature rises. This reduction in crystallite size and particle aggregation reduces light dispersion and hence increases transmittance [19]. The bandgap energy for TiO<sub>2</sub> basically decreases if modification of TiO<sub>2</sub> (for example doping) is done.

Narrowing the band gap allows visible light to be absorbed, promoting solar photon energy conversion. The fundamental reason for band-gap narrowing is increased interfacial Ti-Ti electronic bonding as packing density increases. The newly produced TiO<sub>2</sub>'s reduced band gap can employ a greater fraction of solar energy, and light absorption can be extended to the visible range (approximately 40% of the solar spectrum), making it more efficient for solar energy conversion. [19]. Meanwhile, the rise in band gap can be attributed to the reduction in crystallite size, which determines the quantum size impact and causes a blue shift in the absorption edge in optical reflectance. Lowering the pH resulted in an evident drop in crystallite size, which can be associated with an increase in the band gap [20].

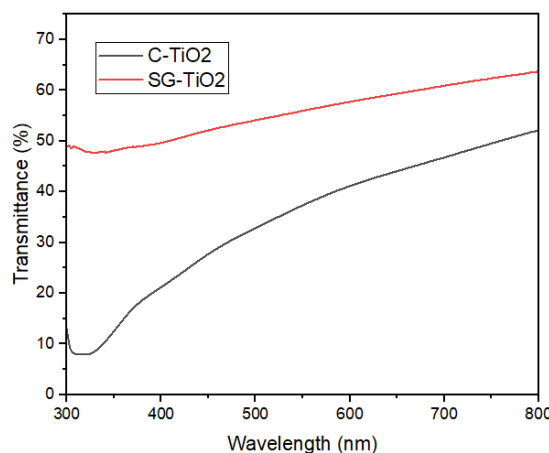


Fig. 4. Transmittance spectra of sol-gel synthesised and commercial TiO<sub>2</sub>

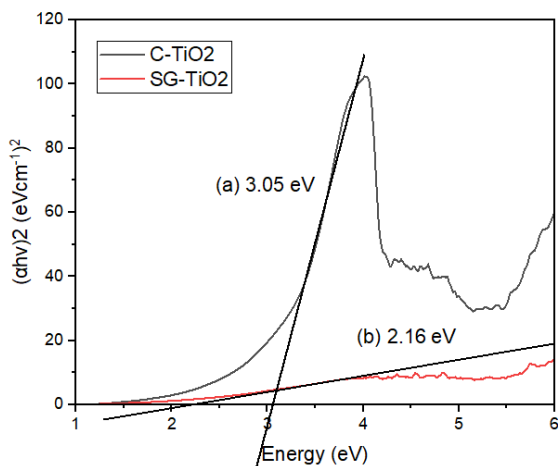


Fig. 5. Tauc plot of sol-gel synthesised and commercial TiO<sub>2</sub>

#### IV. CONCLUSION

Theoretically, the sol-gel process has numerous advantages, including its low crystallisation temperature and high yield, as well as its cost-effectiveness and outstanding compositional control over the arrangement of the atoms. Many factors influence nanoparticle qualities, including basic shape, surface area, porosity, etc. Based on the obtained results, improvisation needed in the sample preparation prior to characterisation to obtain desirable results for DSSC application.

#### ACKNOWLEDGMENT

N.A. would like to thank Universiti Teknologi MARA (UiTM) under FRGS: 600-RMC/FRGS5/3 (119/2021). We acknowledged Nano-Electronic Centre, School of Mechanical Engineering, College of Engineering and Faculty of Applied Science of UiTM Shah Alam for research facilities for laboratory work and characterisation equipment.

#### REFERENCES

[1] S. Kumar et al., "Recent development in two-dimensional material-based advanced photoanodes for high-performance dye-sensitized solar cells," *Solar Energy*, vol. 249, pp. 606-623, 2023/01/01/ 2023, doi: <https://doi.org/10.1016/j.solener.2022.12.013>.

[2] G. Richhariya, A. Kumar, P. Tekasakul, and B. Gupta, "Natural dyes for dye sensitized solar cell: A review," *Renewable and Sustainable Energy Reviews*, vol. 69, pp. 705-718, 2017, doi: [10.1016/j.rser.2016.11.198](https://doi.org/10.1016/j.rser.2016.11.198).

[3] M. Lal, P. Sharma, and C. Ram, "Synthesis and photocatalytic potential of Nd-doped TiO<sub>2</sub> under UV and solar light irradiation using a sol-gel ultrasonication method," *Results in Materials*, vol. 15, p. 100308, 2022/09/01/ 2022, doi: <https://doi.org/10.1016/j.rinma.2022.100308>.

[4] S. Sathyajothi, R. Jayavel, and A. C. Dhanemozhi, "The Fabrication of Natural Dye Sensitized Solar Cell (Dssc) based on TiO<sub>2</sub> Using Henna And Beetroot Dye Extracts," *Materials Today: Proceedings*, vol. 4, no. 2, Part A, pp. 668-676, 2017/01/01/ 2017, doi: <https://doi.org/10.1016/j.matpr.2017.01.071>.

[5] A. A. Hendi et al., "Dye-sensitized solar cells constructed using titanium oxide nanoparticles and green dyes as photosensitizers," *Journal of King Saud University - Science*, vol. 35, no. 3, p. 102555, 2023/04/01/ 2023, doi: <https://doi.org/10.1016/j.jksus.2023.102555>.

[6] R. Singh, "Dye-sensitized Solar Cell Technology: Recent Development and Advancement," in *Low Carbon Energy Supply: Trends, Technology, Management*, A. Sharma, A. Shukla, and L. Aye Eds., (Green Energy and Technology, 2018, pp. 221-250).

[7] C. B. D. Marien, C. Marchal, A. Koch, D. Robert, and P. Drogui, "Sol-gel synthesis of TiO<sub>2</sub> nanoparticles: effect of Pluronic P123 on particle's morphology and photocatalytic degradation of paraquat," *Environ Sci Pollut Res Int*, vol. 24, no. 14, pp. 12582-12588, May 2017, doi: [10.1007/s11356-016-7681-2](https://doi.org/10.1007/s11356-016-7681-2).

[8] T. Soga, *Nanostructured Materials for Solar Energy Conversion*, First ed. Elsevier, 2006, p. 600.

[9] S. B. Vinaayak, V. Balasubramani, M. Shkir, M. A. Manthrammel, and G. Sreedevi, "Enhancing the performance of TiO<sub>2</sub> based N-DSSC using dye extracted from *Cladophora Columbiana*, *Ludwigia repens* and mixed sensitizer," *Optical Materials*, vol. 133, p. 112968, 2022/11/01/ 2022, doi: <https://doi.org/10.1016/j.optmat.2022.112968>.

[10] T. Raguram and K. S. Rajni, "Synthesis and characterisation of Cu - Doped TiO<sub>2</sub> nanoparticles for DSSC and photocatalytic applications," *International Journal of Hydrogen Energy*, vol. 47, no. 7, pp. 4674-4689, 2022/01/22/ 2022, doi: <https://doi.org/10.1016/j.ijhydene.2021.11.113>.

[11] K. T. Low, F. K. Yam, K. P. Beh, A. Abd Manaf, and K. K. Beh, "Characteristics and Sensing of Sol-gel derived Titanium Dioxide-based Ultraviolet Photodetector on Flame Retardant-4 Board," *Sensors and Actuators A: Physical*, vol. 323, p. 112654, 2021/06/01/ 2021, doi: <https://doi.org/10.1016/j.sna.2021.112654>.

[12] I. Morad, A. M. Alshehri, A. F. Mansour, M. H. Wasfy, and M. M. El-Desoky, "Facile synthesis and comparative study for the optical performance of different TiO<sub>2</sub> phases doped PVA nanocomposite films," *Physica B: Condensed Matter*, vol. 597, p. 412415, 2020/11/15/ 2020, doi: <https://doi.org/10.1016/j.physb.2020.412415>.

[13] M.-E. Yeoh et al., "Hydrothermal duration effect on the self-assembled TiO<sub>2</sub> photo-anode for DSSC application," *Optical Materials*, vol. 141, p. 113907, 2023/07/01/ 2023, doi: <https://doi.org/10.1016/j.optmat.2023.113907>.

[14] S. Ibrahim and S. Sreekantan, "Effect of pH on TiO<sub>2</sub> Nanoparticles via Sol-Gel Method," *Advanced Materials Research*, vol. 173, pp. 184-189, 12/01 2010, doi: [10.4028/www.scientific.net/AMR.173.184](https://doi.org/10.4028/www.scientific.net/AMR.173.184).

[15] S. Castilhos, F. Souza, L. Colpini, L. Jorge, and O. Santos, "Assessment comparison of commercial TiO<sub>2</sub> and TiO<sub>2</sub> sol-gel on the degradation of caffeine using artificial radiation," *Environmental Science and Pollution Research*, vol. 27, 06/01 2020, doi: [10.1007/s11356-020-07748-x](https://doi.org/10.1007/s11356-020-07748-x).

[16] T. P. T. T. S. T. A. P. W. Promnopas, "Synthesis and Characterization of TiO<sub>2</sub> Nanopowders for Fabrication of Dye Sensitized Solar Cells," *Digest Journal of Nanomaterials and Biostructures*, vol. 11, pp. 81-90, March 2016 2016.

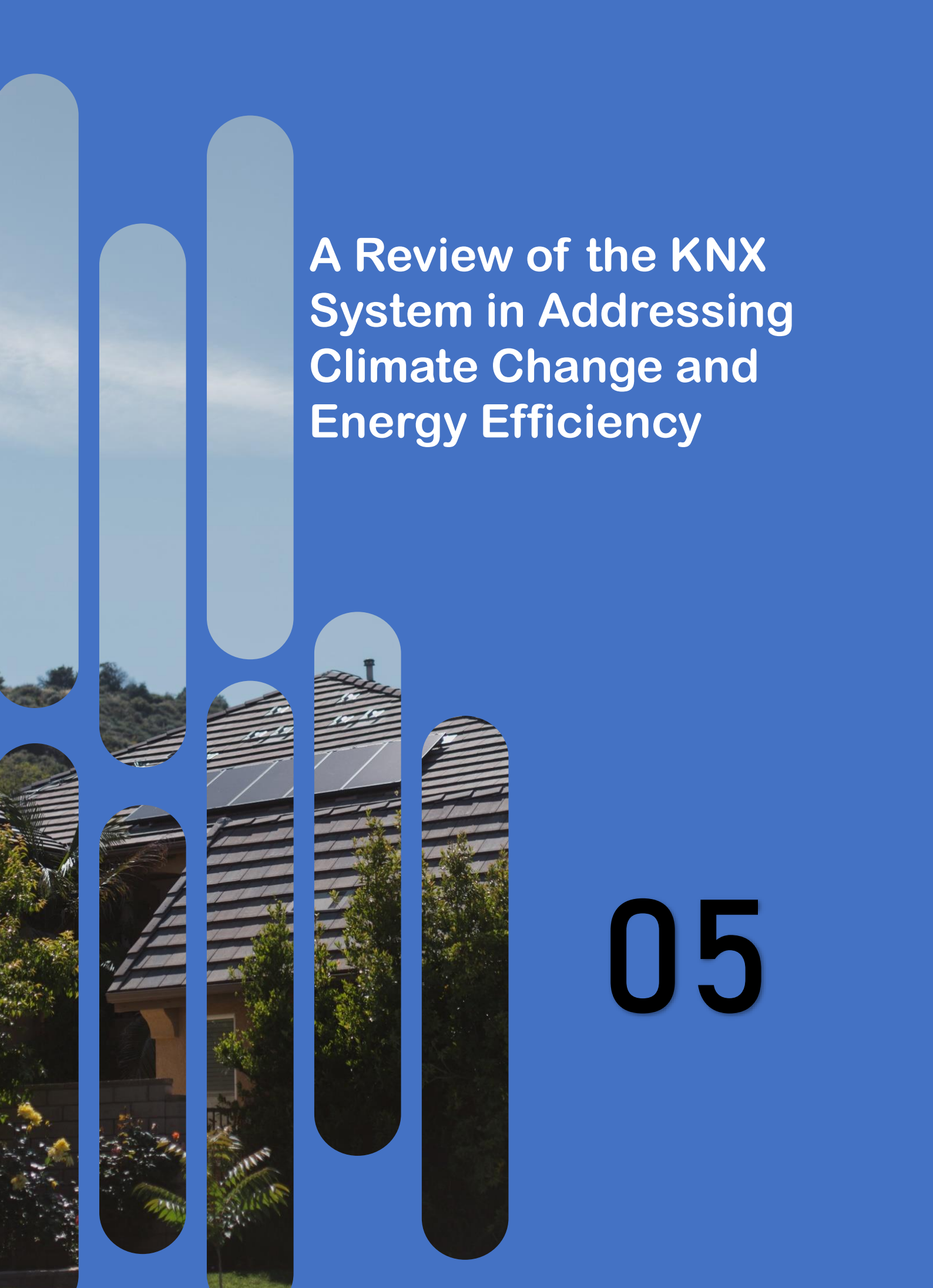
[17] D. Kishore Kumar et al., "Functionalized metal oxide nanoparticles for efficient dye-sensitized solar cells (DSSCs): A review," *Materials Science for Energy Technologies*, vol. 3, pp. 472-481, 2020/01/01/ 2020, doi: <https://doi.org/10.1016/j.mset.2020.03.003>.

[18] N. Ahmad, D. Kamaruzaman, and M. Rusop, "Amorphous Carbon Deposited by a Novel Aerosol-Assisted Chemical Vapor Deposition for Photovoltaic Solar Cells," *Japanese Journal of Applied Physics*, vol. 51, 06/01 2012, doi: [10.1143/JJAP.51.06FD05](https://doi.org/10.1143/JJAP.51.06FD05).

[19] K. Priyalakshmi Devi, P. Goswami, and H. Chaturvedi, "Fabrication of nanocrystalline TiO<sub>2</sub> thin films using Sol-Gel spin coating technology and investigation of its structural, morphology and optical characteristics," *Applied Surface Science*, vol. 591, p. 153226, 2022/07/30/ 2022, doi: <https://doi.org/10.1016/j.apsusc.2022.153226>.

[20] M. Tsega and F. B. Dejene, "Influence of acidic pH on the formulation of TiO<sub>2</sub> nanocrystalline powders with enhanced photoluminescence property," *Heliyon*, vol. 3, no. 2, p. e00246, Feb 2017, doi: [10.1016/j.heliyon.2017.e00246](https://doi.org/10.1016/j.heliyon.2017.e00246).





# A Review of the KNX System in Addressing Climate Change and Energy Efficiency

05

# A Review of the KNX System in Addressing Climate Change and Energy Efficiency

Sharina Safiee  
Department of Electrical Technology  
Kolej Komuniti Kuala Langat,  
Malaysia  
Banting, Selangor, Malaysia  
sharinasafiee@gmail.com

Nofri Yenita Dahlan  
Solar Research Institute  
School of Electrical Engineering,  
College of Engineering  
Universiti Teknologi MARA,  
Shah Alam, Selangor, Malaysia  
nofriyenita012@uitm.edu.my

Rozita Jailani  
School of Electrical Engineering,  
College of Engineering  
Universiti Teknologi MARA,  
Shah Alam, Selangor, Malaysia  
rozitaj@uitm.edu.my

Mohamad Fani Sulaima  
Faculty of Electrical Engineering  
Universiti Teknikal Malaysia Melaka  
Hang Tuah Jaya, Melaka, Malaysia  
fani@utem.edu.my

**Abstract**— As climate change poses significant environmental and societal challenges, there is a growing need for innovative building automation and energy management solutions. This chapter examines the role of the KNX system in combating climate change by increasing energy efficiency, advocating sustainable practices, and adapting to shifting environmental conditions. The beginning of the chapter emphasizes the significance of energy efficiency in preventing climate change. Integrating sensors, actuators, and controllers demonstrates how the KNX system optimizes energy consumption and reduces carbon emissions. By facilitating precise control and automation, the KNX system reduces energy waste and supports the operation of green buildings. In addition, the chapter examines the KNX system's ability to contribute to sustainable practices. The chapter also explores how the KNX system facilitates the surveillance and analysis of energy consumption, thereby providing valuable insights for identifying energy-saving opportunities and optimizing building performance. This chapter concludes by emphasizing the importance of the KNX system in addressing the challenges of climate change. Its ability to increase energy efficiency, promote sustainable practices, and adapt to changing environmental conditions makes it a valuable tool for building automation and energy management strategies to mitigate climate change impacts.

**Keywords**— KNX System, Climate Change, Building Automation System, Energy saving

## I. INTRODUCTION

Climate change is considered one of the 21st century's most significant threats [1]. A total of 195 states agreed to reduce their greenhouse gas (GHG) emissions to prevent irreversible impacts of global warming after the 21st Meeting of the Parties to the United Nations Framework Conference on Climate Change (UNFCCC) convened in Paris [2]. Electricity and heat generation account for a fifth of the overall worldwide GHG emissions [3], which is one of the reasons countries worldwide are trying to make their electricity networks more sustainable.

Energy-efficient activities will help to minimise greenhouse emissions and climate change impacts. In line with the report in [2], Malaysia's Government is implementing various energy efficiency (EE) programs and initiatives. Among them is the National Energy Efficiency Action Plan (NEEAP), where the Government targets to save 8% of energy, that is, 52,223 GWh over a 10-year period from

2016-2025 [4]. Hailing the latest technology elements in the new era will accelerate the EE potential. The presence of an automation system, such as a Building Automation System (BAS), is an essential prerequisite for engaging in a demand response (DR) program. It can also substantially minimise energy usage [5].

BAS consists of a control system to monitor and tracks building facilities for heating, cooling, ventilation, air conditioning, illumination, shading, security and warning [6]. BAS is used to automate the control process of electrical load in domestic or office buildings. As well-built and run, BAS provides comprehensive capabilities to maximise energy efficiency in numerous systems [7]. There are extensive domestic demands to build smart BAS with the required versatility and adaptability at an affordable cost reduction to recover investment in energy efficiency while retaining the desired level of comfort and consumer demands [8]. Integrating the new technology will drive the optimal output to the greatest extent. BAS technology includes BACnet, KNX, LonWorks [9], Modbus [6], ZigBee or EnOcean, X10, and Z-Wave [10]. The authors in [11] suggest that BAS, machine learning, IoT and significant data innovations are alternatives that aim to increase energy efficiency.

This paper aims to investigate how the KNX system can play a part in mitigating the effects of climate change by increasing energy efficiency, fostering more environmentally friendly practices, and better adapting to shifting environmental conditions regarding the critical benefits of KNX Automation [12].



Fig. 1. Key Benefits of KNX Automation for Buildings [12].

## II. KNX SYSTEM IN CLIMATE CHANGE MITIGATION AND ENERGY EFFICIENCY

### A. Optimisation Of Energy Consumption

In modern times, when climate change is getting more drastic, and issues like CO<sub>2</sub> emission and energy efficiency are becoming increasingly important, it is necessary to find possible energy savings in every area. To achieve these possible savings in the residential area, it is essential to establish Intelligent Building Automation in residential buildings. The importance of energy efficiency in climate change mitigation demonstrates how the KNX system optimises energy consumption by integrating sensors, actuators, and controllers. By providing efficient control and automation, the KNX system reduces energy waste and carbon emissions, contributing to sustainability.

Building automation and control systems (BACS), like KNX, are one new strategy [13] proposed for improving building energy efficiency. Therefore, [14] designed a lighting control network to decrease the energy consumption of a commercial building, using the KNX system to calculate an 82.33% reduction in energy consumption. Similarly, carbon dioxide (CO<sub>2</sub>) emissions, one of the leading greenhouse gases contributing to climate change, were 85% lower. With these results, we acquire economic and environmental benefits; as a result, the same procedure is proposed for the control of air conditioning systems, whose operation accounts for 32.8% of an establishment's total energy consumption. Even [15] proposed passive wireless communication as a cutting-edge new technology extensively used in energy-efficient green buildings. Passive wireless lighting switch, a human body infrared sensor, a light sensor, and access to the KNX bus system, saving 40% of lighting transformation costs and 80% of the building's 31 km of cable. In a hotel chain in Germany with 25 hotels (5000 rooms), the regular operation of the air conditioning system for the modification reduces air conditioning energy consumption by 20%. In just two years, the renovation investment is recouped by energy savings.

The KNX and Digital Addressable Interface (DALI) systems were implemented on a megaship, resulting in an 80% decrease in illumination power consumption from 12,935.2 to 2830.3Wh [16]. Therefore, reducing carbon dioxide emissions associated with decreased power generation is possible by implementing an intelligent illumination system on ships and

optimising the power required for lighting. This initiative can impact ship operations positively regarding environmental protection and climate change response. The KNX/DALI protocol is anticipated to play a significant role in researching intelligent ships for automated sailing.

As an Intelligent Building Automation system, the KNX system incorporates sensors, actuators, and controllers to optimise energy consumption and reduce carbon emissions in residential and commercial structures in achieving energy savings. The illustrated examples of how KNX-based control networks for lighting and air conditioning systems result in substantial energy and cost reductions. Moreover, implementing KNX and DALI systems on a megaship significantly reduced illumination power consumption, which may affect environmental protection and climate change response in the maritime industry. Numerous recent studies by BAS researchers demonstrate that the KNX system considerably impacts energy consumption. Table 3 summarises the KNX system's applicability in various building types, control strategies, and savings results.

### B. Adaptive Climate Control

Adaptive Climate Control (ACC) is the dynamic adjustment of cooling, heating, and ventilation systems in response to environmental factors like temperature, humidity, and occupancy variations. Adaptation is the capacity of a human or natural system to respond to climate change (including climate variability and extremes) by mitigating potential damages, exploiting opportunities, or managing the consequences [17]. ACC, also called methods, are used to resolve the challenges and uncertainties associated with building climate dynamics, such as unmodeled dynamics and unknown perturbations [18]. Adaptive climate control methods contribute to effective building energy management and reducing carbon emissions. It enables the control system to continuously adapt and adjust its strategies based on real-time conditions and feedback, improving the overall performance and energy efficiency of HVAC systems [19].

This control strategy was first investigated in 1979 for use in greenhouses [20] and Computer-Aided Cultivation [21]. ACC optimises energy economy, occupant comfort, and climate management by considering surrounding zone interactions [18]. The KNX system can adapt to fluctuating

TABLE I. A SUMMARY OF THE KNX SYSTEM'S APPLICABILITY IN VARIOUS BUILDING TYPES AND CONTROL STRATEGIES

Author	Method/Load/ Control Mechanism	Application of BAS	Building Type	Saving/ Result
[13]	Retrofit sensor and control network	EnOcean, KNX, BACnet, and m-bus for sensing and automation	Campus building	Exhibit similar characteristics; control behaviour differently
[14]	Lighting control	KNX	Green building	Energy consumption: 82.33% Co <sub>2</sub> emissions: 85%
[15]	Passive wireless communication	KNX	Commercial building	Lighting cost: 40% Cable cost: 80%
[16]	Lighting control	KNX/digital addressable lighting interface protocol	Ship	Power consumption: ≥80%
[22]	Heating & lighting control	4-Channel-Pt1000 interfaces & M-bus heat meter Dimming actuators & light sensors	Educational Building	50%
[23]	KNX-Zigbee Integration (wired & wireless HAS)	KNX-Zigbee gateway	Domestic	Integration enabled
[24]	Lighting, heating/cooling system & motorised opening	KNX- Raspberry Pi	Resident building	30%
[25]	Solar energy-powered lighting system	KNX	Smart building	Energy consumption: 50% Co <sub>2</sub> reduction: 0.56 tons Roi: 11.13 years

environmental conditions caused by climate change. For example, it can monitor outdoor temperature, humidity, and weather data to adjust HVAC systems accordingly. This adaptive climate control helps maintain a comfortable interior. The KNX actuator regulates each heating circuit's valves independently for heating control. The indoor temperature is essential for determining when the valve opens and closes. For this purpose, room temperature sensors record the room temperature [26]–[29]. Figure 2 shows the configuration for space heating in an apartment using the KNX system [27].

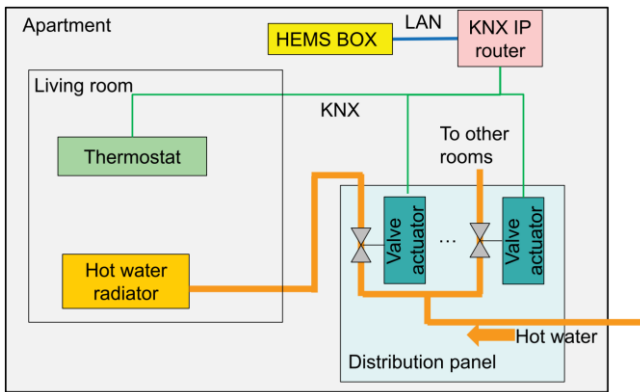


Fig. 2. System configuration for space heating in an apartment using the KNX system [27]

Additionally, [24] investigates the integration of Raspberry Pi in home automation systems utilising the KNX protocol to facilitate the installation and configuration of smart home components, resulting in promising communication between components and a 15% reduction in energy usage. Overall, the ACC enables systems to respond to variations and extremes in the climate, mitigating potential damages and managing consequences. This strategy resolves challenges in building climate dynamics, resulting in efficient energy management and decreased carbon emissions. The KNX system can adapt to changing environmental conditions resulting from climate change, monitoring outdoor data to modify HVAC systems and maintain a comfortable interior.

### C. Integration With Renewable Energy

The latest integration combines an enhanced energy storage management technique with KNX building control and automation systems for demand-side management in a microgrid [30]. yields a KNX system with renewable energy. KNX devices are programmable and can regulate the electrical energy consumption of consumers after being installed at the low-voltage portion of the grid. Integrating KNX into the microgrid significantly enhances the microgrid's power supply reliability.

In [31], the LAMBDA MG LAB integrates the KNX system and renewable energy to accomplish energy savings and control. The KNX protocol is utilised for smart department objectives such as illumination, presence, HVAC, and energy-consuming device control. Integration of additional renewable energy sources, such as wind or hydropower, could be investigated to improve the microgrid's sustainability and efficacy further.

The KNX system and renewable energy integration in [32] were carried out using the KNX system to control and

administer the heating system in intelligent buildings that employ hybrid renewable energy sources. Future research could focus on integrating additional renewable energy sources, such as geothermal or wind energy, with the KNX system in intelligent structures. These additional renewable energy sources would enable a more comprehensive and diverse approach to using renewable energy. In addition, investigating the potential of energy storage technologies, such as batteries or hydrogen storage, in conjunction with the management system could improve the system's overall efficacy and dependability.

According to a previous study by [33], using energy management systems and renewable energy sources in smart home installations can result in significant energy savings and less reliance on external energy infrastructure. The study found that implementing energy management strategies, such as cost-effective or comfort strategies, can result in savings ranging from 11 to 31% and a reduction in energy demand of up to 60%. Photovoltaic installations and other renewable energy sources can help with these energy reductions. While [25] reported that the installation of a solar energy system in an intelligent building with the KNX system in Malaysia resulted in a 50% energy reduction for the lighting system, [26] found that the installation of a solar energy system resulted in a 25% energy reduction for the lighting system. The annual energy consumption of lighting systems fell from 1600 kW to 800 kW. The installation's estimated return on investment (ROI) is approximately 11.13 years. However, the investment costs of implementing such systems must be carefully considered, and the usability must be evaluated based on the energy management strategy adopted.

In [34], integrating the KNX system with renewable energy is discussed in the context of intelligent building management. Figure 3 shows that The KNX protocol controls responsive/non-responsive devices and renewable photovoltaic resources in an intelligent building. Incorporating additional renewable energy sources, such as wind power, into the energy management paradigm for intelligent structures would increase the use of renewable energy and decrease dependence on the grid.

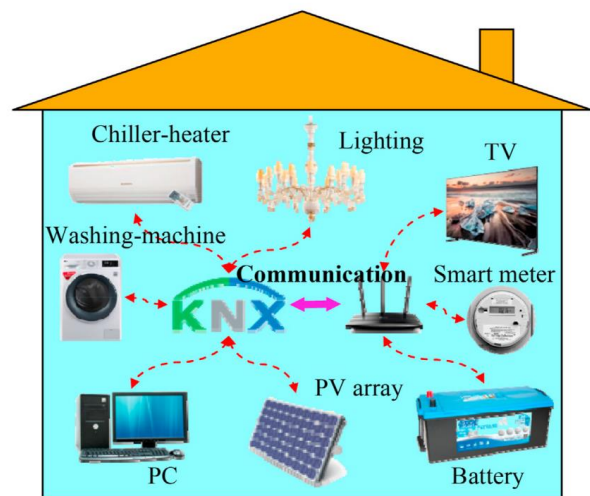


Fig. 3. KNX protocol and renewable photovoltaic resources in the smart building [34]

Ultimately, the integration of KNX and renewable energy highlights how this integration enables efficient management of renewable energy production and consumption within buildings, thereby reducing reliance on fossil fuels and fostering a sustainable energy composition.

#### D. Supporting Demand Respond Strategy

Load shedding is one demand response (DR) strategy available via building automation systems. This strategy involves reducing energy consumption during peak periods to prevent grid instability. During periods of high demand, building automation systems can autonomously adjust energy consumption by turning off or reducing non-critical building systems such as lighting and HVAC [35]. The KNX system is employed in [36] for building automation, which includes HVAC control, sensors, security, and illumination. It is projected that DR will reduce peak demand and increase the load factor. The KNX system plays a role in implementing demand response measures, such as controlling and altering the operation of various building systems to optimise energy consumption and reduce peak demand.

The KNX system facilitates effective demand response and energy management in microgrid systems. The KNX system enables the coordination of multiple production and storage systems to maintain a demand-supply equilibrium. In [37], the KNX system is utilised as a technological platform for home automation to regulate the load/energy consumption of the microgrid testbed. The KNX system enables simple access and compatibility with energy production and consumption data maintained by a server with a web interface. This study devised an algorithm for demand response that combines with the Building Automation System (BAS) using the KNX protocol to accomplish efficient energy management from renewable energy sources and energy storage systems. [38] emphasises the excessive fragmentation of protocols and standards in Building Management Systems (BMS) and building-to-grid communications, which poses a challenge for achieving interoperability, such as KNX. KNX is regarded as more established and is supported by a small number of standards for demand response.

[39] uses the KNX system to facilitate demand response in district heating circuits. Individual heating system components, including sensors and actuators, are linked using the KNX protocol, which enables decentralised, distributed control. The data from the local control systems are then sent to the data management system (DMS) using the MQTT protocol, which works on top of TCP/IP at the Internet Protocol Suite's application layer. The article uses the KNX system and MQTT protocol to show the potential for controlling heating demand and achieving energy savings in district heating systems.

Furthermore, [40] promotes the KNX system's support for demand response strategies, which permit capacity shedding or shifting during peak demand periods. The system reduces strain on the electrical infrastructure by stabilising the power grid. Hence, KNX is a crucial technological platform for effective demand response and energy management in building automation, microgrid systems, and district heating circuits. It facilitates coordinating and controlling multiple production and storage systems, optimising energy consumption during peak periods, and incorporating renewable energy sources. Interoperability with other protocols is a concern despite its benefits, highlighting the need for standardisation in Building Management Systems

and building-to-grid communications. KNX is an established and dependable solution for demand response and energy management strategies.

### III. SUMMARY


In conclusion, the article emphasises the significance of the KNX system in mitigating climate change by promoting energy efficiency, environmentally favourable practices, and adaptability to altering environmental conditions. By integrating sensors, actuators, and controllers, the KNX system optimises energy consumption, thereby reducing energy waste and carbon emissions. In addition, it enables adaptive climate control, which dynamically adjusts HVAC systems in response to environmental factors, resulting in effective building energy management and decreased carbon emissions. In addition, integrating the KNX system with renewable energy sources improves the microgrid's power supply reliability and promotes a sustainable energy composition. In addition, the KNX system facilitates demand response strategies, which reduce stress on the electrical infrastructure during periods of peak demand.

Overall, the KNX system emerges as a crucial technological platform that considerably contributes to climate change mitigation efforts by providing effective energy management solutions and nurturing a greener, more sustainable future. In Building Management Systems and building-to-grid communications, interoperability issues with other protocols must be addressed through standardisation efforts despite their benefits. Despite this, the KNX system remains a well-established and reliable means of attaining energy efficiency and effective demand response strategies in various applications.

### REFERENCES

- [1] D. Subkhankulova, "Exploring future opportunities and challenges of Demand Side Management with Agent Based Modelling," 2018.
- [2] R. Falkner, "The Paris agreement and the new logic of international climate politics," *Int Aff*, vol. 92, no. 5, pp. 1107–1125, Sep. 2016, doi: 10.1111/1468-2346.12708.
- [3] Istanbul Policy Center, *Low Carbon Development Pathways and Priorities for Turkey*. 2017. [Online]. Available: [www.wwf.org.tr](http://www.wwf.org.tr).
- [4] Suruhanjaya Tenaga, "Energy Malaysia," 2020. [Online]. Available: [www.pvmpublish.com.my](http://www.pvmpublish.com.my)
- [5] F. Mancini, G. Lo Basso, and L. de Santoli, "Energy use in residential buildings: Impact of building automation control systems on energy performance and flexibility," *Energies (Basel)*, vol. 12, no. 15, Jul. 2019, doi: 10.3390/en12152896.
- [6] P. Domingues, P. Carreira, R. Vieira, and W. Kastner, "Building automation systems: Concepts and technology review," *Computer Standards and Interfaces*, vol. 45, Elsevier B.V., pp. 1–12, Mar. 01, 2016. doi: 10.1016/j.csi.2015.11.005.
- [7] J. A. Engvang and M. Jradi, "Auditing and design evaluation of building automation and control systems based on eu.bac system audit – Danish case study," *Energy and Built Environment*, vol. 2, no. 1, pp. 34–44, Jan. 2021, doi: 10.1016/j.enbenv.2020.06.002.
- [8] H. C. Sun and Y. C. Huang, "Optimization of power scheduling for energy management in smart homes," in *Procedia Engineering*, Elsevier Ltd, 2012, pp. 1822–1827. doi: 10.1016/j.proeng.2012.06.225.
- [9] G. Lobaccaro, S. Carlucci, and E. Löfström, "A review of systems and technologies for smart homes and smart grids," *Energies*, vol. 9, no. 5, MDPI AG, May 01, 2016. doi: 10.3390/en9050348.
- [10] S. Ilieva, A. Penchev, and D. Petrova-Antonova, "Internet of things framework for smart home building," in *Communications in Computer*

- and Information Science, Springer Verlag, 2016, pp. 450–462. doi: 10.1007/978-3-319-49700-6\_45.
- [11] I. Machorro-Cano, G. Alor-Hernández, M. A. Paredes-Valverde, L. Rodríguez-Mazahua, J. L. Sánchez-Cervantes, and J. O. Olmedo-Aguirre, “HEMS-IoT: A big data and machine learning-based smart home system for energy saving,” *Energies* (Basel), vol. 13, no. 5, Mar. 2020, doi: 10.3390/en13051097.
- [12] Norlect Engineering, “KNX System Integrator,” 2023.
- [13] P. Althaus, F. Redder, E. Ubachukwu, M. Mork, A. Xhonneux, and D. Müller, “Enhancing Building Monitoring and Control for District Energy Systems: Technology Selection and Installation within the Living Lab Energy Campus,” *Applied Sciences* (Switzerland), vol. 12, no. 7, Apr. 2022, doi: 10.3390/app12073305.
- [14] O. Chamorro-Atalaya, A. Quesquen-Porras, and D. Arce-Santillan, “Lighting control network based on KNX protocol, for the reduction of energy consumption,” *Indonesian Journal of Electrical Engineering and Computer Science*, vol. 19, no. 3, pp. 1186–1193, Sep. 2020, doi: 10.11591/ijeecs.v19.i3.pp1186-1193.
- [15] X. J. Feng, “Passive Wireless Communication Technology Applied in Green Building,” *Adv Mat Res*, vol. 1061–1062, pp. 1190–1193, Dec. 2014, doi: 10.4028/www.scientific.net/amr.1061-1062.1190.
- [16] J. Kim and A. Choi, “Reduction of lighting power consumption through lighting control using the KNX/digital addressable lighting interface protocol in liquefied natural gas carrier accommodation mock-up,” *Renewable and Sustainable Energy Reviews*, vol. 182, Aug. 2023, doi: 10.1016/j.rser.2023.113374.
- [17] Environmental Protection Agency, “Climate Adaptation and EPA’s Role – US EPA definition,” Sep. 19, 2022. <https://www.epa.gov/climate-adaptation/climate-adaptation-and-epas-role> (accessed Jul. 09, 2023).
- [18] Y. Jiang, S. Zhu, Q. Xu, B. Yang, and X. Guan, “Building Temperature and Humidity Adaptive Control for a Multi-Zone HVAC System Using Hybrid Modeling Method,” in *Proceedings of the IEEE International Conference on Industrial Technology, Institute of Electrical and Electronics Engineers Inc.*, 2022, doi: 10.1109/ICIT48603.2022.10002727.
- [19] M. Gholamzadehmir, C. Del Pero, S. Buffa, R. Fedrizzi, and N. Aste, “Adaptive-predictive control strategy for HVAC systems in smart buildings – A review,” *Sustainable Cities and Society*, vol. 63, Elsevier Ltd, Dec. 01, 2020, doi: 10.1016/j.scs.2020.102480.
- [20] A. J. Udink ten Cate, “Adaptive Climate Control Systems for Greenhouses,” 18th IEEE Conference On Decision and Control, Fort Lauderdale, Florida, , 1979.
- [21] Hashimoto Y, Morimoto T, and Funada S, “Computer Processing Of Speaking Plant For Climate Control And Computer Aided Plantation (Computer Aided Cultivation),” *Symposium on More Profitable Use of Energy in Protected Cultivation*, 1980.
- [22] M. Mevenkamp, I. Beinaar, and C. Eder, “KNX-based Energy Efficient Heating and Lighting in Educational Buildings \*,” 2006. [Online]. Available: [www.it-gmbh.de](http://www.it-gmbh.de)
- [23] S. L. Woo and H. H. Seung, “Implementation of a KNX-ZigBee gateway for home automation,” in *Digest of Technical Papers - IEEE International Conference on Consumer Electronics*, 2009, pp. 545–549. doi: 10.1109/ISCE.2009.5156866.
- [24] E. Feki, K. Kassab, and A. Mami, “Integration of the small board computers Raspberry PI in Home Automation based on KNX protocol,” *IEEE Antennas and Propagation Society Institute of Electrical and Electronics Engineers*, 2019.
- [25] M. F. Lee, S. C. J. Lim, P. W. Siew, and B. T. Tee, “Technical and Economic Analysis of Solar Energy Powered Lighting System in a Smart Building at Tropical Region,” in *IEEE International Conference on Industrial Engineering and Engineering Management*, IEEE Computer Society, 2022, pp. 407–411. doi: 10.1109/IEEM55944.2022.9989620.
- [26] S. Dimitrios, F. Hermes, V. Georgios, and K. Georgios, “Design and Construction of HVAC and Lighting Controller with Internet of Things Capabilities,” in *2020 3rd World Symposium on Communication Engineering (WSCE)*, Thessaloniki, Greece: IEEE, Oct. 2022.
- [27] T. Yano, “Space Heating Control by Estimating Acceptable Set-Point Temperature Based on Survival Analysis,” *IEEE Access*, vol. 8, pp. 17956–17964, 2020, doi: 10.1109/ACCESS.2020.2967057.
- [28] T. Yano, “Space Heating Control Using Acceptable Set-Point Temperature Estimation by a Statistical Approach in the Lyon Smart Community Project,” in *2018 IEEE International Conference on Industrial Technology (ICIT)*, Lyon, France: IEEE, Apr. 2018.
- [29] T. Yano and S. Imahara, “Field Study on Actual Usage of Occupancy-Reactive Space Heating Control,” *IEEE Access*, vol. 9, pp. 47204–47215, 2021, doi: 10.1109/ACCESS.2021.3067884.
- [30] T. Kollatou et al., “Advanced Demand-Side Management in Microgrids using KNX Technologies,” *2014 KNX Scientific Conference*, vol. 1, no. October, pp. 30–3, Oct. 2014.
- [31] M. Kermani, B. Adelmanesh, E. Shirdare, C. A. Sima, D. L. Carni, and L. Martirano, “Intelligent energy management based on SCADA system in a real Microgrid for smart building applications,” *Renew Energy*, vol. 171, pp. 1115–1127, Jun. 2021, doi: 10.1016/j.renene.2021.03.008.
- [32] J. Szymenderski and D. Typańska, “Management of hybrid renewable energy source in smart building,” *Computer Applications in Electrical Engineering*, vol. 13, pp. 191–196, 2015.
- [33] K. Listewnik and P. Formela, “Multi-Criterion Analysis Of Selected Power Management Strategies In Smart Home Systems,” *Scientific Journal of Gdynia Maritime University*, no. 123, pp. 79–93, 2022, doi: 10.26408/123.07.
- [34] M. H. Dadashi-Rad, A. Ghasemi-Marzbali, and R. A. Ahangar, “Modeling and planning of smart buildings energy in power system considering demand response,” *Energy*, vol. 213, Dec. 2020, doi: 10.1016/j.energy.2020.118770.
- [35] A. M. Al-Ghaili et al., “A systematic review on demand response role towards sustainable energy in the smart grids-adopted buildings sector,” *IEEE Access*, 2023, doi: 10.1109/ACCESS.2023.3287641.
- [36] M. Kermani, E. Shirdare, A. Najafi, B. Adelmanesh, D. L. Carni, and L. Martirano, “Optimal Self-Scheduling of a Real Energy Hub Considering Local DG Units and Demand Response under Uncertainties,” *IEEE Trans Ind Appl*, vol. 57, no. 4, pp. 3396–3405, Jul. 2021, doi: 10.1109/TIA.2021.3072022.
- [37] A. Al Hadi, C. A. S. Silva, E. Hossain, and R. Chaloo, “Algorithm for demand response to maximize the penetration of renewable energy,” *IEEE Access*, vol. 8, pp. 55279–55288, 2020, doi: 10.1109/ACCESS.2020.2981877.
- [38] D. Tzovaras, I. Damousis, A. Papanikolaou, G. Pitsiladis, and G. Barbagelata, “DRIMPAC—Unified Demand Response Interoperability Framework Enabling Market Participation of Active Energy Consumers,” in *Proceedings, MDPI AG*, Jul. 2019, p. 15. doi: 10.3390/proceedings2019020015.
- [39] M. H. Christensen, R. Li, and P. Pinson, “Demand side management of heat in smart homes: Living-lab experiments,” *Energy*, vol. 195, Mar. 2020, doi: 10.1016/j.energy.2020.116993.
- [40] H. F. Chinchero, J. M. Alonso, and H. Ortiz T, “LED lighting systems for smart buildings: a review,” *IET Smart Cities*, vol. 2, no. 3, John Wiley and Sons Inc, pp. 126–134, Sep. 01, 2020, doi: 10.1049/iet-smc.2020.0061.



# A Fuzzy C-Means Clustering Analysis of Global Horizontal Irradiance – A Case Study in Gambang, Pahang, Malaysia

06

# A Fuzzy C-Means Clustering Analysis of Global Horizontal Irradiance – A Case Study in Gambang, Pahang, Malaysia

Norhasnelly Anuar  
Mathematical Science Studies  
College of Computing, Informatics and  
Media  
Universiti Teknologi MARA (UiTM)  
Negeri Sembilan Branch  
Seremban Campus  
Negeri Sembilan, Malaysia  
norhasnelly@uitm.edu.my

Nofri Yenita Dahlan  
Solar Research Institute (SRI)  
Universiti Teknologi MARA Shah Alam  
Selangor, Malaysia  
nofriyenita012@uitm.edu.my

Nur Fadzilah Ahmad  
Solar Research Institute (SRI)  
Universiti Teknologi MARA Shah Alam  
Selangor, Malaysia  
nurfadzilah6344@uitm.edu.my

**Abstract**— As the world transitions to renewable energy, solar photovoltaic (PV) installations play a dominant role. To ensure optimal performance and minimize losses, solar plant monitoring and forecasting are crucial. Numerous articles have previously discussed a variety of monitoring and forecasting activities intended for solar plants. Literature suggests that a crucial step in data pre-processing is the classification of weather patterns. A 50MWp UiTM's Solar Park I (USP I) located in Gambang, Pahang, Malaysia is used as the case study. Four type of weather parameters for this study and electrical parameter are obtained from this plant. The correlation analysis between the weather parameters and electrical parameter is performed to identify highly correlated weather parameters, which will then be further clustered using Fuzzy C-Means to uncover the seasonal patterns. According to correlation analysis, Global Horizontal Irradiance (GHI) is the most highly correlated variable. Fuzzy C-Means clustering of GHI revealed three seasonal patterns. This research highlights the importance of weather parameter behavior in solar plant management and performance analysis.

**Keywords**—Fuzzy C-Means, Correlation Analysis, Seasonal Patterns, Solar Energy Management, Large Scale Solar Plant, Global Horizontal Irradiance

## I. INTRODUCTION

Solar energy has emerged as a prominent renewable energy source, offering sustainable and environmentally friendly solutions to meet the increasing global energy demand. The production of solar energy is also increasing because of cost reductions and the solar photovoltaic (PV) industry's rapid growth [1],[2]. Malaysia has joined and demonstrated interest in the development of solar PV. Furthermore, due to its abundance of sunlight and land, Malaysia is considered to have high potential for solar energy generation. In 2015, Malaysia signed the Paris Agreement pledging to fight climate change alongside the rest of the world. Under the third theme of the most recently announced 12th Malaysia Plan, the government has proposed several initiatives to promote green development and energy sustainability. The energy sector's key highlights include reducing greenhouse gas emissions by 45 percent by 2030 and a clean energy target of 31 percent by 2025.

Solar farms play an important part in generating renewable energy, and their performance is highly dependent on the weather [3],[4]. This study aims to discover the correlation between the weather parameters and the generated

AC power. By recognizing the specific weather patterns that are strongly correlated with variations in the AC power, operators and analysts can make informed decisions and take proactive steps to increase the solar farm's performance and production. This information can result in more precise performance forecasts, efficient maintenance scheduling, and optimized energy production, thereby maximizing the solar farm's productivity and economic viability.

Numerous studies have investigated the correlation between meteorological parameters and electrical parameters. Sharma et al. [3] studied the correlation between weather parameters and solar intensity. They found that sky cover, relative humidity, and precipitation were highly correlated with solar intensity, while temperature, dew point, and wind speed showed partial correlations. The study provided insights into how weather metrics affect solar energy harvesting. Using feature clustering and a Markov transition probability matrix, Fu et al. [5] proposed a simulation approach for solar irradiance data. The algorithm utilized K-Means and Markov modelling to generate simulated solar irradiance data. An example simulation with NREL one-minute data was provided, and the results were analyzed and evaluated. Previous research has extensively examined the relationship between weather parameters and electrical parameters in various contexts. Several studies have investigated the correlation between solar irradiance, temperature, wind speed, and other weather variables, and their impact on electrical parameters such as power output, current, and voltage in solar farms [6], [7], [8], [9].

Wu et al. [10] focused on the classification of weather patterns as a crucial data preprocessing method. Weather patterns were categorized by utilizing the K-Means algorithm, Self-Organising maps, and Pearson correlation coefficient to establish specific prediction models for each category. Various methods were explored, including typical clustering classification, season-based classification, time-based classification, and classification based on the amplitude and variance of the data. The result shows the accuracy of solar power forecasting could be significantly improved. The study by Lyu et.al [11] introduced a new framework to predict solar irradiance accurately by dynamically identifying optimal features. It combined feature extraction, clustering techniques, and deep reinforcement learning (DRL) to determine the minimum set of features needed for precise forecasting. The framework adapted to



different weather conditions and adjusted the selected features accordingly. Real-world case studies confirmed that this approach significantly reduced the data required for accurate irradiance prediction across various weather patterns. Overall, the framework improved solar generation forecasts despite limited and inconsistent data availability. Omar et. al addressed the seasonality-related uncertainty in weather data to improve forecasting accuracy. To achieve this, the study utilized layering and stacking of weather data clusters. Adding high-dimensional heterogeneous weather data to training datasets was crucial for enhancing accuracy. However, traditional forecasting models like long short-term memory (LSTM) were not effective when transitioning from univariate to multivariate analyses, leading to decreased performance [12]. A paper by Lopez-Lorente et al. [4] aimed to analyze the impact of temporal variability in solar irradiance on solar energy integration and intra-day forecasting models. The study investigated a classification approach for day types in solar energy applications and assessed its effect on intra-day solar generation forecasting. The proposed approach utilized unsupervised learning, combining self-organized maps and mean-shift clustering with six location-independent metrics related to irradiance variability and energy yield.

Additionally, several methods have been applied to do the clustering of the weather patterns to uncover the underlying variations such as Spectral clustering [13] and Long-Short Term Memory (LSTM) [12]. It is also worth noting that these studies utilized various statistical methods, such as correlation coefficients and regression analysis, to quantify the relationship between weather parameters and electrical parameters. Overall, previous research provides a solid foundation for understanding the correlation between weather parameters and electrical parameters in solar plant. However, there is still a need for further investigation, particularly in the context of specific solar farms in a specific environment to gain a more comprehensive understanding of this relationship and its implications for optimizing energy generation and efficiency.

## II. METHODOLOGY

### A. Data Collection

Weather data was collected from Solar Park I, a 50 MWp solar power plant located in Gambang, Pahang, Malaysia. The data collection period covered one year, from May 2020 to April 2021, during which measurements were recorded at regular 5-minute intervals, specifically from 7 am to 7 pm. The dataset comprised four essential weather parameters which are the Global Horizontal Irradiance (GHI), PV module temperature, ambient temperature and wind speed along with data on generated AC power. Weather parameters play a crucial role in determining the solar plant's overall efficiency and power generation capacity under varying weather conditions.

### B. Correlation Analysis

A fundamental step in the study involved performing a correlation analysis to understand the relationships between the collected weather parameters and the generated AC power. In this study, the method used for correlation analysis is the Pearson correlation coefficient. The Pearson correlation coefficient measures the linear correlation between two

variables and provides a value between -1 and 1 where value 1 indicates high correlation. By evaluating the degree of correlation, either positive or negative, between each weather parameter and the AC power, the most influential factors affecting the solar plant's performance were identified. Parameter with the highest correlation coefficients were considered as key indicator of the solar plant's sensitivity to certain weather conditions.

### C. Fuzzy C-Means Clustering

To unveil the underlying weather patterns, the Fuzzy C-Means (FCM) clustering algorithm was employed. FCM is a soft clustering technique that assigns data points to clusters based on their degrees of membership, allowing for the flexibility of partial belonging. In this context, FCM enabled the discovery of multiple weather patterns that affect the AC power output of the solar plant. Each data point was assigned to one or more clusters, reflecting its similarity to different weather patterns.

### D. Optimal Cluster Selection

To determine the optimal number of clusters for FCM clustering, the elbow method using silhouette analysis was utilized. The silhouette analysis measured the compactness and separation of data points within each cluster for different numbers of clusters. By plotting the silhouette scores against the number of clusters, the "elbow point," which represents the optimal number of clusters, was identified. The elbow point corresponds to the highest average silhouette score, indicating the most meaningful clustering solution for the dataset. Determining the optimal number of clusters was essential to avoid overfitting or underfitting the data during the clustering process.

Following the FCM clustering, each cluster was interpreted and characterized to understand the unique weather patterns it represented. A detailed analysis of the weather parameters associated with each cluster was conducted to identify specific meteorological conditions leading to variations in the solar plant's AC power output. This interpretation provided valuable insights into the diverse range of weather scenarios affecting solar energy generation.

## III. RESULT AND DISCUSSION

### A. Correlation Analysis

The correlation analysis was conducted to investigate the relationship between weather parameters and the generated AC power at Solar Park I, located in Gambang, Pahang, Malaysia. The study aimed to identify the most influential weather factors impacting solar energy generation. Figure 1 presents the correlation coefficients between various weather parameters and the generated AC power at Solar Park I. The correlation analysis aimed to investigate the relationship between weather conditions and solar energy generation. The weather parameters considered in the analysis are Global Horizontal Irradiance, PV module temperature, ambient temperature and wind speed. AC power represents the actual electricity generation from the solar park. The correlation coefficients range from -1 to 1, where a positive value indicates a positive correlation, a negative value indicates a negative correlation. A value close to 0 suggests a weak or no correlation. Table 1 provides a summary of the correlation coefficients between each weather parameter and the AC power generated at Solar Park I. The correlation values

quantify the strength and direction of the relationship between the weather parameter and solar energy generation.

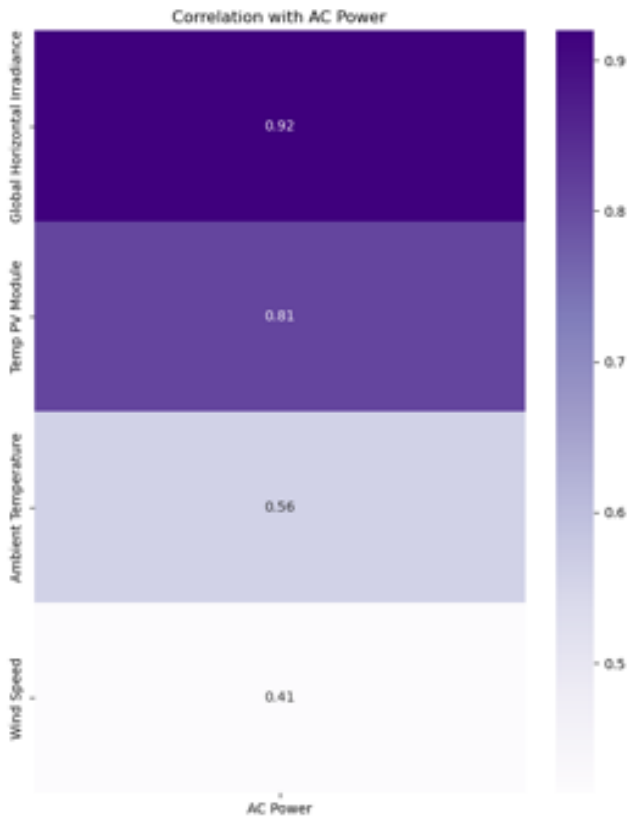


Fig. 1. Weather Parameter and Correlation with Generated AC Power

TABLE I. PARAMETER AND CORRELATION WITH GENERATED AC POWER

Weather Parameter	Correlation
Global Horizontal Irradiance	0.92
PV Module Temperature	0.81
Ambient Temperature	0.56
Wind Speed	0.41

Higher GHI levels on sunny days result in increased power generation, while lower GHI levels on cloudy days lead to decreased power generation. The temperature of PV modules demonstrated a significant positive correlation of 0.81 with AC power. As the temperature of the PV modules increases, the efficiency of the solar cells decreases, resulting in a decrease in power output. Managing the temperature of PV modules is essential for optimising energy production. On the other hand, there was a moderately positive correlation of 0.56 between ambient temperature and AC power. Higher ambient temperatures can affect the effectiveness of various solar power plant components, thereby affecting overall energy production. Temperature control measures may be beneficial for optimising facility operation. Lastly, wind speed demonstrated a moderate positive correlation of 0.41 with AC power. Wind speed may not be the most important factor influencing solar energy production, but it can still have an effect, particularly in strong winds conditions. It may be

relevant to consider wind-induced movement or cooling effects on solar panels.

The correlation analysis highlights the crucial impact of Global Horizontal Irradiance (GHI) on the AC power output at Solar Park I. Understanding these relationships is of utmost importance for optimizing solar energy generation and enhancing the overall performance of the solar power plant. To gain deeper insights into GHI's influence, the weather parameter is further subjected to Fuzzy C-Means (FCM) clustering analysis. Through FCM clustering, this study aim to uncover underlying patterns in GHI data that significantly impact Solar Park I's energy production. This will enable us to identify distinct weather conditions or trends that influence the plant's efficiency and guide informed decision-making for effective energy operation and maintenance.

### B. Optimal Cluster Selection

Clustering is an essential unsupervised learning technique used to group similar data points into distinct clusters. The challenge lies in determining the appropriate number of clusters, as it directly impacts the interpretability and effectiveness of the analysis. The optimal number of clusters in the dataset is determined by using the Elbow method. The analysis was conducted to identify the ideal number of clusters required to capture meaningful patterns in the data. The Elbow method involves plotting the within-cluster sum of squares (WCSS) against the number of clusters. WCSS quantifies the compactness of the clusters, and the goal is to minimize this value. The Elbow method seeks to find the "elbow point" on the plot, which represents the optimal number of clusters, where adding more clusters does not lead to a significant reduction in WCSS. Figure 2 demonstrate the application of the Elbow method to the dataset to identify the optimal number of clusters. Based on the Elbow method analysis, the optimal number of clusters for the dataset was determined to be three. At this point, adding more clusters would not result in a substantial gain in clustering accuracy, while a smaller number of clusters could lead to a loss of significant patterns in the data.

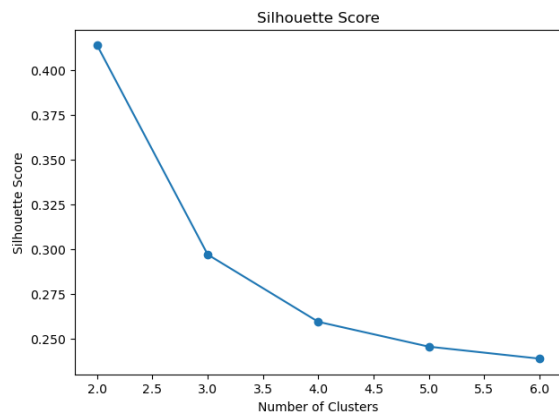


Fig. 2. Silhouette Score - Optimal Number of Cluster Selection

### C. FCM Clustering

Having identified the significant impact of Global Horizontal Irradiance (GHI) on the AC power output at Solar Park I, the study endeavors to gain deeper insights into the underlying patterns of this crucial weather parameter. To achieve this, the Fuzzy C-Means (FCM) clustering analysis

was employed. FCM clustering aims to partition data points into distinct clusters based on their similarities to each other. Unlike traditional hard clustering algorithms, FCM allows data points to belong to multiple clusters with varying degrees of membership, reflecting the fuzzy nature of data distribution. This soft clustering approach enables us to discover subtle patterns and associations within the GHI data.

The clustering analysis of the GHI data collected over one year from May 2020 to April 2021, with 5-minute intervals between 7 am and 7 pm, revealed three distinct weather patterns significantly influencing solar irradiance. Figure 3 presents the time series plot depicting the average Global Horizontal Irradiance (GHI) values for each of the three identified clusters. The time series plot showcases the distinct patterns observed for Cluster 1 (blue line), Cluster 2 (yellow line), and Cluster 3 (green line).

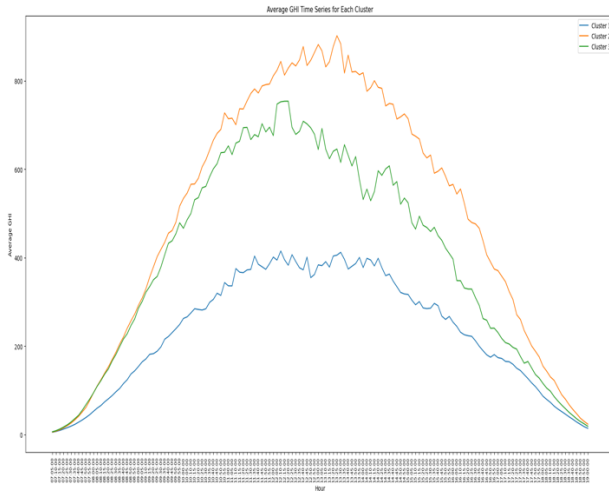


Fig. 3. Time series plot for average GHI for Cluster 1,2 and 3

Additionally, Table 2 provides a summary of the minimum and maximum average GHI values for each cluster.

Cluster	Min GHI Average Value (W/m <sup>2</sup> )	Max GHI Average Value (W/m <sup>2</sup> )
Cluster 1	4.4	422.05
Cluster 2	4.4	901.94
Cluster 3	4.9	758.17

Among the three clusters identified in the clustering analysis, Cluster 1 exhibits the lowest average value of GHI as shown in Figure 4. This cluster is associated with heavy cloud cover and potential rain, resulting in GHI levels ranging from a minimum average value of 4.4 W/m<sup>2</sup> to a maximum average value of 422.05 W/m<sup>2</sup>. These values represent the lowest solar irradiance levels observed during the analyzed period. Identifying this pattern can aid in predicting periods of reduced solar energy production and help plan for necessary adjustments to compensate for energy shortfalls.

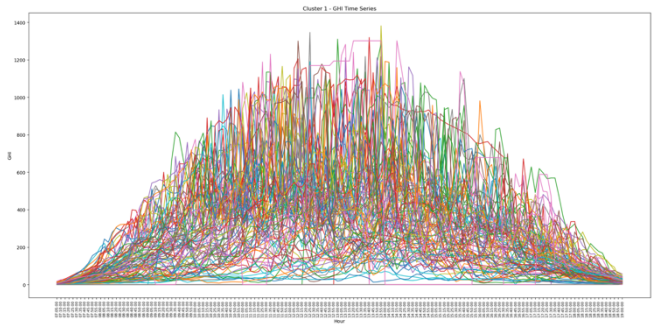


Fig. 4. Time series plot for GHI - Cluster 1

Cluster 2 is shown in Figure 5 and demonstrates the highest average value of GHI. This cluster is characterized by favourable weather conditions, including clear skies and minimal cloud cover, resulting in GHI levels ranging from a minimum average value of 4.4 W/m<sup>2</sup> to a maximum average value of 901.94 W/m<sup>2</sup>. These values indicate the highest solar irradiance levels observed during the analysed period, making this weather pattern highly suitable for optimizing solar energy generation and scheduling.

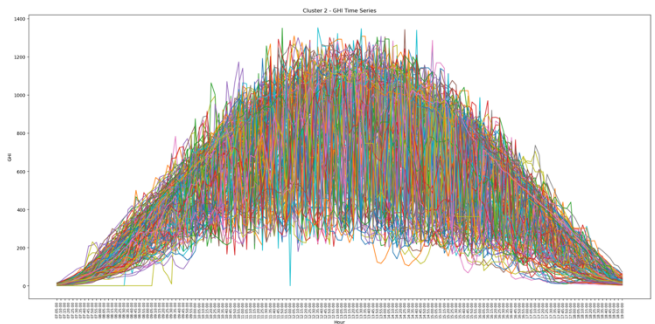


Fig. 5. Time series plot for GHI - Cluster 2

Cluster 3 represents a weather pattern with moderate cloud cover and intermittent sun, resulting in moderate fluctuations of GHI as observed in Figure 6. The GHI levels in this cluster range from a minimum average value of 4.9 W/m<sup>2</sup> to a maximum average value of 758.17 W/m<sup>2</sup>. This pattern indicates varying solar irradiance levels throughout the day, making it crucial for predicting fluctuations in solar energy generation and implementing strategies to maintain a stable power supply during changing weather conditions.

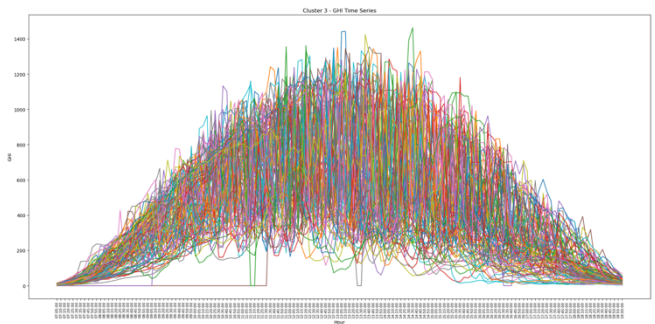


Fig. 6. Time series plot for GHI - Cluster 3

The identified weather patterns provide valuable insights for various applications in the renewable energy sector. Developing predictive models based on historical weather

patterns and GHI data can enable accurate forecasting of solar energy generation, optimizing grid management, and scheduling. Integrating energy storage systems to mitigate the impact of fluctuating GHI levels resulting from different weather patterns can enhance the reliability and stability of solar energy as a viable power source. Furthermore, understanding the long-term trends of the identified weather patterns is crucial for assessing potential shifts in solar irradiance due to climate change. Analyzing these trends will aid in long-term planning in the renewable energy sector and contribute to sustainable power generation strategies.

#### IV. CONCLUSION

In conclusion, the clustering analysis of GHI data into three distinct patterns offers valuable insights into the underlying weather dynamics influencing solar irradiance. These findings open opportunities for more efficient solar energy management and utilization, contributing to the development of sustainable and environmentally friendly power generation systems. As research in this area progresses, the knowledge gained from this study will be essential in advancing renewable energy technologies and addressing the challenges of climate change. To generalize the findings, replicating this study in different regions with similar data collection setups can identify region-specific weather patterns and optimize solar energy utilization on a broader scale. Additionally, incorporating other meteorological variables, such as temperature, humidity, and wind speed, will provide a more comprehensive understanding of the complex interactions between various weather factors and solar irradiance.

#### ACKNOWLEDGMENT

We would like to express our gratitude and appreciation to the University Teknologi MARA (UiTM) for providing us with the invaluable opportunity to advance the study.

#### REFERENCES

- [1] G. S. Sharma *et al.*, "Performance Evaluation of a MW-Size Grid-Connected Solar Photovoltaic Plant Considering the Impact of Tilt Angle," *Sustainability (Switzerland)*, vol. 14, no. 3, Feb. 2022, doi: 10.3390/su14031444.
- [2] A. Livera, M. Theristis, L. Micheli, E. F. Fernandez, J. S. Stein, and G. E. Georghiou, "Operation and Maintenance Decision Support System for Photovoltaic Systems," *IEEE Access*, vol. 10, pp. 42481–42496, 2022, doi: 10.1109/ACCESS.2022.3168140.
- [3] N. Sharma, P. Sharma, D. Irwin, and P. Shenoy, "Predicting solar generation from weather forecasts using machine learning," *2011 IEEE International Conference on Smart Grid Communications, SmartGridComm 2011*, pp. 528–533, 2011, doi: 10.1109/SmartGridComm.2011.6102379.
- [4] J. Lopez-Lorente, S. Theocharides, G. Makrides, and G. E. Georghiou, "Impact of Daily Irradiance Profiles on Intra-Day Solar Forecasting," in *Conference Record of the IEEE Photovoltaic Specialists Conference*, Institute of Electrical and Electronics Engineers Inc., 2022, pp. 156–163. doi: 10.1109/PVSC48317.2022.9938936.
- [5] "A Simulation Method of Solar Irradiance Data Based on Feature Clustering and Markov Transition Probability Matrix."
- [6] M. Sun, C. Feng, and J. Zhang, "Probabilistic solar power forecasting based on weather scenario generation," *Appl Energy*, vol. 266, May 2020, doi: 10.1016/j.apenergy.2020.114823.
- [7] R. Singhal, P. Singhal, and S. Gupta, "Solar-Cast: Solar Power Generation Prediction from Weather Forecasts using Machine Learning," in *2022 IEEE 10th Power India International Conference, PIICON 2022*, Institute of Electrical and Electronics Engineers Inc., 2022. doi: 10.1109/PIICON56320.2022.10045237.
- [8] M. S. Hossain and H. Mahmood, "Short-term photovoltaic power forecasting using an LSTM neural network and synthetic weather forecast," *IEEE Access*, vol. 8, pp. 172524–172533, 2020, doi: 10.1109/ACCESS.2020.3024901.
- [9] I. M. Moreno-García, R. López-Luque, M. Varo-Martínez, L. M. Fernández-Ahumada, J. C. Ramírez-Faz, and F. C. De La Torre, "An Approach for the Solar Energy Assessment using Weather Medium-Range Forecasting," in *Proceedings - 2019 IEEE International Conference on Environment and Electrical Engineering and 2019 IEEE Industrial and Commercial Power Systems Europe, EEEIC/I and CPS Europe 2019*, Institute of Electrical and Electronics Engineers Inc., Jun. 2019. doi: 10.1109/EEEIC.2019.8783583.
- [10] Y. K. Wu, Y. J. Zhong, and Q. T. Phan, "Overview of Day-ahead Solar Power Forecasts Based on Weather Classifications," in *Conference Record - Industrial and Commercial Power Systems Technical Conference*, Institute of Electrical and Electronics Engineers Inc., 2023. doi: 10.1109/ICPS57144.2023.10142132.
- [11] C. Lyu, S. Eftekharijad, S. Basumallik, and C. Xu, "Dynamic Feature Selection for Solar Irradiance Forecasting Based on Deep Reinforcement Learning," *IEEE Trans Ind Appl*, vol. 59, no. 1, pp. 533–543, Jan. 2023, doi: 10.1109/TIA.2022.3206731.
- [12] N. Omar, H. Aly, and T. Little, "Seasonal Clustering Forecasting Technique for Intelligent Hourly Solar Irradiance Systems," *IEEE Trans Industr Inform*, vol. 19, no. 3, pp. 2520–2529, Mar. 2023, doi: 10.1109/TII.2022.3177746.

## List of contributors

Ahmad Ihsan bin Mohd Yassin, *Microwave Research Institute, Universiti Teknologi MARA*

Mohamad Fani Sulaima, *Fakulti Kejuruteraan Elektrik, Universiti Teknikal Malaysia Melaka*

Muhammad Ikram bin Ahmad Zaidi, *UiTM Solar Research Institute, Universiti Teknologi MARA*

Nofri Yenita Dahlan, *UiTM Solar Energy Research Institute, Universiti Teknologi MARA*

Norhasnelly Anuar, *Mathematical Science Studies, College of Computing, Informatics and Media, Universiti Teknologi MARA (UiTM)*

Nurfadzilah Ahmad, *UiTM Solar Research Insitute,Universiti Teknologi MARA*

Nurliyana Binti Baharin, *Kejuruteraan Elektrik, Universiti Teknikal Malaysia Melaka*

Nur Alfarina Pirdaus, *UiTM Solar Research Insitute,Universiti Teknologi MARA*

Nur Fadhilah Jamaludin, *School of Electrical Engineering, College of Engineering, Universiti Teknologi MARA*

Rijalul Fahmi bin Mustapha, *School of Electrical Engineering, College of Engineering, Universiti Teknologi MARA*

Rozita Jailani, *School of Electrical Engineering, College of Engineering, Universiti Teknologi MARA*

Sharina Safiee, *Department of Electrical Technology, Kolej Komuniti Kuala Langat*

## Index

Artificial Neural Network 2-3  
battery electric buses 2-8  
BEB *see* battery electric buses  
Building Automation System 2,4-5,7-8  
Charging scheduling 35-37  
Climate Change 2-3, 5-7, 10, 29-30, 32  
Commercial TiO<sub>2</sub> 2, 6  
Correlation Analysis 2, 4-6  
Distributed Combiner Box 2, 4  
DSSC *see* dye-sensitized solar cells  
dye-sensitized solar cells 10, 31, 35  
Energy saving 10, 16-17, 19  
enhanced time-of-use 10, 16, 21  
eToU *see* enhanced time-of-use  
Fuzzy  
    C-Means 10-14, 36  
    logic 4, 35  
GHI *see* Global Horizontal Irradiance  
Global Horizontal Irradiance 4, 16-17, 19, 38  
KNX System 16, 18  
Large Scale  
    Solar 16-17  
    Plant 16,18  
    Photovoltaic 16  
Load profile 24-27  
LSSPV *see* Large-Scale Solar Photovoltaic 24-27  
Matrix Laboratory 24-27  
Maximum Power Point Tracking 29-32  
Mean Square Error 10, 29-32  
MSE *see* Mean Square Error  
Perturb and Observe 29-32  
Photovoltaic 29-32  
Regression 35-37  
Seasonal Patterns 35-37  
Solar  
    cell 35  
    Energy Management 35, 39  
sol-gel 35  
Standard Test Condition 35, 37-39  
TiO<sub>2</sub> 11, 35-38

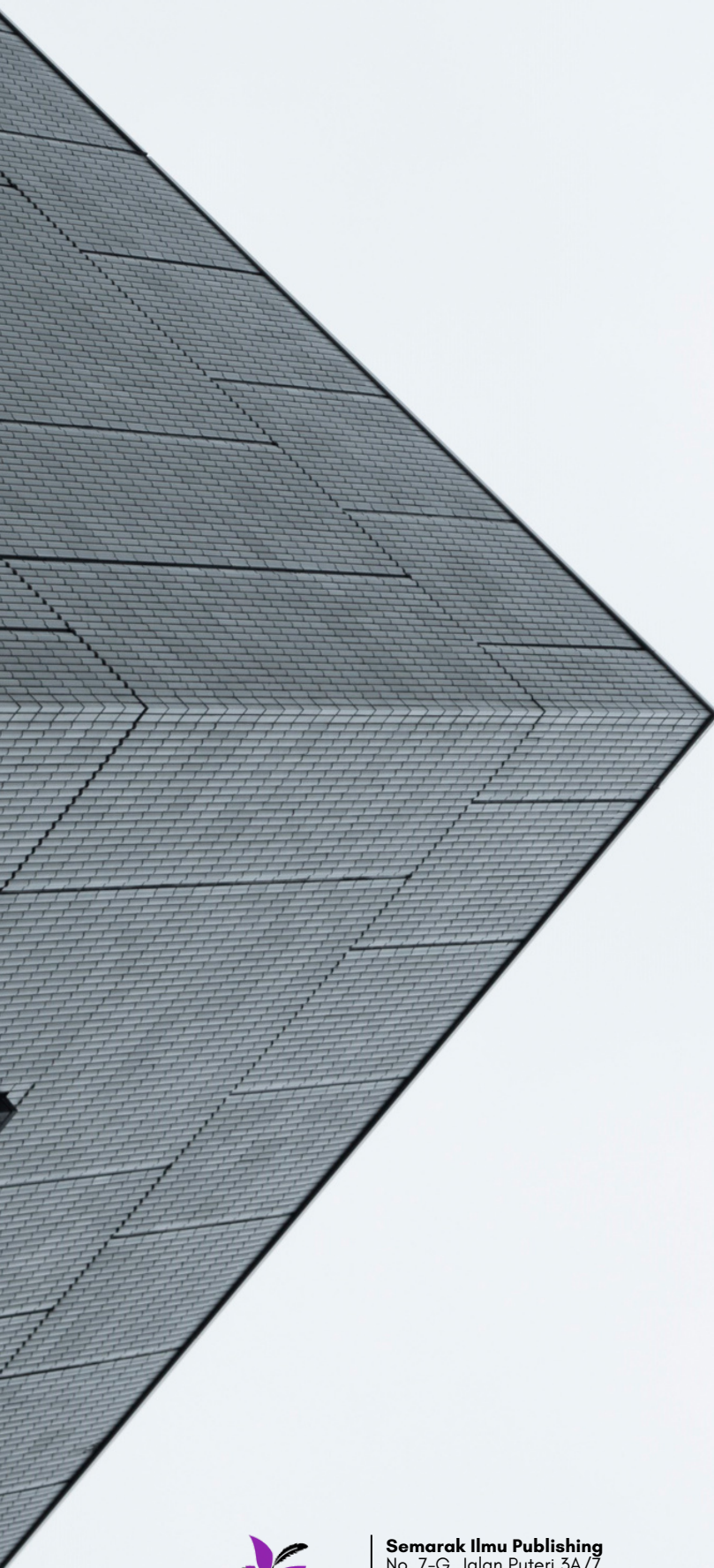
Climate Change and Renewables Progressing Towards a Greener and Cleaner Future

e ISBN 978-629-98779-0-5



SEMARAK ILMU PUBLISHING

(online)



**Semarak Ilmu Publishing**  
No. 7-G, Jalan Puteri 3A/7  
Bandar Puteri Bangi  
43000 Kajang, Selangor  
Tel: 017-7541097  
Web: <https://semarakilmu.com.my>

e ISBN 978-629-98779-0-5

